

ELECTRONIC BIOSENSORS FOR EARLY CANCER DETECTION

by

WAQAS ALI

Presented to the Faculty of the Graduate School of
The University of Texas at Arlington
in Partial Fulfillment of the Requirements
for the Degree of

DOCTOR OF PHILOSOPHY

UNIVERSITY OF TEXAS AT ARLINGTON

April 2016

ACKNOWLEDGEMENTS

All praise to Almighty Allah, the most merciful. Peace be upon Prophet Muhammad.

I would like to thank my parents and my family members for their full support in every part of my life and I would like to express my deepest respect for my advisor Dr. Samir Iqbal for guiding me and helping me throughout this work.

April 20, 2016

ABSTRACT

ELECTRONIC BIOSENSORS FOR EARLY CANCER DETECTION

Waqas Ali, PhD

University of Texas at Arlington, 2016

Supervising Professor: Dr. Samir M. Iqbal

Nanotechnology is an emerging field that holds promise to improved disease diagnosis and better health care. It has revolutionized the medical industry and is continuing to mesmerize in other research areas as well. Even after tremendous advancements in disease detection and treatment techniques, high mortality rate due to cancer necessitates the need for new sensing platforms for early cancer detection.

The focus of this dissertation is development of new sensing platforms that are highly sensitive and selective and are able to detect the tumor at an early stage i.e. cellular or molecular level. We demonstrated that breast cancer tumor cells and lung cancer tumor cells could be successfully differentiated with the micropore biosensor. This biosensor was fabricated using standard device fabrication technology. Micropore sensor differentiated tumor cells using the difference in their cell properties. Since the cell properties of tumor cells are different than the normal cells, this property was used as an inherent cell marker alleviating the need of any external cell markers that are conventionally being used for tumor detection. With micropore sensor tumor can be detected even before it gets metastasized: a primary requirement for early cancer detection. With nanopore sensor epidermal growth factor receptor (EGFR) was detected with high sensitivity and selectivity. Selectivity was imparted using the anti-EGFR

aptamer. These devices are easy to use, require minimal processing of the sample and can potentially be used at point-of-care.

TABLE OF CONTENTS

Acknowledgements.....	ii
Abstract	iii
Chapter 1	
Background.....	1
Overview of Research Work.....	8
Differentiating Metastatic and Non-metastatic Tumor Cells.....	9
Discriminating between Lung Cancer Cell Sub-types.....	9
Solid-state Nanopore for Label Free Detection of EGFR.....	10
References.....	11
Chapter 2	
Abstract.....	15
Introduction.....	16
Experimental Section.....	20
Tumor Cell Interrogating Micropores.....	20
Measurement Setup and Data Analysis.....	21
Flow Rate and Sampling Frequency.....	23
Microchannel Device.....	24
Cell Culture.....	25
Results.....	26
Cell Detection Efficiency.....	26
Electrical Signatures of MTCs and NMTCs.....	26
Reliability of Electrical Signatures from Micropore Device.....	28
Quantitative Cellular Discrimination from a Mixture.....	29

Detection Limit.....	32
Cellular Discrimination from an Impure Sample.....	33
Breast Cancer Cell Migration through Tightly Confined Microchannels....	35
Discussion.....	36
References.....	41
Acknowledgement & Financial Interest Statement.....	44
 Chapter 3	
Abstract.....	47
Introduction.....	49
Materials and Methods.....	51
Micropore Device Fabrication.....	51
Measurement Setup.....	53
Lung Cancer Cell Line Culture.....	55
Measurement of Lung Cancer Cell Diameter.....	55
Lung Cancer Cell Migration through Tightly Confined Microchannels.....	55
Results.....	57
Cell Detection Efficiency.....	57
Electrical Signatures of Lung Cancer Cells.....	59
Discussion.....	64
Conclusion.....	66
Acknowledgements and Financial Interest Statement.....	67
References.....	68
 Chapter 4	
Abstract.....	73
Introduction.....	74

Results and Discussion.....	76
Materials and Methods.....	87
Materials.....	87
Nanopore Fabrication and Electrical Measurements.....	88
In-solution Binding of Protein and Aptamer.....	88
Conclusions.....	89
Acknowledgements.....	89
References.....	91
Chapter 5	
Future Directions.....	95
Early Detection of Leukemia from Blood Serum.....	95
Self-referenced Nanopore Array for Multiple Biomarker Detection.....	96
Spiral Microfluidics Interfaced with Micropore – Lab on a Chip.....	97
Conclusions.....	98
Appendices.....	100

CHAPTER 1

INTRODUCTION

1.1 Background

Nanotechnology is an interdisciplinary field that has undergone tremendous growth and development in the last couple of decades. It has evolved as a disruptive technology that has impacted almost every scientific area. It holds promise to change the paradigms of current scientific knowledge especially in the field of biology and medicine. The intersection of nanotechnology and biology is referred as Bio-Nanotechnology and based on that new diagnostic and treatment methods are evolving. Further advancement in this area will change the way diseases are being diagnosed and treated.

In the last decade, one of the biggest focus of researchers has been to develop new drug delivery methods to treat cancer and devise new mechanisms to detect cancer during its inception. Due to the advancement in technology, disease diagnosis and treatment has improved a lot. Over the past few decades mortality rate due to all major life threatening diseases like heart diseases, cardiovascular diseases and pneumonia etc. have reduced significantly but cancer is a disease for which mortality rate has not changed as can be seen in Figure 1.1. Cancer is the 2nd most common disease and it claims 1 out of every 4 deaths in the world. Every year, \$250 billion is the

cost of the diagnosis and treatment of this disease and the figures are continuously increasing. This is a huge burden on the world economy. According to the American Cancer Society, 1.68 million new cancer cases have been reported so far in U.S. in 2016. Despite a massive investment in the treatment and prevention of cancer the mortality rate for this disease has fallen a meager 8% since 1975 among people under age of 85 years in the US. Among people of age more than 85 years, mortality rate has actually increased rather than decreasing.

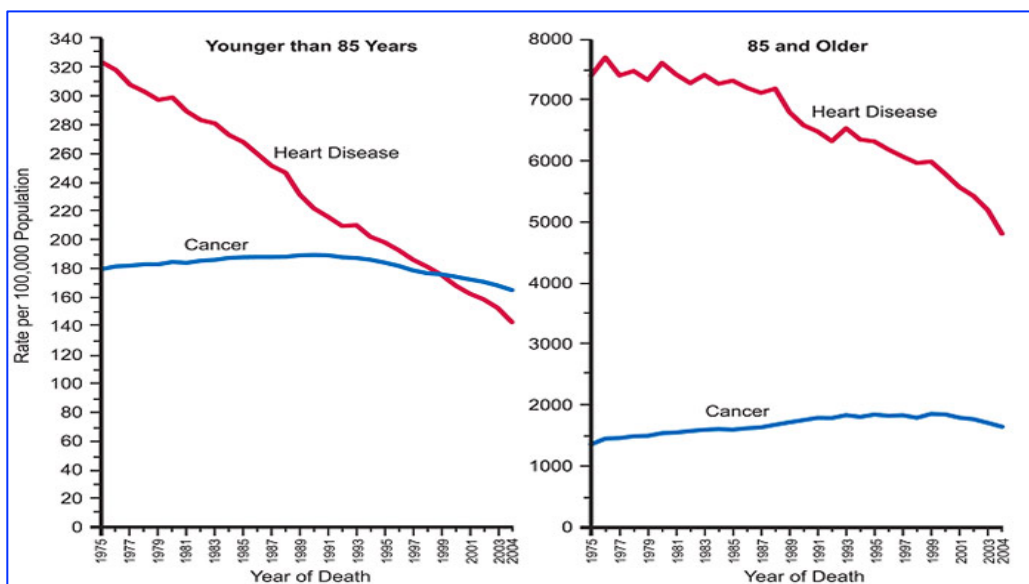


Figure 1.1: Comparison of Improvement in the Mortality Rate for Heart Disease and Cancer among people of age (a) Younger than 85 Years (b) 85 Years and Older [1].

The main reasons for this failure are our inability to provide low cost and rapid diagnostic platforms that can detect the cancer at its early stage. The current diagnostic tools lack the sensitivity and selectivity for early cancer detection. Early detection is the key to successful treatment of cancer [2,3]. As can be seen in figure 1.2 that the survival

rate for cancer is highest at early stages that decreases gradually as the disease matures.

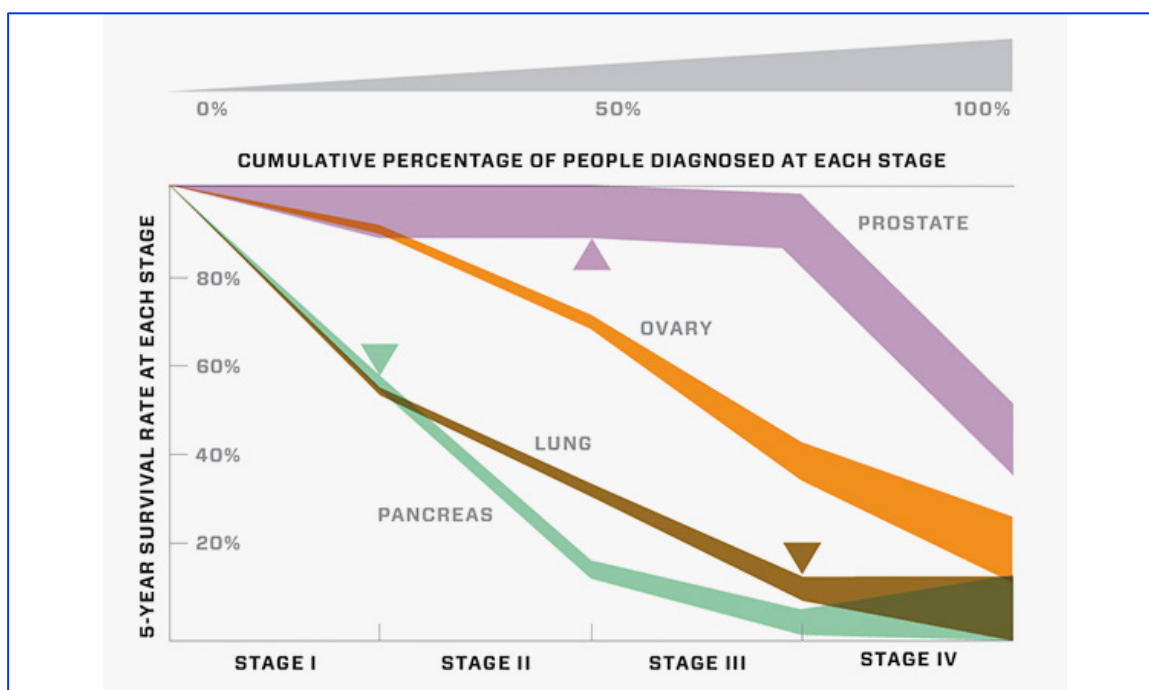


Figure 1.2: 5-Year Survival Rate for Various Types of Cancer [3].

From Figure 1.2 one can also see the cumulative percentage of people who are being diagnosed at each cancer stage. At stage 1 of the disease, the disease detection rate is 0% whereas at stage 4, its 100%. At stage 1, cancer is curable but not detectable and at stage 4, cancer is easily detectable but not curable. At one end, there is need for better cancer treatment and on the other end better diagnostic platforms are required that can detect the disease as soon as it starts.

An unprecedented growth in the field of nanotechnology has led researchers and scientists to fabricate devices at the scales that were just impossible few decades ago. Now it has become possible to self-assemble the atoms to make useful structures

(bottom-up fabrication) or to fabricate thin films of few nanometer thickness (top-down fabrication). Such well-controlled and precise fabrication has led to the use of nanowires, nanotubes and quantum dots etc. in real world applications. The use of nanoparticles for controlled and targeted dose delivery is one such application where nanotechnology has revolutionized the medical industry [4-6]. Some of these new applications and the scale at which they are useful are mentioned in Figure 1.3.

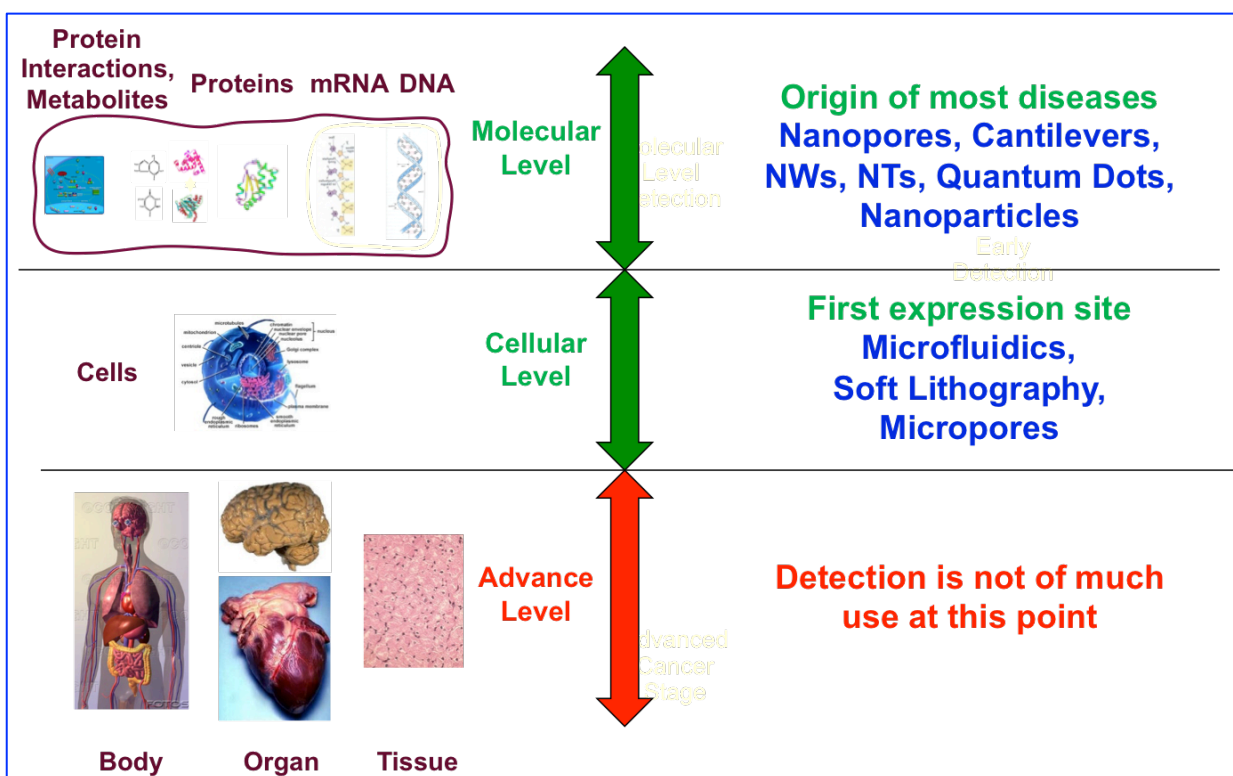


Figure 1.3: Cancer Detection Stage – Early Detection is the key to successful cancer treatment and it is possible only when cancer is detected at molecular or cellular level. Survival rate is too low once cancer enters into its advanced stages.

One of the major advancement in cancer diagnosis was detection of circulating tumor cells (CTCs) in human blood. Ashworth was the first one to find CTCs in the blood stream in 1869 [7]. Around 10 years ago, Cristofanilli et. al. elaborated the

prognostic value of CTCs in metastatic breast cancer patients for the first time [8]. Since then a lot of progress has been made for the detection of CTCs and various methods have been developed.

Immunomagnetic systems, reverse transcription polymerase chain reaction system (RT-PCR), CellSearch™ assay and isolation by size of epithelial tumor cells (ISET) are more common. Immunomagnetic detection methods require mixing of whole blood with magnetic particles-bound antibodies [9,10]. Due to antibody interactions, cells attach to beads/particles and are separated by the magnetic force.

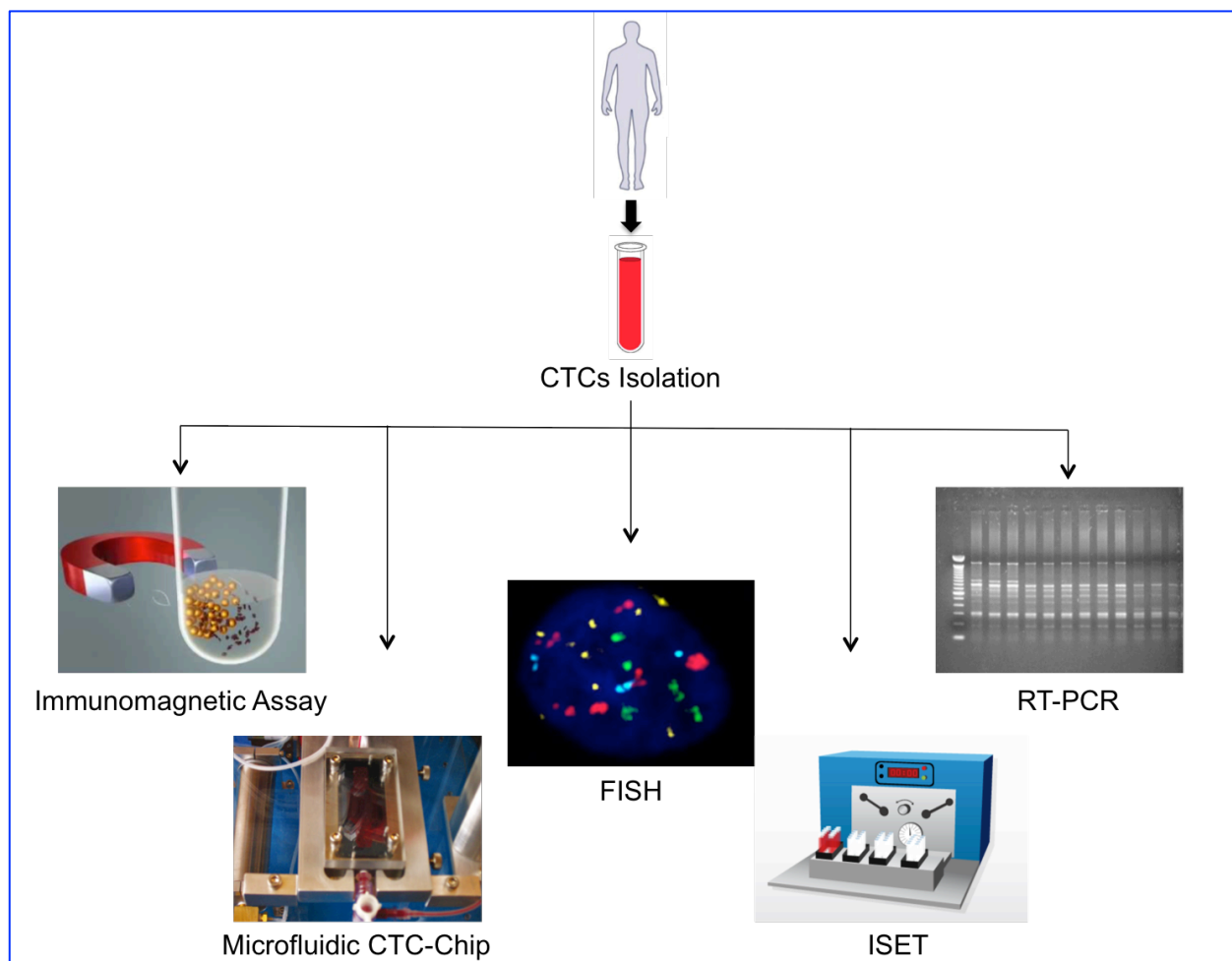


Figure 1.4: CTCs Isolation Techniques [11-14]

CellSearch™ assay uses beads coated with epithelial cell adhesion molecule (EpCAM) antibody to immunomagnetically capture epithelial cells followed by fluorescent labeling of cells. ISET is a method based on cell filtering. Diluted blood is filtered with polycarbonate membrane with the mean diameter of 8 µm. Due to their comparatively larger size epithelial cells remain on the membrane [11]. Then cells are fluorescently tagged and a laser cytometer is used to scan them. This method has been utilized to successfully isolate breast tumor cells [12]. RT-PCR method uses gel electrophoresis to investigate specific genes from CTCs. This method is sensitive enough to detect 1 cancer cell from 10^7 normal cells. Even though it has highest sensitivity, this method has limited usage because of high false positive rate [13].

More recently, microfluidics and microchips have been used as well for the detection of CTCs. In this regard, microchip platform developed by Nagrath et al. and micropore biosensor developed by Asghar et al. looked very promising. The first one utilized EpCAM antibody to functionalize the microposts to selectively attach CTCs whereas later one did size based filtering to separate CTCs from the blood [14,15].

Though CTC detection and quantification can provide cancer progression information and better monitoring of cancer therapy but presence of CTCs in the blood itself is an indication of an advanced stage of cancer. At the most, it can indicate the start of metastatic stage if CTCs are detected early. It will be more important to detect the tumor even before it has reached its metastatic stage since the survival rate for patients who has not reached metastatic stage is very high whereas once tumor become metastatic, survival rate goes down drastically [1,2,15]. For example, in the case of breast tumor, survival rate goes down to only 22% once it reaches its metastatic

stage [7,16]. Analysis of tumor cells from the biopsy sample or a lesion can lead us to detect the tumor even before it reaches its metastatic stage. Those tumor cells can be analyzed to check their tendency to become metastatic. That will be a big breakthrough towards early cancer detection.

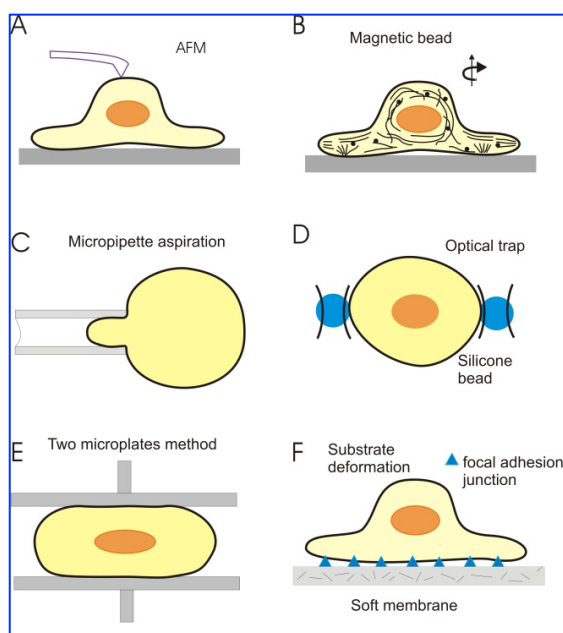


Figure 1.5: Methods to probe cell properties [17]

There are several methods to investigate cell properties from the biopsy sample. Previously, micropipette aspiration (MA), microneedle probes, atomic force microscopy (AFM), microplate manipulation and optical tweezers etc. have been used to investigate cell mechanical properties [18-22]. Lekka et al. probed the mechanical properties of normal and cancerous cells with AFM and found an order of magnitude difference in the cell rigidity [23]. Ward et al. have reported 50% difference in elasticity of malignant and

normal cells using MA. All these methods have their limitations [24,25]. They all require labor-intensive pre-processing of the samples, specialized equipment and very well trained manpower to get the results. The results can't be obtained quickly. Probing the cell cytoskeleton directly requires fluorescent tagging [26]. There are no convenient methods to investigate mechanical properties of cells and to differentiate them on that basis.

1.2 Overview of Research Work

The research presented in this dissertation focuses on the development of highly sensitive and selective molecular & cellular platforms for early cancer detection. There are peculiar differences in the cell properties of normal and tumor cells. The cell attributes of one type of tumor cells are also different from the other types of tumor [22]. Malignant transformations in cells go side by side with very specific changes in cell mechanical properties. One most pronounced change is in their cell deformability. Malignant cells become more compliant in the sense that they lose their stiffness and it is easier to deform them as compared to normal or benign tumor cells [27]. Cell deformability has become an inherent cell marker to check the malignancy and metastatic potential of tumor cells where higher cell deformability corresponds to higher malignancy and metastatic potential [23,27]. This important property can be used to differentiate tumor cells. We used mechanophysical properties of tumor cells to differentiate breast cancer cells and lung cancer cells.

First two projects were to develop micropore biosensors for detection and differentiation of tumor cells. First project aimed at discriminating between metastatic

and non-metastatic tumor cells, and second one aimed at detecting between three types of non-small cell lung cancer cells (NSCLC). The third project was on nanopore biosensor for the detection of epidermal growth factor receptor (EGFR) overexpression from patients sample. Micropore biosensors are suitable for cellular level detection whereas nanopore biosensors are ideal for molecular level detection.

1.2.1 Differentiating Metastatic and Non-metastatic Tumor Cells from their Translocation Profile through Solid-state Micropores

Metastatic and Non-metastatic tumor cells of breast cancer (MB-231 and MCF7) were translocated through a micropore, the size (diameter) of which was kept smaller than the cell size of these tumor cells. Since metastatic tumor cells are more elastic and pliable than their non-metastatic counterpart, the former were able to squeeze through the micropore easily whereas the non-metastatic cells faced much more steric hindrance during their translocation due to their rigidity and less pliable cell characteristics. The electrical pulses registered due to the translocation of metastatic tumor cells were shallow and narrower whereas those registered by non-metastatic tumor cells were much deeper and wider. These pulses were analyzed to quantify the two types of tumor cells present in the sample. This information was pivotal in determining the cancer stage.

1.2.2 Discriminating between Lung Cancer Cell Sub-types

Non-small cell lung cancer cells (H1155, A549 and H460) were translocated through the micropore to differentiate them from their translocation profile. Two cell types had size larger than the pore diameter whereas the cell diameter for third one was smaller than the pore diameter. It was observed that the three cell types were

differentiable on the basis of their translocation profiles through the micropore. The difference in translocation profile stemmed from the difference in the mechanophysical properties of the three cell types. It was observed that the cell size was a dominant cell property in dictating the translocation characteristics of the cells and other mechanical properties of cell like elasticity, rigidity and shape become important only when the cells had same size. The cell differentiation was useful to prescribe the right treatment for the disease.

1.2.3 Solid-State Nanopore for Label Free Detection of EGFR

Nanopore biosensor was used to detect EGFR. Anti-EGFR aptamer was used as the targeting agent. Sample was translocated through a 40 nm nanopore before and after incubation with anti-EGFR aptamer. There was a shift in the event population (translocation time vs peak amplitude scatter plot) between the two types of translocations when there was EGFR present in the sample. Thrombin was used to check the specificity of this assay. This is a simple but very efficient, low cost and rapid assay to check the presence of EGFR in a sample.

References

- [1] Jemal, A., et al., *Cancer Statistics, 2008*. CA: A Cancer J for Clinicians 2008. **58**(2): pp. 71-96.
- [2] Cheng, M.M.C., et al., *Nanotechnologies for biomolecular detection and medical diagnostics*. Current Opinion in Chemical Biology, 2006. **10**(1): pp. 11-19.
- [3] Goetz, T., *The Riddle of Early Detection!*. Wired Magazine 2008.
- [4] Park, K., *Controlled drug delivery systems: Past forward and future back*. Journal of Controlled Release, 2014. **190**: pp 3-8.
- [5] Muller, R. H., Mader, K., and Gohla, S., *Solid lipid nanoparticles (SLN) for controlled drug delivery – a review of the state of the art*. European Journal of Pharmaceutics and Biopharmaceutics, 2000. **50**(1): pp. 161-177.
- [6] Hwang, A. A., Lu, J., Tamanoi, F., and Zink, J. I., *Functional Nanovalves on Protein-Coated Nanoparticles for In vitro and In vivo Controlled Drug Delivery*. Small, 2015. **11**(3): pp. 319-328.
- [7] Cristofanilli, M., et al., *Circulating tumor cells: a novel prognostic factor for newly diagnosed metastatic breast cancer*. Journal of Clinical Oncology, 2005. **23**(7): p. 1420- 1430.
- [8] Cristofanilli, M. et al. *Circulating tumor cells, disease progression, and survival in metastatic breast cancer*. The New England J of Medicine, 2004. **351**: pp. 781–791.
- [9] Witzig, T.E., et al., *Detection of circulating cytokeratin-positive cells in the blood of breast cancer patients using immunomagnetic enrichment and digital microscopy*. Clinical Cancer Research, 2002. **8**(5): pp. 1085-1091.
- [10] Gauthier, L.R., et al., *Detection of circulating carcinoma cells by telomerase activity*. British J of Cancer, 2001. **84**(5): pp. 631.
- [11] Zabaglo, L., et al., *Cell filtration-laser scanning cytometry for the characterisation of circulating breast cancer cells*. Cytometry Part A, 2003. **55**(2): pp. 102-108.
- [12] Vona, G., et al., *Isolation by Size of Epithelial Tumor Cells: A New Method for the Immunomorphological and Molecular Characterization of Circulating Tumor Cells*. American Journal of Pathology, 2000. **156**(1): pp. 57.
- [13] Zieglschmid, V., Hollmann, C., and Bocher, O., *Detection of disseminated tumor cells in peripheral blood*. Critical Reviews in Clinical Laboratory Sciences, 2005. **42**(2): pp. 155-196.
- [14] Nagrath, S., et al., *Isolation of rare circulating tumour cells in cancer patients by microchip technology*. Nature, 2007. **450**(7173): pp. 1235-1239.
- [15] Asghar, W., Wan, Y., Ilyas, A., Bachoo, R., Kim, Y. T., and Iqbal, S. M., *Electrical fingerprinting, 3D profiling and detection of tumor cells 649 with solid-state micropores*. Lab on Chip, 2012. **12**: pp. 2345–2352.
- [16] Ohnishi, Y., Watanabe, M., Yasui, H., and Kakudo, K., *Effects of epidermal growth factor on the invasive activity and cytoskeleton of oral squamous cell carcinoma cell lines*. Oncology Letters, 2014. **7**(5): pp.1439-42.
- [17] Holecek, M., Kochova, P., and Tonar, Z., *Mechanical Properties of Living Cells and Tissues Related to Thermodynamics, Experiments and Quantitative Morphology – A Review in Theoretical Biomechanics*. Intech 2011. pp.1-26.

- [18] Benitez, R., and Toca-Herrera, J. L., *Looking at cell mechanics with atomic force microscopy: Experiment and theory*. Microscopy Research and Technique, 2014. **77**: pp. 947-958.
- [19] De la Rica, R., Thompson, S., Baldi, A., Fernandez-Sanchez, C., Drain, C. M., and Matsui, H., *Label-free cancer cell detection with impedimetric transducers*. Analytical Chemistry, 2009. **81**(24): pp. 10167-71.
- [20] Dehoux, T., et al., *Probing single-cell mechanics with picosecond ultrasonics*. Ultrasonics, 2014. **56**: pp.160-71.
- [21] Kuznetsova, T. G., Starodubtseva, M. N., Yegorenkov, N. I., Chizhik, S. A., and Zhdanov, R. I., *Atomic force microscopy probing of cell elasticity*. Micron, 2007, **38**(8): pp. 824-33.
- [22] Li, Q. S., Lee, G., Ong, C. N., Lim, C. T., *AFM indentation study of breast cancer cells*. Biochemical and Biophysical Research Communications, 2008. **374**(4): pp. 609-13.
- [23] Lekka, M., Laidler, P., Gil, D., Lekki, J., Stachura, Z., Hryniewicz, A., *Elasticity of normal and cancerous human bladder cells studied by scanning force microscopy*. European Biophysics Journal with Biophysics Letters, 1999. **28**(4): pp. 312-6.
- [24] Ward, K. A., Li, W. I., Zimmer, S., Davis, T., *Viscoelastic properties of transformed cells: role in tumor cell progression and metastasis formation*. Biorheology, 1991. **28**(3-4): pp. 301-13.
- [25] Guo, Y., Sun, G., Zhang, L., Tang, Y., Luo, J., and Yang, P., *Multifunctional optical probe based on gold nanorods for detection and identification of cancer cells*. Sensors and Actuators B-Chemical, 2014. **91**: pp. 741-9.
- [26] Lukinavicius, G., et al., *Fluorogenic probes for live-cell imaging of the cytoskeleton*. Nature Methods, 2014. **11**(7): pp. 731-3.
- [27] Katira, P., Bonnacaze, R. T., and Zaman, M. H., *Modeling the Mechanics of Cancer: Effect of Changes in Cellular and Extra-Cellular Mechanical Properties*. Frontier in Oncology, 2013. **3**: pp. 145.

CHAPTER 2

DIFFERENTIATING METASTATIC AND NON-METASTATIC TUMOR CELLS FROM THEIR TRANSLOCATION PROFILE THROUGH SOLID-STATE MICROPORES

Reprinted (adapted) with permission from (Ali, W., Ilyas, A., Bui, L., Sayles, B., Hur, Y., Kim, Y. T., and Iqbal, S. M. *Differentiating Metastatic and Non-metastatic Tumor Cells from their Translocation Profile through Solid-state Micropores*. Langmuir, 2016. Just Accepted Manuscript, DOI: 10.1021/acs.langmuir.6b00016).

Copyright (2016) American Chemical Society.

Differentiating Metastatic and Non-metastatic Tumor Cells from their Translocation Profile through Solid-state Micropores

Waqas Ali^{1,2,3}, Azhar Ilyas^{1,2,3}, Loan Bui⁴, Bailey Sayles⁴, Yeun Hur⁴, Young-Tae Kim⁴
and Samir M. Iqbal^{1,2,3,4,5,*}

¹Nano-Bio Lab, ²Department of Electrical Engineering, ³Nanotechnology Research Center, ⁴Department of Bioengineering, University of Texas at Arlington, Arlington, Texas 76019. ⁵Department of Urology, University of Texas Southwestern Medical Center at Dallas, Dallas, Texas 75235.

*Contact Author:
Samir M. Iqbal, Ph.D.
Associate Professor,
UT Arlington.
500 S. Cooper St #217
Arlington, TX 76019
Email: SMIQBAL@uta.edu
Ph: 817-272-0228
Fax: 817-272-7458

Abstract

Cancer treatment, care and outcomes are much more effective if started at early stages of the disease. The presence of malignant cancer cells in human samples such as blood or biopsied tissue can be used to reduce over-treatment, under-diagnosis as well as for prognosis monitoring. Reliable quantification of metastatic tumor cells (MTCs) and non-metastatic tumor cells (NMTCs) from human samples can help in cancer staging as well. We report a simple, fast and reliable approach to identify and quantify metastatic and non-metastatic cancer cells from whole biological samples in a point-of-care manner. The metastatic (MDA MB-231) and non-metastatic (MCF7) breast cancer cells were pushed through solid-state micropore made in 200 nm thin SiO₂ membrane while measuring current across the micropore. The cells generated very distinctive translocation profiles. The translocation differences stemmed from their peculiar mechanophysical properties. The detection efficiency of the device for each type of tumor cells was ~75%. Metastatic cells showed faster translocation (36%) and 34% less pore blockage as compared to non-metastatic tumor cells. The micropore approach is simple, exact and quantitative for metastatic cell detection in a lab-on-a chip setting, without the need for any pre-processing of the sample.

Keywords: Solid-state micropores; Metastasis; Cell Mechanics; Early cancer treatment; Breast cancer; Cancer prognosis; Tumor staging.

Introduction

Metastatic tumor cells (MTCs) and non-metastatic tumor cells (NMTCs) are both cancer derivatives of normal cells, but there are significant differences between the two^{1,2}. These are different in their mechanophysical behavior, in their cytoskeleton structure and the way they operate in human body³⁻⁷. At the early stages of cancer, only NMTCs are dominant in a lesion but with time these cells start transforming into MTCs^{3,8}. As the disease matures, the number of MTCs surpasses the number of NMTCs. Hence the advanced stages of cancer are marked by the abundant number of MTCs^{1,9}. At any time, during the course of the disease, exact quantification of MTCs and NMTCs present in a human body can give a precise measure for cancer stage and can indicate the maturity level of the disease.

It is important to determine the stage and monitor the progress for suitable therapy for all diseases. For cancer, this is of utmost importance. At early stages, many cancer types are dormant and curable. On the other hand, at the advanced stages, the disease is easily detectable but the chances of complete recovery are drastically reduced^{2,5}. For instance, in the case of breast cancer, 5-year relative survival rate after breast cancer diagnosis and treatment is 93-100% for stage 0-2, but it significantly decreases to 22% for stage 4. Similarly, in the case of lung cancer, 5-year relative survival rate is 31% for stage 1, but it drops to 2% at stage 4. Therefore, it is very important to reliably and precisely detect any type of cancer in early stages (stage 1-2)¹⁰. MTCs are much more dangerous and pose a greater health risk than NMTCs. These cells are the primary cause of 90% of the deaths of breast cancer patients^{11,12}. Determining the exact ratio of MTCs and NMTCs present in cancer patients can be vital

in prescribing the right cancer treatment. Though it is advantageous to quantify these two types of tumor cells from entire biological samples, at the same time, it is very challenging because there is no suitable technique to completely discriminate these cells in a point-of-care manner. All the existing methods to investigate cell properties require labor intensive pre-processing of the biological samples¹³. For example, magnetic twisting cytometry, atomic force microscopy and micropipette aspiration have been shown to mechanically probe the cell surface, whereas microplate stretcher and laser/optical tweezers approaches do the same but optically¹³⁻¹⁸. All these assays require labor intensive sample preparation, and none of these can claim assessment of every cell in the biological sample^{14,17,19}. In a recent development engineered microbes have also been used to detect metastasis in liver²⁰. It required oral delivery of the engineered probiotic to the patient followed by the analysis of patient's urine sample. Bacterial diagnostic techniques like this are still in their infancy and there are several challenges like selective trafficking of programmable probiotic and interaction of bacterial species etc. that must be addressed before the clinical trial can be made possible. We report a simple and efficient electrical detection approach to distinguish MTCs and NMTCs directly from the blood/tissue sample based on their translocation profile through a solid-state micropore. A single micropore device is a resistive pulse sensor that works on the principle of a coulter counter, in which any particle while translocating through the micropore causes a physical blockage which shows as a dip in the ionic current²¹. The travel of different species with different shapes, physical, mechanical and chemical properties through the solid-state micropores causes unique electrical pulses in the ionic current²²⁻²⁵. Previously, a similar device was used to detect

circulating tumor cells (CTCs) from the whole blood of a cancer patient²⁶. That was primarily a size based detection scheme. Adamo et al. used a microfluidic device to relate the translocation time of cells through narrow constrictions with the cell stiffness and found that stiffer cells took longer to pass through when compared to less stiff ones, through same diameter constriction²⁷. They used Foster Shawn theory and an analogy with Coulter principle to infer that the cell diameter can be determined by measuring the cell travel time through the constriction until a certain threshold. When the cell size increases that threshold value (i.e. when constriction is filled by the cell) the cell travel time becomes independent of cell size. At this point device becomes more sensitive to cell deformability²⁷. Though there is not too much difference between the cells' size as well as the size of the nuclei for MTCs and NMTCs, as shown in Figure 1, it has been reported that the two types of tumor cells differ significantly from each other in behavior and other cell properties^{2,5,28}. NMTCs exhibit cell qualities similar to normal cells, whereas MTCs are more robust, dynamic, elastically deformable and flexible^{2,16,28,29}. Due to these differences, both types of cells give characteristic electrical signals while translocating through a micropore. NMTCs pass through the micropore slowly and cause much more ionic charge blockage whereas MTCs translocate much faster and exhibit less micropore blockage as indicated by their shorter dwell times and smaller peak amplitudes of the current pulses. This method provides a convenient and inexpensive way of differentiating MTCs and NMTCs in a lab-on-a-chip setting. It can be very useful for proper diagnosis of cancer and for prescribing the right treatment by detecting the maturity level of the disease. This method is free from preprocessing

requirements and does not need any particle/bead attachment, surface functionalization, or fluorescent tagging.

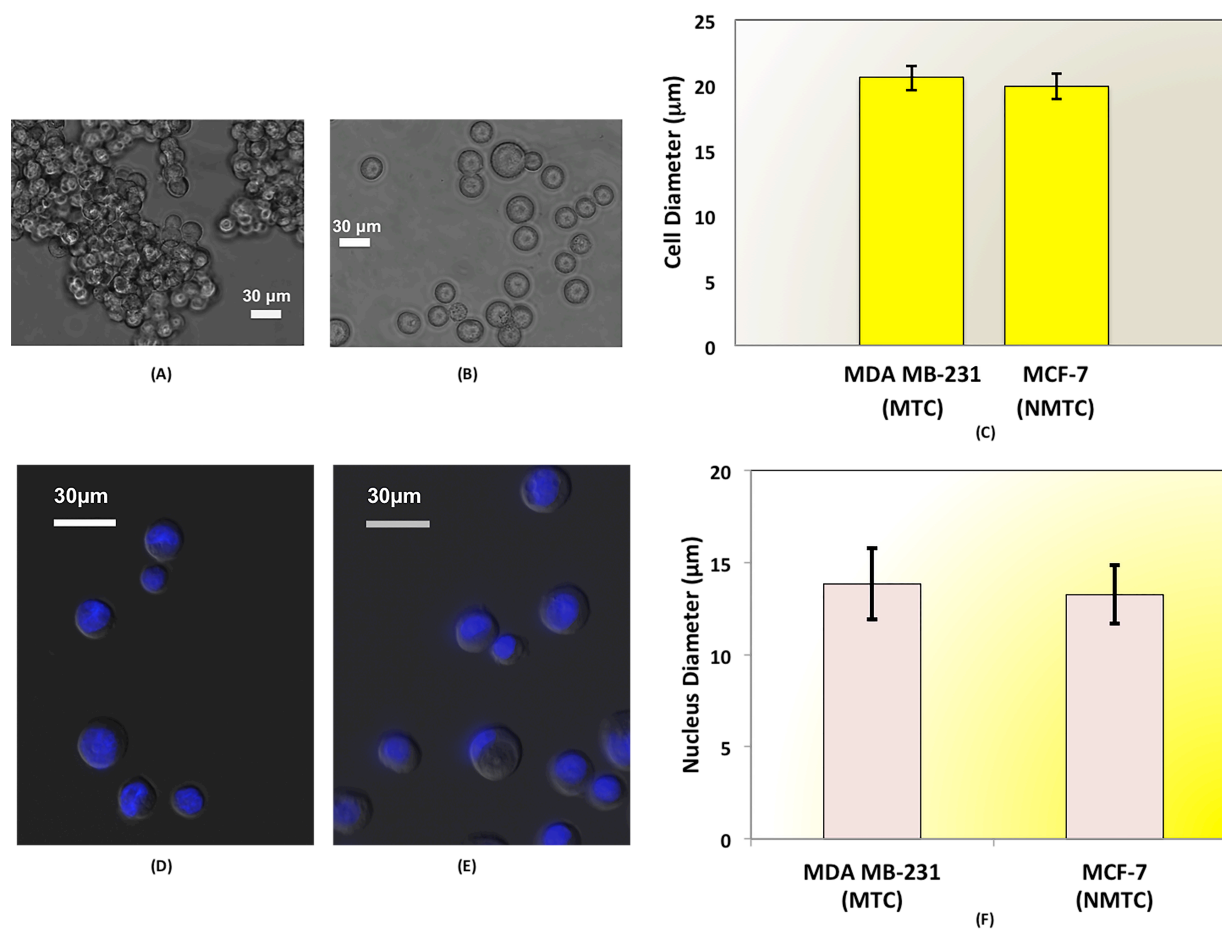


Fig. 1. Cell and nucleus size comparison of the suspended (A) NMTCs (MCF7) and (B) MTCs (MDA MB-231). The cell diameter was measured from the optical images of cells (N=30) of each tumor type and average cell size was calculated. (C) The average cell size of MTCs and NMTCs was found to be very close. Average \pm S.D. Suspended MDA MB-231 and MCF-7 were stained for nuclei by incubating with Hoechst 33342 (Invitrogen) for 15 minutes at 37°C. The fluorescence images of MTCs and NMTCs are shown in (D) and (E) respectively. The nucleus diameter was measured based on the fluorescence images using Image J, and quantitative analysis (N=30 per cell line) provided the average and standard deviation of the nucleus size shown in (F).

Experimental Section

All chemicals were obtained from Sigma-Aldrich unless otherwise noted. All processes and methods were as per the approved institution policies.

Tumor Cell Interrogating Micropores

The micropores were fabricated with standard CMOS processing technology. A 4-inch double-side polished Si wafer of thickness 500 μm and orientation (100) was first oxidized to grow a thin silicon dioxide layer of 200 nm. The wafer was cleaned with Piranha solution ($\text{H}_2\text{SO}_4:\text{H}_2\text{O}_2$, 1:1) and spin-coated with positive photoresist (PR) (Shipley S1813) on one side. After spin-coating the wafer was exposed to a UV source to pattern square etch windows on the spin-coated PR. The wafer was then dipped in developer solution (MF319) for a few seconds to remove the exposed PR. This step left patterned square windows in PR through which the bare silicon dioxide was etched (Fig. 2). During this process, the other side of the oxidized wafer was kept masked with PR layer. The wafer was immersed in buffered hydrofluoric acid (BHF) to etch away the exposed silicon dioxide through the patterned PR window. At this point, the whole PR pattern was transferred to the underlying layer of oxide. After thorough rinsing with deionized (DI) water, the wafer was washed thoroughly with acetone to remove PR from both sides.

The wafer was immersed in 25% tetramethylammonium hydroxide (TMAH) at 90 $^\circ\text{C}$ to anisotropically etch silicon. TMAH etches silicon at a rate of $\sim 1 \mu\text{m}/\text{min}$ ³⁰. After around 8 hours, all of the silicon was etched away from the exposed area and etching ultimately stopped after reaching the oxide layer on the other side of the wafer. The

whole wafer was then cut into $5 \times 5 \text{ mm}^2$ chips. Each chip had a membrane of silicon dioxide. Each chip was then drilled with Focused Ion Beam (FIB) to make micropores of $20 \text{ }\mu\text{m}$ diameter. Diameters of drilled micropores can be controlled from $1\text{-}50 \text{ }\mu\text{m}$ by adjusting exposure time, beam current and acceleration voltage^{24,25}. The micropores for this work were drilled using acceleration voltage of 30 kV and beam current of 1 nA . The complete drilling occurred in 300 sec for 200 nm thin oxide membranes. After drilling, each chip was annealed by exposing to very high temperatures for a few seconds to release mechanical stresses of the oxide membrane (Fig. 2B)²⁵.

Measurement Setup & Data Analysis

The overall device assembly ensured that all paths for cell translocation were aligned and no solution leakage occurred. The micropore chip was sandwiched between two PDMS gaskets and these gaskets were further sandwiched between two Teflon blocks (Fig. 2). PDMS gaskets properly sealed the micropore chip. The gaskets and both blocks had 1 mm holes and the assembly was done in a way that the holes in the gaskets and blocks remained in alignment with the membrane in the chip. Both of the Teflon blocks had independent reservoirs that were connected to each other only through the micropore. One reservoir was the inlet and the other was the outlet, and both were filled with 0.85% (*w/v*) NaCl solution. Phosphate buffered saline (PBS) is a better medium for ensuring cell morphology, which was very crucial for these experiments. However NaCl was used because the electrical signals were less noisy and conductivity change due to pore blockage was more prominent. The downside was that one must run the experiments within 1 hour of suspending the cells in NaCl

otherwise the cell activity would degrade and the cells might die or lose their characteristics, causing them to become undistinguishable.

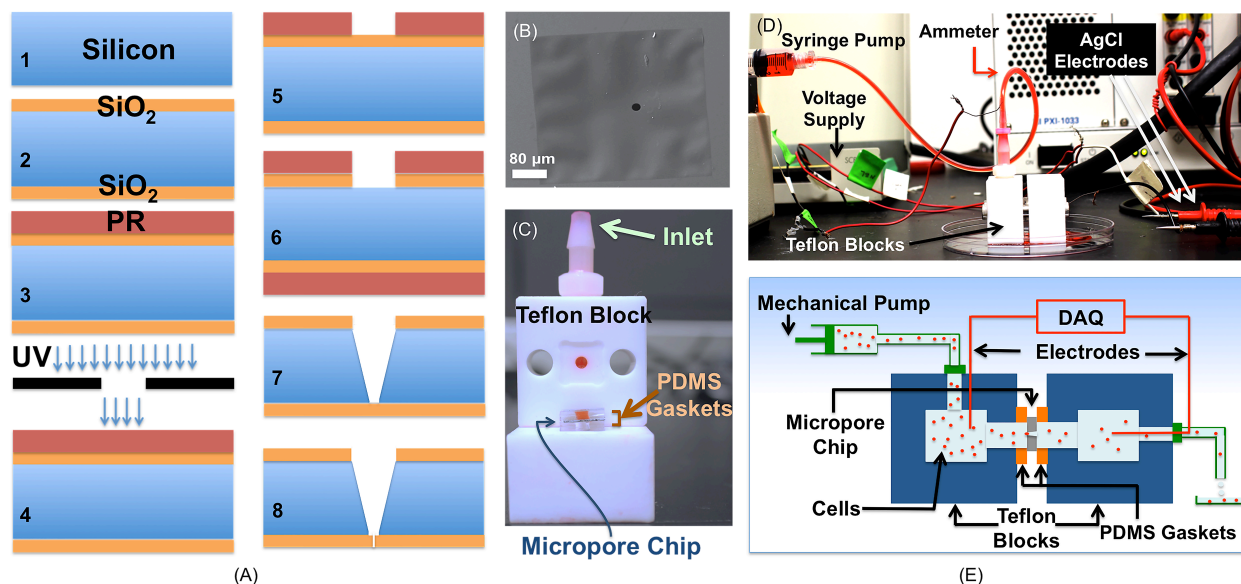


Fig. 2. Device fabrication, assembly and cancer cell measurement setup. (A) Fabrication of silicon dioxide membranes using UV-lithography followed by oxide and silicon etching in BHF and TMAH respectively. The free-standing membrane of silicon dioxide is drilled with FIB to fabricate the micropores of 20 μm diameter. (B) SEM micrograph of a drilled micropore in the silicon dioxide membrane is shown in inset. (C) Micropore chip is sandwiched between two PDMS gaskets and held between two Teflon blocks. Each Teflon block has a reservoir, one is the inlet as shown and the other one is the outlet. (D) The micropore device is connected in series with the voltage supply and ammeter through Ag/AgCl electrodes. The Ag/AgCl electrodes are used to apply 5V constant voltage and to measure the flow of ionic current through the micropore. (E) Micropore system schematic.

To apply voltage bias and to measure resulting current, Ag/AgCl electrodes were used. The electrodes were connected to the data acquisition cards (DAQ) and were dipped in each reservoir. DAQ block included a digital multimeter (NI PXI-1033 & NI PXI-4071) and a DC voltage supply (NI SCB-68A, NI PXIe-6361 & NI SHC68-68-EPM).

Cells were pushed into the inlet reservoir using a syringe pump (Harvard Apparatus).

Micropore conductivity is given by the relation, $G = \frac{\sigma\pi r^2}{L}$, where ' σ ' is the conductivity of NaCl solution, ' r ' is micropore radius and ' L ' is the channel length/membrane thickness²⁶. When cells passed through the micropore, these caused physical blockage of the micropore and reduced the effective radius that resulted in a decrease in conductivity. A LabView program was used to collect and store ionic current data which was further processed and analyzed with MATLAB scripts³¹. For statistical analysis, the average and the standard deviation were calculated and t -test was carried out.

Flow Rate and Sampling Frequency

Special care had to be taken in selecting the flow rate of cells and the sampling frequency for micropore measurements. A very high flow rate would increase the device throughput but would be prone to miss subtle differences in translocation events between MTCs and NMTCs, hence causing the device to lose selectivity. A low flow rate would increase the device selectivity as there would be pronounced differences between the pulses from two types of cells, but the device throughput will deteriorate. Also using a very high sampling frequency adds too much noise to the system, decreasing the device sensitivity, but can potentially give higher resolution. A very small sampling frequency would have less noise but it would result in missed translocation events, again reducing the sensitivity²⁶. Taking these trade-offs into consideration, experiments were performed at a flow rate of 1 ml/hour and sampling was done at 0.2 MHz.

Microchannel Device

The microchannels used in cell migration experiment had height and length of 5 μm and 530 μm , respectively. The microchannel widths decreased from 20 μm to 15, 10, 8, and finally became 5 μm just before the receiving reservoir (Figs. 3A and 3B).

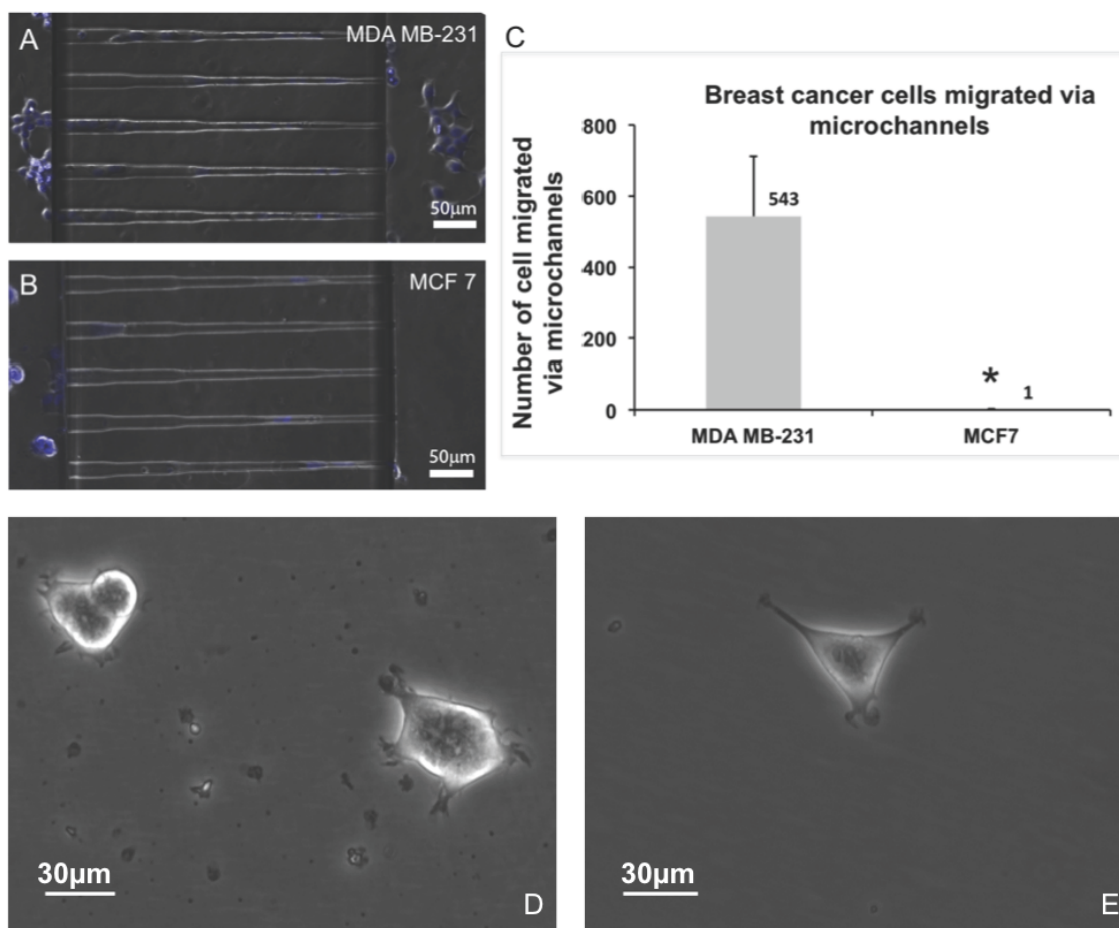


Fig. 3. Quantitative comparison of migration ability between (A) MTCs and (B) NMTCs. Representative micrographs show migration through the tapered microchannels. (C) Number of cells migrated from the seeding reservoir to the receiving reservoir via tapered microchannels; results are average \pm standard deviation (* $P < 0.01$). (D) MDA MB-231 cells growing on a cultured petri dish were first imaged prior to passing through the micropore device. (E) After passing through the micropore, MDA MB-231 cells were collected, re-cultured on a petri dish and then imaged after three hours. Comparison of the phenotype integrity was performed based on the morphology of the cells before and three hours after passing through the micropore device.

All devices were coated with collagen type 1 in advance. Dulbecco's modified eagle's medium/F-12 medium with 10% fetal bovine serum (FBS) was used and renewed as necessary during cell culture.

The devices were incubated at 37 °C and in 5% CO₂ environment. The cells were allowed to migrate via microchannels for 96 hours. After 96 hours, the cells were fixed with 4% paraformaldehyde in 1X PBS and stained with DAPI. The cells that had migrated from the microchannels into the receiving reservoirs were then counted with a fluorescent microscope. For statistical analysis, the average and the standard deviation were calculated and *t*-test was carried out.

Cell Culture

MDA MB-231 and MCF7 breast cancer cell lines and human fibroblast cell lines were obtained from the University of Texas Southwestern Medical Center (Dallas, TX). These cells were cultured in Dulbecco's modified Eagle's medium (DMEM/F-12, Cellgro, Corning) with 10% heat inactivated fetal bovine serum. Gentamycin and L-glutamine (Invitrogen) were also added to the cell culture medium. HUVEC were purchased from Lonza and cultured in Medium 200 (Life Technologies) supplemented with low serum growth supplement (LSGS, Life Technologies). The cells were cultured under sterile, humidified, 95% air, 5% CO₂ and 37 °C environment.

Results

Cell Detection Efficiency

The experiments were repeated multiple times for both NMTCs and MTCs with known concentrations. Each peak in the data represented one cell. The number of peaks were used to calculate the detection efficiency of the device as follows.

$$\text{Cell Detection Efficiency } (\eta) = \frac{\text{No. of Cells Detected}}{\text{Total No. of Cells}} \times 100 \% \quad (1)$$

The efficiency was always more than ~75% for both cell types. Cell detection efficiency is strongly dependent on cell flow rate and sampling frequency and changing any of these from their optimized value severely deteriorated the peak capture rate and hence the efficiency.

Electrical Signatures of MTCs and NMTCs

Separate solutions were prepared for each tumor cell type by suspending 10,000 cells of each in 10 ml NaCl solution. Each mixture was processed for 15-20 minutes through a 20 μm micropore (Fig. 2B) one after the other, and data was recorded at the optimized settings. Both types of cells caused significant current blockage while translocating through the micropore and a pulse was registered for almost each cell without any missed events. The experiments were repeated thrice and every time more than 75% cells were detected from the acquired pulses.

Analysis of the acquired data revealed that the distinguishing traits between the electrical pulses from the two tumor cells were the pulse width and pulse peak amplitude (Fig. 4). Pulse width depicted the cell dwell time in the micropore.

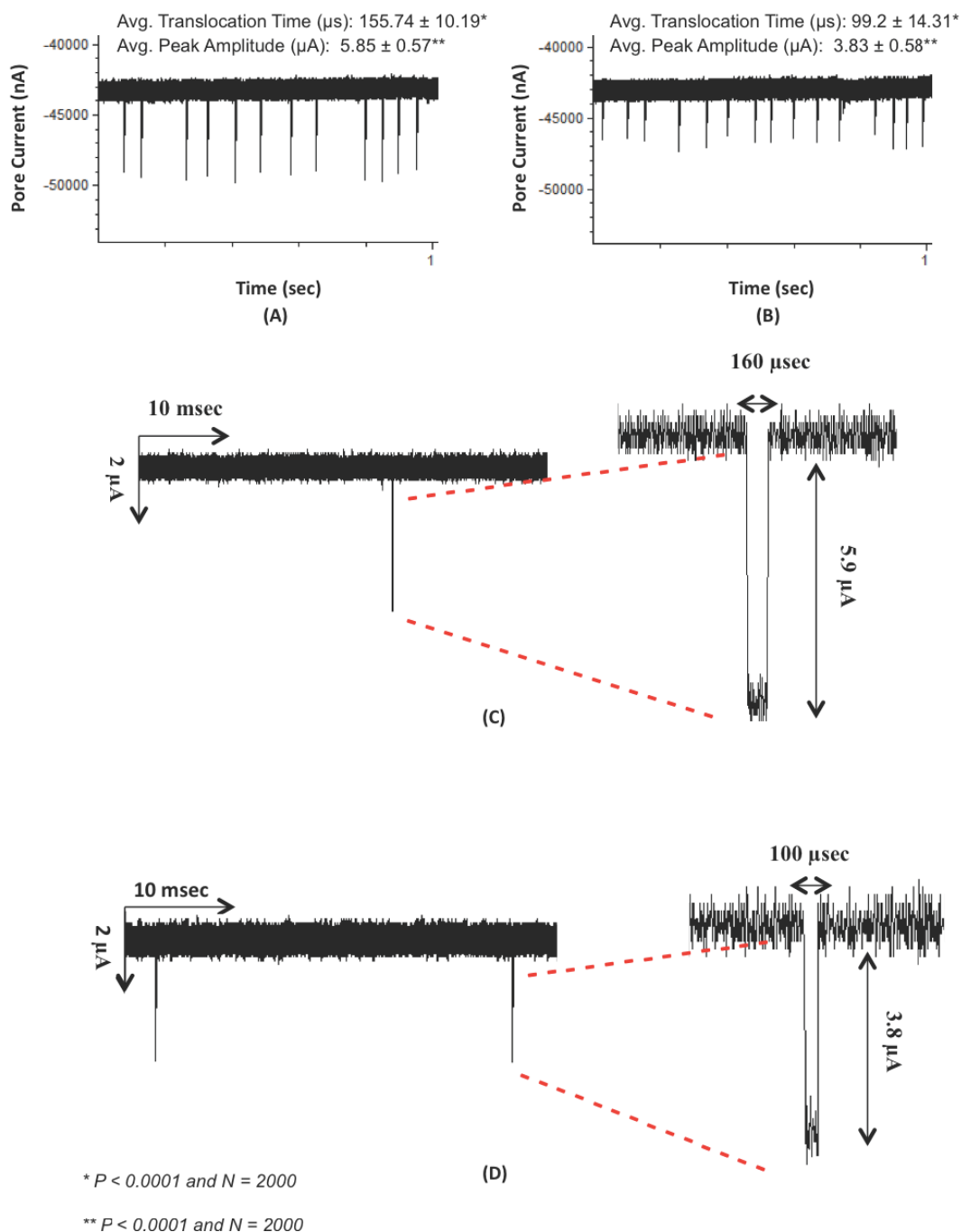


Fig. 4. Temporal trace of ionic current showing pulses from the translocations of (A) NMTCs only, and (B) MTCs only. (C) & (D) shows the ionic current profile of a representative pulse for NMTCs translocation and MTCs translocation respectively. The characteristic pulse for NMTCs is wider and deeper i.e. higher translocation time (~ 160 μ sec) and higher peak amplitude (~ 5.9 μ A) whereas the characteristic pulse for MTCs is thinner (translocation time ~ 100 μ sec) and shallow (peak amplitude ~ 3.8 μ A).

It was observed that the electrical pulses registered by NMTC translocations were significantly wider and deeper in contrast to those obtained from MTC translocations. NMTCs registered pulses had average peak amplitude of 5.85 μA (S.D. 0.57) and average pulse width of 155.74 μs (S.D. 10.19). On the contrary, the average peak amplitude and average width of the pulses obtained from MTCs translocation was 3.83 μA (S.D. 0.58) and 99.2 μs (S.D. 14.31), respectively (Fig. 4). The 34% difference in peak amplitude and 36% difference in widths of the pulses were sufficient enough to uniquely identify these two tumor cell populations from their respective pulses.

Statistical data analysis was done by performing the *t*-test (unpaired). First, the test was conducted to check how significantly different were the registered pulses of NMTCs and MTCs in terms of their translocation times. The two populations (N=2000) were found to be significantly different ($p < 0.0001$). Similar test was conducted to check the discrimination efficiency of the registered pulses of NMTCs and MTCs in terms of their peak amplitude and again the two populations (N=2000) were found to be significantly different with $p < 0.0001$.

Reliability of Electrical Signatures from Micropore Device

The translocation profile was found to be steady throughout the measurements without any cell blockage. Figure 5 shows the comparison of electrical signal profiles for two cell types at three different time points (1, 10 and 30 minutes) of the recorded data. These results clearly demonstrated that the unique electrical signature of each cell reliably remained the same during entire analysis period.

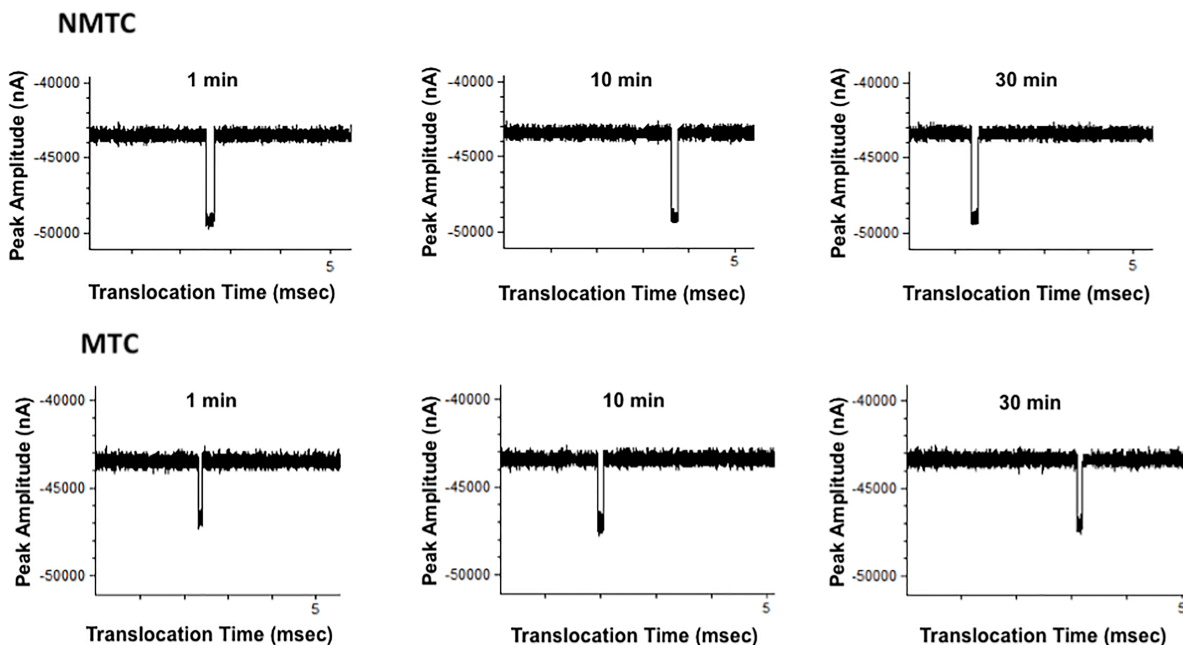


Fig. 5. The translocation profile for both tumor cells is stable throughout the experiments. The current signals at 1, 10 and 30 minutes after initial cell detection for each cell type are at same baseline indicating the reliable operation of the device.

Quantitative Cellular Discrimination from a Mixture of NMTCs and MTCs

The count of MTCs is expected to be too few at the outset of metastasis. For a true application, this framework has to be able to distinguish relatively small concentration of MTCs from NMTCs. It has been reported that on average as few as 5 CTCs are found in 7.5 ml blood sample of breast cancer patients³². It is still a question of debate as to how many of these would go through mesenchymal–epithelial transition and extravasate and start a new tumor. In nude mice, as fewer as 100 tumor cells have been shown to start new tumors³³. To this end, mixtures of NMTCs and MTCs with known concentrations of each cell type were processed with the micropore device. Both tumor cells were suspended in 10 ml NaCl solution at two different relative concentrations (MTCs:NMTCs in 1:1 and 1:10). The solutions were mixed thoroughly to

make homogenous mixtures and were processed with the micropore device at a flow rate of 1 ml/hour. The pulse counts for separate suspensions and the two mixtures are shown in Figure 6. The representative sample of 1 second for mixed suspension of equal concentrations of MTCs and NMTCs (1:1) shows 4 pulses for MTCs and 7 pulses for NMTCs (Fig. 6A) whereas the representative sample for mixed suspension of unequal concentrations of MTCs and NMTCs (1:10) shows 1 pulse for MTCs and 10 pulses for NMTCs in 1 second time duration (Fig. 6B).

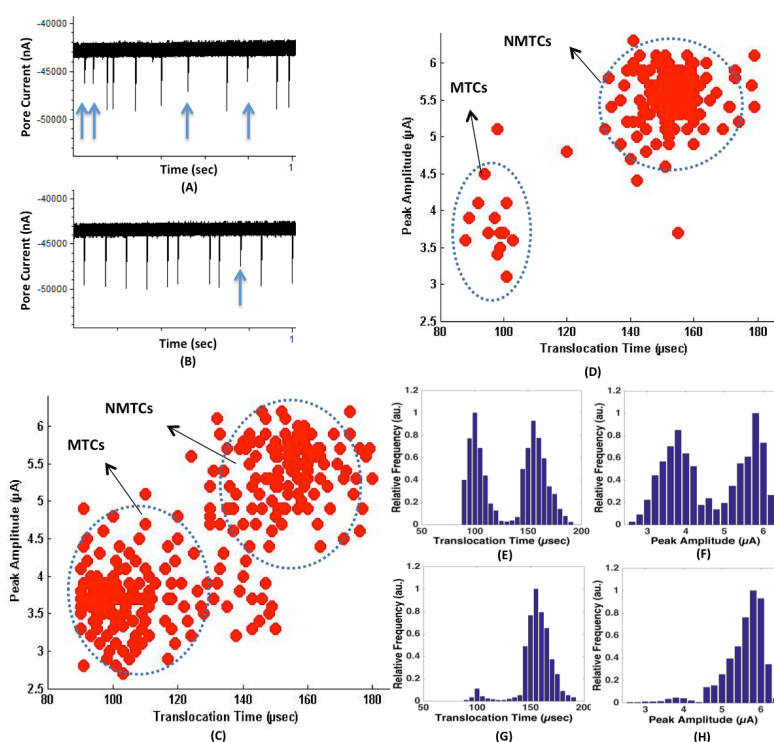


Fig. 6. Temporal trace of the ionic current showing pulses from the translocations of MTCs and NMTCs in (A) 1:1 ratio (Mixture 1) and (B) 1:10 ratio (Mixture 2). Arrow indicates MTCs. (C) & (D) shows the data density scatter plot of pulse attributes from mixed cell suspensions of MTCs:NMTCs in 1:1 ratio and 1:10 ratio respectively. In both (C) & (D) population of MTCs and NMTCs obtained from pulse attributes is inline with the actual ratio of MTCs and NMTCs in the mixed suspension. The distribution plots of translocation time and peak amplitude for mixture 1 and mixture 2 are shown in (E), (F), (G) and (H) respectively. From the distribution plots, it can be seen that the variables (Translocation Time and Peak Amplitudes) are normally distributed.

The detection efficiency for each cell type was again more than 75% and pulses were clearly distinguishable. Further analysis of the electrical pulses also indicated the presence of equal concentrations of both types of tumor cells for 1:1 mixture. The second mixture contained 10,000 NMTCs and 1,000 MTCs (10:1). Again, the detection efficiency for each cell type was more than 75% and the statistical analysis of the pulses revealed the presence of NMTCs and MTCs in ~10:1 ratio. The density plots, shown in Figure 6, indicate these results more clearly.

Statistical analysis was done by conducting the *t*-test. In Figure 6C, it can be seen that there are two populations. The one closer to origin is of MTCs as these have shorter translocation times and peak amplitudes and the one far from origin is of NMTCs due to their longer translocation times and higher peak amplitudes. The *t*-test analysis revealed that the two populations were statistically different with respect to translocation times ($p < 0.0001$) as well as in peak amplitudes ($p < 0.0001$). Further, it can be seen from the plot that the two distinct populations have almost same population density, which indicates the presence of equal number of NMTCs and MTCs in the mixture. In Figure 6D, there are two distinct populations. The population close to the origin has much lower density as compared to the other one indicating presence of fewer MTCs than NMTCs (1:10). The *t*-test analysis revealed that the two populations were significantly different with respect to translocation times ($p < 0.0001$) as well as peak amplitudes ($p < 0.0001$). These results indicate that precise quantification of NMTCs and MTCs can be done in a mixture. All the experiments were done in triplicate. The data shown here is representative of the trends of other runs.

Detection Limit

To determine the limit of detection of the micropore device, a series of translocation experiments were conducted. For these experiments, three mixtures of MTCs and NMTCs were prepared in 10 ml NaCl solution each. The cell count of NMTCs was kept fixed at 10,000 cells for all the three mixtures whereas the cell count for MTCs was gradually reduced. First mixture had 400 MTCs, second had 200 and the third mixture contained only 100 MTCs. The temporal traces of the ionic current and the scatter plots for mixture 1, 2 and 3 are shown in Figures 7A, 7B, 7C, 7D, 7E and 7F, respectively. In 1 hour, 1 ml solution translocated through the micropore for each mixture and MTCs were detected reliably for each mixture. To check the discrimination efficiency of the two populations i.e. one from NMTCs and one from MTCs, in terms of their respective translocation times and peak amplitudes, the t-test was conducted. The test results for the three mixtures are shown in Table 1.

Table 1: *t*-test analysis results to discriminate MTCs and NMTCs population in a limited range

	<i>t</i> -test statistics to discriminate NMTCs and MTCs populations with respect to the Translocation Time			<i>t</i> -test statistics to discriminate NMTCs and MTCs populations with respect to the Peak Amplitude		
	df	t-value	p-value	df	t-value	p-value
Mixture 1 $N_1 = 400$ & $N_2 = 27$	424	41.49	<0.0001	424	28.91	<0.0001
Mixture 2 $N_1 = 400$ & $N_2 = 14$	410	30.25	<0.0001	410	21.51	<0.0001
Mixture 3 $N_1 = 400$ & $N_2 = 9$	406	25.55	<0.0001	406	16.28	<0.0001

N_1 = Sample size for NMTCs, N_2 = Sample size for MTCs

From the test results it was inferred that the micropore device could easily detect MTCs even if these were as low as 10 cells/ml. It is also possible to detect even a lower concentration of MTCs than 10 cells/ml through this micropore device but then we would need to make sure that no cells cluster together in the suspension. This would require the addition of a chemical agent in the mixture that would break the EpCAM and hence reduce the chances of cell agglomeration. This limit of detection is very much in line with the real samples MTCs as few as 100 are known to develop tumors in immunocompromised host mice³³.

Cellular Discrimination from An Impure Sample

In the actual patient samples, there are many other cells than just MTCs and NMTCs. White blood cells (WBCs), red blood cells (RBCs), endothelial cells and fibroblasts are few of these. Since it has already been established that tumor cells can be differentiated from the WBCs and RBCs through the micropore device²⁶, it was more important to make sure that cells like endothelial and fibroblasts did not interfere with the detection of MTCs and NMTCs through the micropore device. To check the viability of this device for processing of actual patient samples, a mixture of human umbilical vein endothelial cells (HUVEC), human fibroblasts, MTCs and NMTCs was prepared by mixing 5000 cells of endothelial cells and fibroblasts each and 2000 cells of MTCs and NMTCs each, in 10 ml NaCl solution. The mixture was processed through the micropore for 1 hour. A representative sample of the registered pulses is shown in figure 7G and the scatter plot of the registered events is shown in Figure 7H.

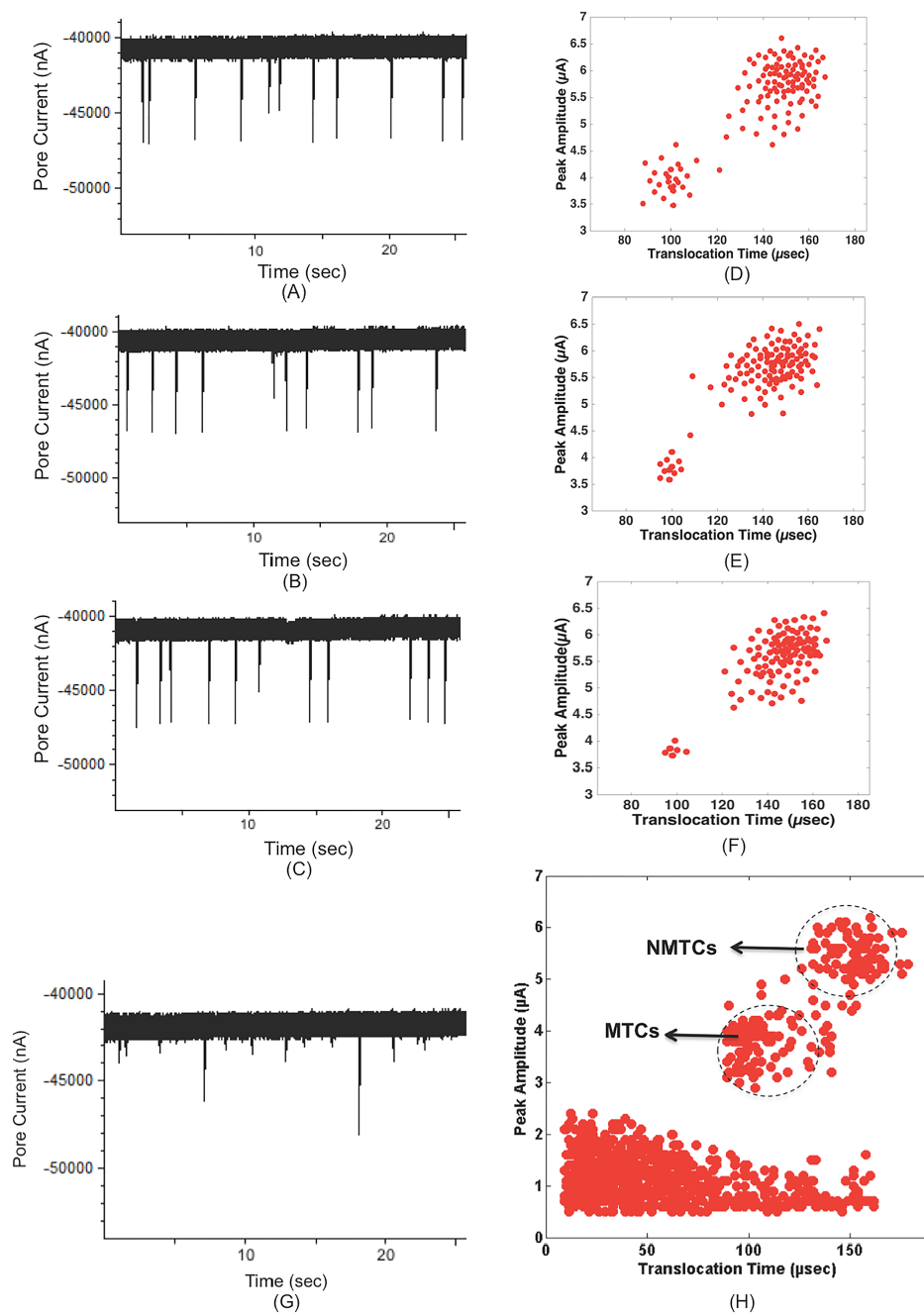


Fig. 7. Temporal trace of the ionic current showing pulses from the translocation of three mixtures (10 ml each) containing fixed number of NMTC's (10,000 cells) and MTCs (A) 400 cells (1:25) (B) 200 cells (1:50) and (C) 100 cells (1:100) and their corresponding scatter plots (D), (E) and (F) respectively. (G) and (H) shows the temporal trace of the ionic current and scatter plot for the mixture of 5000 cells of endothelial cells and stromal fibroblasts each and 2000 cells of NMTC's and MTC's each.

Quantitatively, there are no direct ways to compare number of rare subpopulations within tumors that may form secondary tumors but a thousand of breast tumorigenic cells have been known to form tumors when injected into the mammary fat pad of SCID mice³³.

The sizes of endothelial cells and fibroblasts are around 13 μm and 10-15 μm , respectively³⁴⁻³⁷. The translocation of these cells through a 20 μm micropore caused pulses that were very different from those of MTCs and NMTCs. The translocation time of the pulses registered due to the translocation of endothelial cells and fibroblasts ranged from around 15 μsec up to 150 μsec but majority of the population was centered around 40 μsec . The peak amplitude of the pulses was in the range of 0.7-2 μA . It can be clearly seen from Figure 7H that MTCs and NMTCs can still be detected from the sample and can be differentiated from each other without any problem since the pulses associated with MTCs and NMTCs are significantly different than those of endothelial cells and stromal fibroblasts.

Breast Cancer Cell Migration through Tightly Confined Microchannels

To further investigate the mechanical differences between two cell types, and to see whether the translocation difference was indeed due to the difference in mechanical natures of the two cell types, cell migration was also observed through tightly confined microchannels. The MTCs and NMTCs were separately seeded (10,000 cells/device, n=18 devices/each cell type) in a microchannel device as described elsewhere³⁸. The device design had two reservoirs, one to seed the cells and another to receive them through tapered microchannels.

MTCs had an average of 542.3 ± 168.8 cells that completely migrated to the receiving reservoir in contrast to an average of 1.22 ± 1.66 NMTCs (Figure 3). This clearly showed that MTCs had the ability to quickly move through tightly confined microchannels like micropores whereas NMTCs were challenged by the spatial confinement.

Discussion

Elastic deformability differences between non-metastatic breast cancer cells and metastatic breast cancer cells were exploited to electrically differentiate NMTCs and MTCs with the use of micropores. Since the syringe pump pushed the sample from the inlet towards the outlet at a stable rate of 1 ml/hour, both MTCs and NMTCs were forced to pass through the micropore, the size of which was deliberately kept smaller than both types of tumor cells. The reason is that, to investigate the elastic deformability as discriminating factor between two types of tumor cells, they should deform to pass through the micropore that is only possible when the micropore size is smaller than the tumor cell size. Table 2 shows the calculated values of shear rate, shear stress and velocity of cells inside and in the vicinity of the micropore and for comparison these values for blood inside the arteries and veins of a human body have also been noted here³⁹. For calculations, the liquid medium (NaCl) was assumed to be a Newtonian fluid. Inside the micropore, the values are orders of magnitude higher than that of arteries and veins as well as micropore vicinity that is primarily because of the size difference between arteries ($d \sim 4$ mm), veins ($d \sim 5$ mm) and micropore ($d \sim 20$ μ m). Shear stress and shear rate are strong function of the size of the flow path. A very high value of shear rate inside the micropore implies that very high degree of deformability is induced

in cells while translocating through the micropore which is an indication that the translocation profile is a true reflection of the deformability properties of the cells.

Cell deformability is directly linked to the elasticity of the cells. Staunton et al. have reported a four-fold elasticity difference between the cellular deformability of metastatic cells and their non-metastatic counterparts¹. Byun et al. also demonstrated the nexus between deformability of cells and their metastatic potential⁴⁰. They reported the reduced friction of cancer cells as another factor for their enhanced metastatic potential and demonstrated that cell entrance velocity into a narrow constriction is an indicator of its deformability whereas cell transit velocity tells whether the cell offers reduced friction or not while travelling through a narrow constriction. Metastatic cells are known to be more elastically deformable and softer, and these are capable of exerting increased force^{28,41-43}. While translocating through the micropore, both NMTCs and MTCs deformed to adjust to the size of the micropore. A lower translocation time for MTCs as compared to NMTCs stands to the reason. Since MTCs are known to depict higher elastic deformability and are more pliable than the NMTCs they took lesser time to deform and adjust according to the micropore size. On the other hand, NMTCs took comparatively longer time to deform due to their lower elasticity and hence hindered the ionic flow through the micropore for a longer time yielding a higher translocation time. More time a cell takes to deform and adjust to the size of micropore, longer it will hinder the ionic flow through the micropore and ultimately will result in a higher translocation time and vice versa. So the cell translocation time is an indirect measure of the cell elasticity. Due to higher cell elasticity, MTCs spent less time in the micropore because these could squeeze through more easily than NMTCs, which were rigid. The two cell

types are known to have different elastic moduli (341 ± 41 Pa for MDA MB-231 MTC and 425 ± 31 Pa for MCF-7 NMTC)⁴⁴ as well as drastically different levels of strain energy when measured in an elastic matrix (~ 0.8 pJ for MTCs vs. ~ 0.4 pJ for NMTC)⁴⁵. The two tumor cell types are also known to have different properties of motility. Metastatic cells are capable to travel farther and in a spontaneous manner whereas non-metastatic cells are inclined to move in a non-linear manner^{4,28,29}. The fact that the nuclei are much more stiffer and viscous than the surrounding cytoplasm, the nuclei are also possibly contributing to the resulting differences in the behavior⁴⁶. These known cell traits of MTCs and NMTCs are also inline to our experimental observations and support our findings.

It is also important that experimental conditions don't affect the phenotype of the cells so that post-processing and standard cytometry can be done later on. In this regard, one might think that very high values of shear rate and velocity of fluid inside the micropore may jeopardize the phenotype of translocating cells, rendering them useless for post-processing. Luckily this is not the case and such a high velocity and shear rate in the micropore did not affect the cell microenvironment and the cells stayed in their native state. Comparison of the phenotype integrity was performed based on the morphology of the cells before and 3 hours after passing through the micropore device (Fig. 3D & 3E). MDA MB-231 cells growing on a cultured Petri dish were first imaged prior to passing through the micropore device. Then after passing through the micropore, MDA MB-231 cells were collected, re-cultured on a Petri dish and then imaged again after three hours. As can be seen in Figure 3E, the cells did not show any change in their morphology. The rapid transaction through the micropore made the cell

boundary squeeze only for so small a time that the internal rearrangement was for a very short transient. For the rest of the time, when cells were not inside the micropore, these experienced shear rate and velocity very close to what these would experience in arteries and veins of the human body (Table 2). These cells thus did not undergo any change in their phenotype and can be used for post-processing and standard cytometry. Post-processing can tell us a lot about new genes and cellular pathways that have been involved in the metastasis.

Table 2: Comparison of shear rate, shear stress and velocity of fluid inside and just outside the micropore with that for blood in arteries and veins³⁹

	Arteries	Veins	Micropore	Micropore Vicinity
Shear Rate (sec⁻¹)	900	160	3.53 x 10 ⁸	353
Shear Stress (dyn/cm²)	4-30	1-4	3.53 x 10 ⁶	3.53
Velocity (m/sec)	0.45	0.1	882	0.088

Micropore devices have been used as a filter in the past for size based detection of cells and their 3D profiling²⁶ but in this work we have demonstrated its use as an electromechanical transducer. Our micropore device works as a transducer that probes the mechanophysical properties of the translocating cells and generates electrical pulses based on those properties. These pulses can be analyzed then for cell differentiation and quantification. This whole process i.e. from the time when patient samples are collected till the analysis is completed using this device, takes not more than 1-2 hours and that too without the aid of specialized equipment and well-trained staff or physician. All that needed to get the timely results is a micropore device and the accompanying data acquisition and analysis setup that can be used for patient's

diagnoses in an ambulance, in the physician's office, home or in a hospital. The presented scheme is not limited to breast cancer but is also suitable for differentiating any types of cells which differ in their biomechanical properties like stiffness, viscosity, elastic deformability, shape, etc. This approach has the potential to empower physicians to make timely decisions at the "point-of-care" and will help fight cancer in a better way. It can also be very useful in cancer therapy monitoring as cancer therapists almost always need to stage the cancer to determine outcomes and prognosis. Presence of more MTCs would indicate an advanced cancer stage. This device can conveniently be used to get these results quickly and reliably in a lab-on-a chip setting.

References

- (1) David A. *et al.* A Physical Sciences Network Characterization of Non-Tumorigenic and Metastatic Cells. *Sci. Rep.* **2013**, 3, 1449.
- (2) Chaffer, C. L.; Weinberg, R. A. A Perspective on Cancer Cell Metastasis. *Science* **2011**, 331, 1559-1564.
- (3) Chambers, A. F.; Groom, A. C.; MacDonald, I. C. Dissemination and growth of cancer cells in metastatic sites. *Nat. Rev. Can.* **2002**, 2, 563-572.
- (4) Ward, K. A.; Li, W. I.; Zimmer, S.; Davis, T. Viscoelastic properties of transformed cells: role in tumor cell progression and metastasis formation. *Biorheology* **1991**, 28, 301-313.
- (5) Sahai, E. Illuminating the metastatic process. *Nat. Rev. Can.* **2007**, 7, 737-749.
- (6) Suresh, S. Biomechanics and biophysics of cancer cells. *Acta Mat.* **2007**, 55, 3989-4014.
- (7) Chakraborty, J.; Von Stein, G. A. Pleomorphism of human prostatic cancer cells (DU 145) in culture--the role of cytoskeleton. *Exp. and Mol. Pat.* **1986**, 44, 235-245.
- (8) Gao, Y.; Xie, J.; Chen, H.; Gu, S.; Zhao, R.; Shao, J.; Jia, L. Nanotechnology-based intelligent drug design for cancer metastasis treatment. *Biotech. Adv.* **2013**.
- (9) Yoshioka, S. *et al.* [The efficacy of early diagnosis of brain metastasis and systemic treatment after radiotherapy in patients with metastatic breast cancer]. *Gan To Kagaku Ryoho. Cancer & Chemo.* **2013**, 40, 2381-2383.
- (10) Jemal, A.; Siegel, R.; Ward, E.; Hao, Y.; Xu, J.; Murray, T.; Thun, M. J. Cancer statistics, 2008. *CA: A Can. J for Cli.* **2008**, 58, 71-96.
- (11) Olivia, J.S.; Boon-Huat, B.; George, Y.; Yingnan, Y. Breast Cancer Metastasis. *Can. Gen. & Pro.* **2012**, 9, 311-320.
- (12) Marino, N.; Woditschka, S.; Reed, L. T.; Nakayama, J.; Mayer, M.; Wetzel, M.; Steeg, P. S. Breast cancer metastasis: issues for the personalization of its prevention and treatment. *The Ame. J of Pat.* **2013**, 183, 1084-1095.
- (13) Kuttel, C.; Nascimento, E.; Demierre, N.; Silva, T.; Braschler, T.; Renaud, P.; Oliva, A. G. Label-free detection of babesia bovis infected red blood cells using impedance spectroscopy on a microfabricated flow cytometer. *Acta Tro.* **2007**, 102, 63-68.
- (14) Binnig, G.; Quate, C. F.; Gerber, C. Atomic force microscope. *Phy. Rev. Let.* **1986**, 56, 930-933.
- (15) Hessler, J. A.; Budor, A.; Putschakayala, K.; Mecke, A.; Rieger, D.; Banaszak Holl, M. M.; Orr, B. G.; Bielinska, A.; Beals, J.; Baker, J., Jr. Atomic force microscopy study of early morphological changes during apoptosis. *Langmuir : The ACS J of Sur. and Col.* **2005**, 21, 9280-9286.
- (16) Sleep, J.; Wilson, D.; Simmons, R.; Gratzer, W. Elasticity of the red cell membrane and its relation to hemolytic disorders: an optical tweezers study. *Biophy. J* **1999**, 77, 3085-3095.
- (17) Evans, E. A. New membrane concept applied to the analysis of fluid shear- and micropipette-deformed red blood cells. *Biophy. J* **1973**, 13, 941-954.

- (18) Mills, J. P.; Qie, L.; Dao, M.; Lim, C. T.; Suresh, S. Nonlinear elastic and viscoelastic deformation of the human red blood cell with optical tweezers. *Mech. & Che. of Biosys. : MCB* **2004**, 1, 169-180.
- (19) Dao, M.; Lim, C. T.; Suresh, S. Mechanics of the human red blood cell deformed by optical tweezers. *J of the Mech. and Phy. of Sol.* **2003**, 51, 2259-2280.
- (20) Danino, T.; Prindle, A.; Kwong, G. A.; Skalak, M.; Li, H.; Allen, K.; Hasty, J. & Bhatia, S. N. Programmable probiotics for detection of cancer in urine. *Sci Transl Med* **2015**, 7, 289.
- (21) Saleh, O. A.; Sohn, L. L. Quantitative sensing of nanoscale colloids using a microchip coulter counter. *Rev. Sci. Instrum.* **2001**, 72, 4449.
- (22) Ilyas, A.; Asghar, W.; Ahmed, S.; Lotan, Y.; Hsieh, J.-T.; Kim, Y.-t.; Iqbal, S. M. Electrophysiological analysis of biopsy samples using elasticity as an inherent cell marker for cancer detection. *Ana. Meth.* **2014**, 6, 7166-7174.
- (23) Venkatesan, B. M.; Bashir, R. Nanopore sensors for nucleic acid analysis. *Nat. Nano* **2011**, 6, 615-624.
- (24) Asghar, W.; Ilyas, A.; Deshmukh, R. R.; Sumitsawan, S.; Timmons, R. B.; Iqbal, S. M. Pulsed plasma polymerization for controlling shrinkage and surface composition of nanopores. *Nanotechnology* **2011**, 22, 285304.
- (25) Asghar, W.; Ilyas, A.; Billo, J. A.; Iqbal, S. M. Shrinking of solid-state nanopores by direct thermal heating. *Nanoscale Res. Let.* **2011**, 6, 372.
- (26) Asghar, W.; Wan, Y.; Ilyas, A.; Bachoo, R.; Kim, Y. T.; Iqbal, S. M. Electrical fingerprinting, 3D profiling and detection of tumor cells with solid-state micropores. *Lab on a Chip* **2012**, 12, 2345-2352.
- (27) Adamo, A.; Sharei, A.; Adamo, L.; Lee, B.; Mao, S. & Jensen, K. F. Microfluidics-based assessment of cell deformability. *Analytical chemistry* **2012**, 84, 6438-6443.
- (28) Swaminathan, V.; Mythreye, K.; O'Brien, E. T.; Berchuck, A.; Blobe, G. C.; Superfine, R. Mechanical stiffness grades metastatic potential in patient tumor cells and in cancer cell lines. *Can. Res.* **2011**, 71, 5075-5080.
- (29) Fraley, S. I.; Feng, Y.; Krishnamurthy, R.; Kim, D. H.; Celedon, A.; Longmore, G. D.; Wirtz, D. A distinctive role for focal adhesion proteins in three-dimensional cell motility. *Nat. Cell Bio.* **2010**, 12, 598-604.
- (30) Tabata, O.; Asahi, R.; Funabashi, H.; Shimaoka, K.; Sugiyama, S. Anisotropic etching of silicon in TMAH solutions. *Sen. and Act. A: Physical* **1992**, 34, 51-57.
- (31) Billo, J. A.; Asghar, W.; Iqbal, S. M. An implementation for The detction and analysis of negative peaks in an applied current signal across a silicon nanopore. *Proc. of SPIE* **2011**, 8031, 80312T-80312T-80317.
- (32) Cristofanilli, M. *et al.* Circulating tumor cells, disease progression, and survival in metastatic breast cancer. *The New Eng. J of Med.* **2004**, 351, 781-791.
- (33) Ponti, D.; Costa, A.; Zaffaroni, N.; Pratesi, G.; Petrangolini, G.; Coradini, D.; Pilotti, S.; Pierotti, M. A.; Daidone, M. G. Isolation and in vitro propagation of tumorigenic breast cancer cells with stem/progenitor cell properties. *Can. Res.* **2005**, 65, 5506-5511.
- (34) Garipcan, B.; Maenz, S.; Pham, T.; Settmacher, U.; Jandt, K. D.; Zanow, J.; Bossert, J. Image analysis of endothelial microstructure and endothelial cell

- dimensions of human arteries - a preliminary study. *Adv. Eng. Mat.* **2011**, 13, B54-B57.
- (35) Iwanaga, K.; Murata, T.; Hori, M.; Ozaki, H. Isolation and characterization of bovine intestinal subepithelial myofibroblasts. *J Pha. Sci.* **2010**, 112, 98-104.
- (36) Brouty-Boye, D.; Mainguene, C.; Magnien, V.; Israel, L.; Beaupain, R. Fibroblast-mediated differentiation in human breast carcinoma cells (MCF-7) grown as nodules in vitro. *Int J Can.* **1994**, 56, 731-735.
- (37) Kusahara, M.; Yamaguchi, K.; Nagasaki, K.; Hayashi, C.; Suzuki, A.; Hori, S.; Handa, S.; Nakamura, Y.; Abe, K. Production of endothelin in human cancer cell lines. *Can. Res.* **1990**, 50, 3257-3261.
- (38) Wan, Y.; Tamuly, D.; Allen, P. B.; Kim, Y. T.; Bachoo, R.; Ellington, A. D.; Iqbal, S. M. Proliferation and migration of tumor cells in tapered channels. *Biomed. Microdev.* **2013**, 15, 635-643.
- (39) Wirtz, D.; Konstantopoulos, K.; Searson, P. C. The physics of cancer: the role of physical interactions and mechanical forces in metastasis. *Nat. Rev. Can.* **2011**, 11, 512-522.
- (40) Byun, S. *et al.* Characterizing deformability and surface friction of cancer cells. *Proceedings of the National Academy of Sciences of the United States of America* **2013**, 110, 7580-7585.
- (41) Fuchs, E.; Weber, K. Intermediate filaments: structure, dynamics, function, and disease. *Ann. Rev. of Bioche.* **1994**, 63, 345-382.
- (42) Zhu, C.; Bao, G.; Wang, N. Cell mechanics: mechanical response, cell adhesion, and molecular deformation. *Ann. Rev. of Biomed. Eng.* **2000**, 2, 189-226.
- (43) Denis, W.; Konstantinos, K.; Peter, C. S. The physics of cancer: the role of physical interactions and mechanical forces in metastasis. *Nat. Rev. Can.* **2011**, 11, 512-522.
- (44) Jonas, O.; Mierke, C. T.; Kaes, J. A. Invasive cancer cell lines exhibit biomechanical properties that are distinct from their noninvasive counterparts. *Soft Matter* **2011**, 7, 11488-11495.
- (45) Koch, T. M.; Muenster, S.; Bonakdar, N.; Butler, J. P.; Fabry, B. 3D traction forces in cancer cell invasion. *PLOS ONE* **2012**, 7.
- (46) Lim, C. T.; Zhou, E. H.; Quek, S. T. Mechanical models for living cells--a review. *J of Biomech.* **2006**, 39, 195-216.

Acknowledgements

We thank M. U. Raza, M. Arif I. Mahmood, M. M. Bellah and M. Islam for their help and useful discussions during this work. We would also like to thank the staff at Nanotechnology Research Center at UTA for trainings at various stages and thank Dr. Robert Bachoo at UT Southwestern Medical center for providing us the breast cancer cells. The work was supported by the NSF grant ECCS-1201878 and CPRIT grant RP110041.

Competing Financial Interests

The authors have no financial interests to disclose.

CHAPTER 3

ELECTROMECHANICAL TRANSDUCER FOR RAPID DETECTION OF LUNG CANCER CELLS, CELLULAR DISCRIMINATION AND QUANTIFICATION

© IOP Publishing. Reproduced with permission. All rights reserved

Ali, W., Moghaddam, F. J., Raza, M. U., Bui, L., Sayles, B., Kim, Y. T., and Iqbal, S. M. *Electromechanical transducer for rapid detection, discrimination and quantification of lung cancer cells*. *Nanotechnology*, 2016. **27**(19): 195101.

Electromechanical Transducer for Rapid Detection of Lung Cancer Cells, Cellular Discrimination and Quantification

Waqas Ali^{1,2,3}, Fatemeh Jalvhei Moghaddam⁴, Muhammad Usman Raza^{1,2,3}, Loan Bui⁴,
Bailey Sayles⁴, Young-Tae Kim^{4,5} and Samir M. Iqbal^{1,2,3,4,5,*}

¹Nano-Bio Lab, ²Department of Electrical Engineering, ³Nanotechnology Research Center, ⁴Department of Bioengineering, University of Texas at Arlington, Arlington, Texas 76019, USA. ⁵Department of Urology, University of Texas Southwestern Medical Center at Dallas, Dallas, TX 75235, USA.

*Contact Author:
Samir M. Iqbal, Ph.D.
Associate Professor
Department of Electrical Engineering
University of Texas at Arlington
500 S. Cooper St #217
Arlington, TX 76019, USA
Email: SMIQBAL@uta.edu
Ph: +1-817-272-0228
Fax: +1-817-272-7458

Abstract

Tumor cells are malignant derivatives of normal cells. There are characteristic differences in the mechanophysical properties of normal and tumor cells, and these differences stem from the changes that occur in the cell cytoskeleton during cancer progression. There is need for viable whole blood processing techniques for rapid and reliable tumor cell detection without need for tagging. Micropore biosensors have been used earlier to differentiate tumor cells from the normal cells and we have used micropore based electromechanical transducer to differentiate one type of tumor cells from the other types. This device generated electrical signals, which were characteristic of the cell properties. Three non-small cell lung cancer (NSCLC) cell lines NCI-H1155, A549 and NCI-H460 were successfully differentiated. NCI-H1155, due to their comparatively smaller size, were found quickest in translocating through the micropore. Their translocation through a 15 μm micropore caused electrical pulses with average translocation time of 101 ± 9.4 μsec and average peak amplitude of 3.71 ± 0.42 μA whereas translocation of A549 and NCI-H460 caused pulses with average translocation time of 126 ± 17.9 μsec and 148 ± 13.7 μsec , respectively and average peak amplitude of 4.58 ± 0.61 μA and 5.27 ± 0.66 μA , respectively. This transformation of difference in cell properties into difference in electrical profile (i.e. difference in peak amplitude and translocation time) with this electromechanical transducer is a quantitative way to differentiate these lung cancer cells. The solid-state micropore device processed the whole biological samples without any pre-processing requirements and is ideal for point-of-care applications.

Keywords: Lung Cancer; Cell Cytoskeleton; Cell Mechanics; Electromechanical Transducer; Cancer Diagnosis; Point-of-care.

Introduction

The efficacy of cancer treatment largely depends on the extent of tumor spread [1, 2]. Detecting the tumor at early stages makes the treatment much easier and also elevates the chances of recovery [3-5]. There are various transformations that happen at molecular and cellular levels before cancer matures and appears at the tissue and organ levels [2, 3]. It has been reported that cytoskeletons of cells characteristically alter during cancer transformations [6-9]. Cell's cytoskeleton is a complex polymer network that defines the molecular architecture of cells and is involved in many cellular functions. It evolves during differentiation of cells [10, 11]. The mechanical properties and morphology of cells depend on the cytoskeleton, and thus, any change in cytoskeleton affects the mechanical properties of cells. The mechanical properties of individual living cells are closely related to the health and function of the human body [3, 6, 12]. Cancer inception and progression can be related to the changes in cell cytoskeleton. Continuous monitoring and tracking of cell cytoskeleton modifications can give a better insight into understanding of this disease and can make timely detection possible. During cancer progression, cytoskeleton transforms to a more compliant and irregular state from an ordered and rigid structure [7, 12, 13]. This restructuring of the cytoskeleton makes malignant cells more motile and pliable compared to normal cells and also helps them in replicating themselves quickly [14, 15]. Owing to these well known facts, cell elasticity, rigidity, size, shape irregularity and lower resistance to deformation (i.e. softness) have emerged as new biological cell markers to differentiate tumor cells from normal cells and also to distinguish one type of tumor cells from other tumor types (e.g. metastatic vs. non-metastatic) [15-17].

Previously micropipette aspiration (MA), microneedle probes, atomic force microscopy (AFM), microplate manipulation and optical tweezers etc. have been used to investigate cell mechanical properties [18-22]. Lekka et al. probed the mechanical properties of normal and cancerous cells with AFM and found an order of magnitude difference in the cell rigidity [14]. Ward et al. have reported 50% difference in elasticity of malignant and normal cells using MA. All these methods have their limitations [13, 23]. They all require labor-intensive pre-processing of the samples, specialized equipment and very well trained manpower to get the results. The results can't be obtained quickly. Probing the cell cytoskeleton directly requires fluorescent tagging [7]. There are no convenient methods to investigate mechanical properties of cells and to differentiate them on that basis. To address these challenges, we report an electromechanical transduction approach that is capable of transforming these mechanical properties of individual cells into electrical signals. The micropore transducer generates unique electrical pulses for each cell type based on the mechanical properties of individual cells. Distinct electrical pulses are obtained for cells with different physical and mechanical properties (elasticity, motility, shape, size, malignancy etc.). Where as similar electrical pulses are seen for cells with same properties.

Micropore electromechanical transducer is a resistive-pulse sensor. The ionic current through micropore changes as the cells pass through it under a mechanical force. Smaller and more elastic and motile cells can squeeze through micropore easily and quickly whereas cells with less elasticity, motility and larger size face more resistance to their passage and as a result these spend more time in the micropore and

are characterized by slow translocation. Narrow and shallower electrical pulses mark fast translocation, whereas slow translocation is registered by deeper and wider pulses.

About 85-90% of lung cancers are NSCLCs [24]. There are three subtypes of NSCLC cells that are squamous cell (epidermoid) carcinoma, adenocarcinoma and large cell (undifferentiated) carcinoma [24-26]. About 25-30% of all lung cancers are squamous cell carcinomas, 40% are adenocarcinomas and about 10-15% are large cell carcinoma [24]. The cells in these subtypes differ in size, shape, and chemical make-up when observed optically. Experiments with micropore translocation differentiated NSCLC cell lines A549, NCI-H460 and NCI-H1155. NCI-H1155 and NCI-H460 are large cell lung cancer subtypes and A549 is adenocarcinoma subtype of NSCLC [25]. The device successfully enumerated more than 75% cells for each cell type and generated unique electrical profiles for each of these based on their unique physic-mechanical properties.

Materials and Methods

Micropore Device Fabrication

The micropore membrane that is the backbone of the device is fabricated using MEMS fabrication techniques. A double side polished (DSP), silicon wafer of (100) crystallographic orientation is used to create the device. The DSP wafer is first cleaned in piranha solution ($\text{H}_2\text{SO}_4:\text{H}_2\text{O}_2::1:1$) and then oxidized in dry oxygen ambient in a three zone furnace at 1100 °C. Exposing the wafer to such an ambient yields a 1 micron thick oxide layer on both sides of the wafer. A reflectometer is used to determine the exact thickness of the oxide layer.

After this, the wafer is prepared for photolithography by first cleaning it in piranha solution for 10 minutes. Then the wafer is dried using dry nitrogen and dehydrated on a hot plate at 150 °C. Shipley 1813 positive photoresist (PR) is then spin coated on both sides of the DSP wafer. Then the wafer is processed under UV light with a dark field mask which transfers the pattern of the etch windows on to the wafer. Then MF319 developer is used to develop the transferred pattern. Buffered hydrofluoric acid (BHF) is used next to etch away the oxide and transfer the square window patterns in the oxide and reveal the bare silicon underneath. After this, acetone is used to remove the remaining resist from both sides of the wafer.

The wafer is then immersed in 25% tetramethylammonium hydroxide (TMAH) solution at 90 °C with steady stirring at 200 rpm. TMAH is an anisotropic etchant of silicon and etches with high selectivity into the (100) face of the silicon at etch rate of about 1 $\mu\text{m}/\text{min}$ [27]. As the wafer is 525 μm thick, it takes about 10 hours for the etching of the (100) layer to reach the backside and reveal the 1 μm thick silicon dioxide membranes on other side of the wafer. The fabrication steps are shown in detail in Fig 1.

The wafer is then cut into 5x5 mm^2 individual chips, each of which has a SiO_2 membrane. Each chip is then processed under a focused ion beam (FIB) to drill the freestanding SiO_2 membrane that creates a single micropore of about 15 μm in diameter in each chip. Acceleration voltage of 30 kV and beam current of 1 nA were used for 200 sec to fabricate the 15 μm diameter micropore. By varying the exposure time, beam current and acceleration voltage, micropores of 1-50 μm can be fabricated [17, 28-30]. After drilling, each chip was annealed at high temperature for a few seconds

to smoothen out the walls of the micropore and to relieve stresses in the oxide membranes that could crack these during experiments [28].

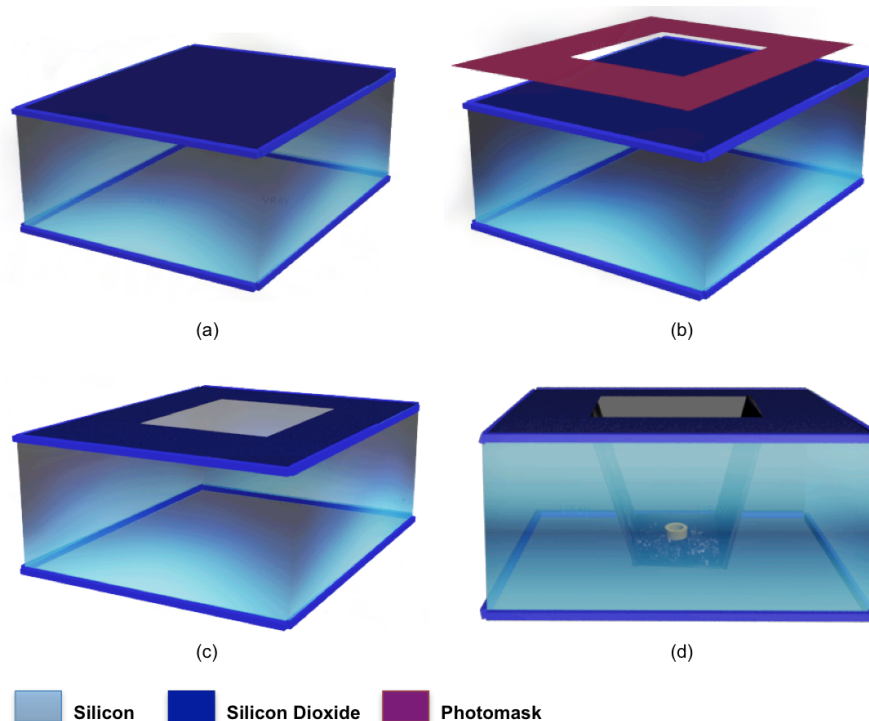


Fig. 1. Micropore device fabrication steps. A DSP silicon wafer is oxidized and one side of the wafer is patterned with optical photolithography to open square etch windows. Silicon is etched through these windows with TMAH to make thin suspended silicon dioxide membranes.

Measurement Setup

Micropore chip was sandwiched between PDMS gaskets, which were further sandwiched between two Teflon blocks. Teflon blocks contained the buffer solution (0.85% (w/v) NaCl). The assembly ensured that during the experiments, the only translocation path was through the micropore and the solution did not leak through or around the assembly. The PDMS gaskets and the Teflon blocks had 1 mm holes.

Micropore chip was placed inside the gaskets in such a way that all the holes of Teflon blocks and gaskets were aligned with the micropore membrane (Fig. 2).

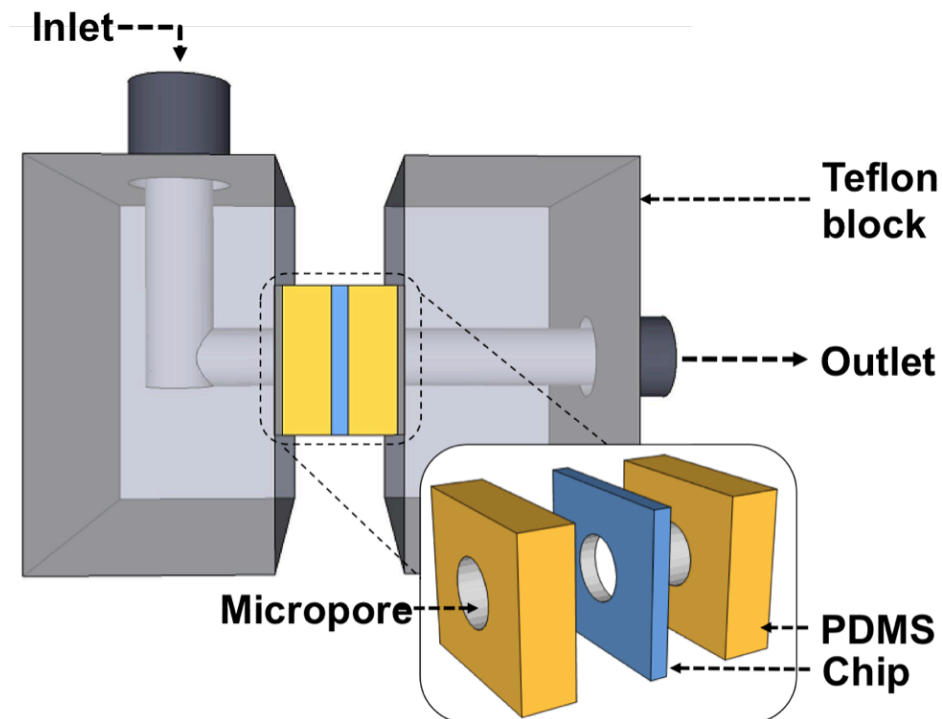


Fig. 2. Experiment setup for cancer cell discrimination. A 5x5 mm² micropore chip is sandwiched between PDMS gaskets, which are further sandwiched between two Teflon blocks. Teflon blocks contain the electrolyte solution and cells are inserted into one of the blocks (i.e. inlet) with a syringe pump.

Voltage bias and ionic current recordings were done through Ag/AgCl electrode pair. One electrode was dipped in each reservoir and these were connected to the data acquisition cards in a computer. After this, the cells were pumped into the inlet reservoir using a syringe pump. When a cell passed through the micropore, it physically blocked the micropore for a certain period of time leading to a change in conductivity of the micropore. This conductivity is measured by the relation, $G = \sigma\pi r^2/L$, where ' σ ' is the conductivity of NaCl solution, ' r ' is micropore radius and ' L ' is the channel

length/membrane thickness. When the cell physically blocked the micropore, its effective radius was reduced; leading to a reduction in the ionic current passing through the micropore. The data acquisition relayed the information to a LabView program that was used to collect and store the experimental data. Acquired data was analyzed with MATLAB routines [31].

Lung Cancer Cell Line Culture

Three NSCLC cell lines (A549, NCI-H460 and NCI-H1155) were obtained from the University of Texas Southwestern Medical Center at Dallas in Texas, USA. These cells were maintained as per standard approved protocols. The cells were cultured in RPMI-1640 Medium with 10% heat inactivated fetal bovine serum. Gentamycin and L-glutamine (Invitrogen) were also added to the cell culture medium. The cells were cultured under sterile, humidified, 95% air, 5% CO₂ and 37 °C environment.

Measurement of Lung Cancer Cell Diameter

Three lung cancer cell lines were dissociated with Trypsin-EDTA (0.05%) and seeded on a hemocytometer to measure the cell diameters. The dissociated cancer cells were imaged (n=30/cell line) and their diameters were measured by *ImageJ* software. For statistical analysis, the averages and the standard deviations were calculated and ANOVA was carried out.

Lung Cancer Cell Migration through Tightly Confined Microchannels

To investigate the mechanical and elastic differences among three different lung cancer cell types, cell migration via tightly confined microchannels was quantified. The

lung cancer cells were separately seeded (10,000 cells/device, $n=20$ /each cell type) in a microchannel device described before [32]. The microchannel device had two reservoirs, one to seed the cells and another to receive them through tapered microchannels. The microchannels were 5 μm high and 530 μm long. Their widths gradually decreased from 20 μm to 15, 10, 8, and finally became 5 μm just before the receiving reservoir (Figs. 3(c—e)).

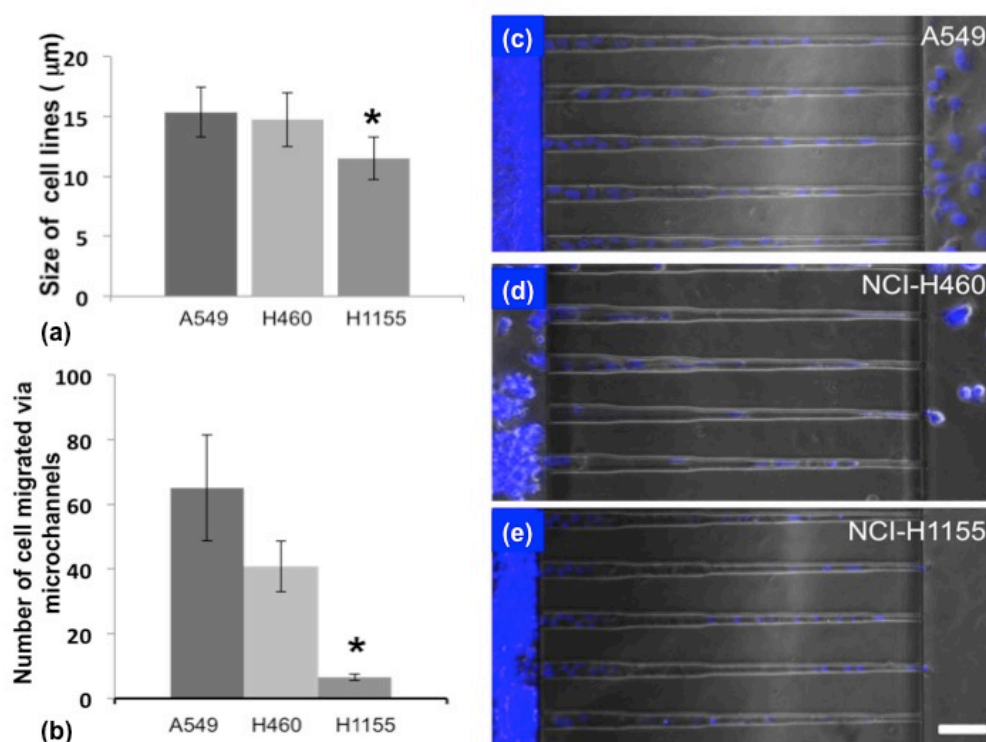


Fig. 3. Quantitative comparison of cell size and migration ability. (a) The cell diameter was measured from the optical images of cells ($n=30$) of each tumor type and average cell size was calculated. The average cell sizes of A549 and NCI-H460 were found to be very similar, whereas NCI-H1155 was found to be much smaller in size. Average \pm S.D. * $p < 0.01$ between NCI-H1155 and others. (b) Number of cells migrated from the seeding reservoir to the receiving reservoir via tapered microchannels. Average \pm S.E.M. * $p < 0.05$ between NCI-H1155 and others. $n = 20$ / each cell line. Representative micrographs of (c) A549, (d) NCI-H460 and (e) NCI-H1155 traveling through microchannels. Scale bar = 50 μm . Migration experiments were repeated three times.

All devices were coated with Collagen type 1 overnight at 37 °C. The microchannel devices were incubated at 37 °C and 5% CO₂, and the cells were allowed to migrate through microchannels for 7 days. After 7 days, the cells were fixed with 4% paraformaldehyde in 1X PBS and stained with DAPI. The cells that had migrated from the microchannels into the receiving reservoirs were then counted with a fluorescent microscope. For statistical analysis, the average and the standard deviation were calculated and *t*-test was carried out.

Results

Cell Detection Efficiency

For each lung cancer cell line, a sample with known concentration was translocated through the micropore chip. The process was repeated twice. Each cell registered one pulse when it translocated through. The efficiency of cell registration was calculated from the recorded pulses as:

$$\text{Cell Detection Efficiency } (\eta) = \frac{\text{No. of Single Cell Pulses Detected}}{\text{Total Number of Cells Introduced}} \times 100 \%$$

The detection efficiency for each cell type was more than ~75% for a flow rate of 1 ml/hour and 0.2 MHz sampling frequency. Cell detection efficiency is a strong function of the sampling frequency and cell flow rate. This combination of flow rate and sampling frequency was chosen after a series of experiments as this gave highest detection efficiency. Using very high flow rate deteriorated device selectivity. On the other hand, if the flow rate was too low or if the sampling frequency was too high or too small then the

device lost sensitivity [33]. Tradeoffs between device sensitivity, selectivity and throughput are essential to decide the flow rate and sampling frequency.

High detection efficiency is a much needed trait for this technology. At the initial stages of cancer, number of tumor cells are extremely low in the lesion [25, 34, 35]. If the device is not sensitive enough, detection efficiency will be low resulting in false negatives. The detection efficiency of 75% indicates that there were 25% cells that were either clumped together or too small for registration. Pulses with multiple spikes were from cell clumps and were discarded during the analysis. This caused reduction in cell detection efficiency. The device was thus sensitive enough to register all pulses for almost all the cells that translocated through the micropore. Cell clumping is also a property of metastatic cells. A single spike thus indicated the presence of a single cell inside the micropore and multiple spikes showed that there were multiple cells traversing the micropore simultaneously [17].

Roughly in ten experiments, at least one clogging event occurs. In our case, it required un-assembling the device and washing the micropore. Cell clumps have also been observed and these are one of the major causes of device' detection efficiency reduction. To get rid of both of these issues i.e. cell clustering and pore clogging, a chemical agents can be used to break the EpCAM. This would break clumps into single cells and would avoid any cell clustering as well as pore clogging but that will add a sample pre-processing requirement to the protocol. Even without adding this additional sample pre-processing requirement, we are getting ~75% cell detection efficiency and the pore clogging is not a very likely event and doesn't happen often enough to jeopardize the process.

Electrical Signatures of the Lung Cancer Cells

The cancer cells were suspended in NaCl buffer solution at concentration of 1000 cells/ml. Each vial was thoroughly shaken to suspend the cells homogeneously in the buffer. The three cell suspensions were then pumped through the micropore, one by one, with the aid of a syringe pump for 40-60 minutes. While translocating through the micropore, each type of cell caused significant blockage to the ionic current flow and that reduction in ionic current was recorded as dips in the baseline current of the micropore.

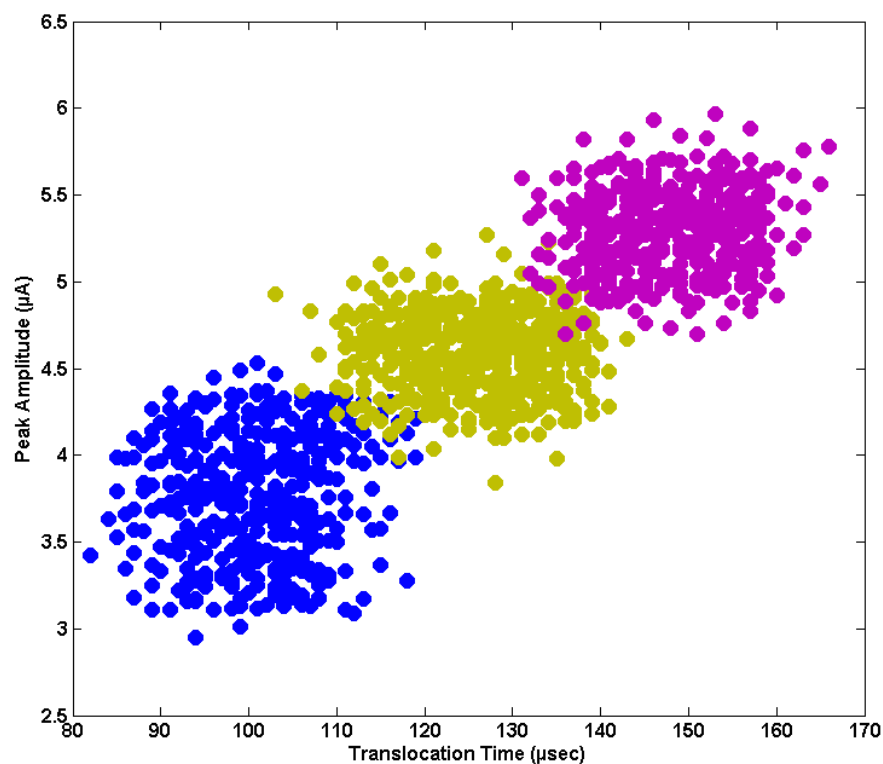


Fig. 4. Scatter plot for NCI-H1155, A549 and NCI-H460. Data points for all three NSCLC cell lines are plotted together for comparison. The density population for NCI-H1155, A549 and NCI-H460 is confined in separate regions indicating that the electrical pulses associated with them have different peak amplitude and pulse width characteristics.

After data acquisition for all three NSCLC cell lines, the recorded pulses were analyzed. First, the pulse statistics (pulse width and amplitude values) were extracted using a MATLAB routine and then statistical analysis of the data was done by ANOVA test. The test confirmed that there were three different populations of data. Each data cluster was associated with a particular cell type. These populations are plotted in Fig 4. Each cell type shows a unique cluster that is different from the cluster recorded by other two cell lines. The signature pulses of each cell type are shown in Fig 5.

The unique characteristics of the electrical pulses were their peak amplitude and the pulse width (Table 1). Pulses registered by NCI-H1155 had average peak amplitude of 3.71 μ A (S.D. 0.42) and average pulse width of 101 μ s (S.D. 9.4), for A549 the average peak amplitude was 4.58 μ A (S.D. 0.61) and average pulse width was 126 μ s (S.D. 17.9) and for NCI-H460 the average peak amplitude and the average pulse width were 5.27 μ A (S.D. 0.66) and 148 μ s (S.D. 13.7) respectively.

Table 1. Pulse statistics for NSCLC cells through micropore.

Cell Line	Average Translocation Time (μ sec)	Average Peak Amplitude (μ A)
NCI-H1155	101 \pm 9.4*	3.71 \pm 0.42**
A549	126 \pm 17.9*	4.58 \pm 0.61**
NCI-H460	148 \pm 13.7*	5.27 \pm 0.66**

* $P < 0.0001$ & $N = 1500$

** $P < 0.0001$ & $N = 1500$

Cell Quantification from a Mixed Lung Cancer Cell Suspension

After identifying the electronic signatures of each lung cancer cell type, two separate mixtures were prepared and processed through the micropore one by one. In the first mixture, 5000 cells of each cell type were suspended in 10 ml NaCl solution

(total 15000 cells). In the second mixture, different number of cells of each cell type were suspended in 10 ml NaCl.

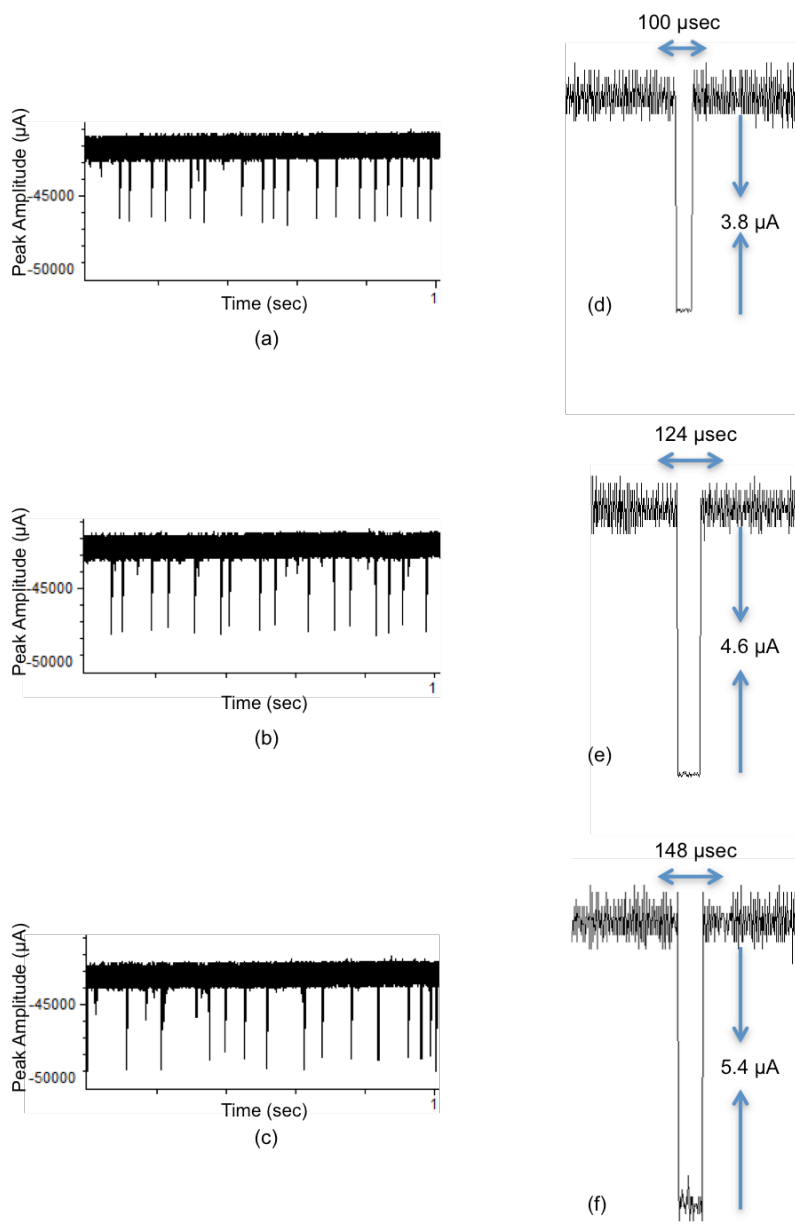


Fig. 5. Signature pulses of 3 cancer cell types. Ionic current through a 15 μm micropore showing representative pulses from the translocation of (a) NCI-H1155, (b) A549 and (c) NCI-H460 in a 1 second duration. Zoomed-in views of representative pulses for NCI-H1155, A549 and NCI-H460 are shown in (d), (e) and (f), respectively.

This mixture contained 1000 cells of NCI-H1155, 5000 cells of A549 and 10000 cells of NCI-H460. So the final mixture had total 16000 cells in 10 ml solution with NCI-H1155, A549 and NCI-H460 in 1:5:10 ratio. Each mixture was processed through a 15 μm micropore for 40-60 minutes. For each suspension, again, the cell detection efficiency was $> \sim 75\%$. The registered pulses associated with a particular cell line were counted to determine the number of cells of that cell line present in each mixture. The pulse count obtained from the acquired data was found to be in close match to the known numbers of the introduced cells in the suspension for each cell type. The registered pulses for mixture 1 (1:1:1) and 2 (1:5:10) are shown in Figures 6(a) and 6(b) respectively, for a period of 1 second. Three different types of pulses can be readily identified in these representative samples.

For mixed suspension of equal concentration of three lung cancer cell types, the representative sample of 1 second contained 8 pulses that had features of NCI-H1155 and 6 pulses each with the features of A549 and NCI-H460 (Fig. 6(a)). The similar representative sample for the mixed suspension of unequal concentrations (NCI-H1155:A549:NCI-H460:::1:5:10) shows 2 pulses with features of NCI-H1155. 6 pulses characteristics of A549 and 13 pulses of NCI-H460 features (Fig. 6(b)).

The scatter plots in Figure 6(c) and 6(d) show the density population of pulses obtained from the translocation of mixture 1 and mixture 2, respectively. In both plots, there are three distinct populations that indicate the presence of three different types of cells in each mixture. In the first scatter plot (Fig. 6(c)) three distinct populations have similar densities which confirms that the three types of cells present in the mixture have same concentration whereas the second scatter plot (Fig. 6(d)) shows that the

three types of cells present in the mixture are not in the same concentration, as expected.

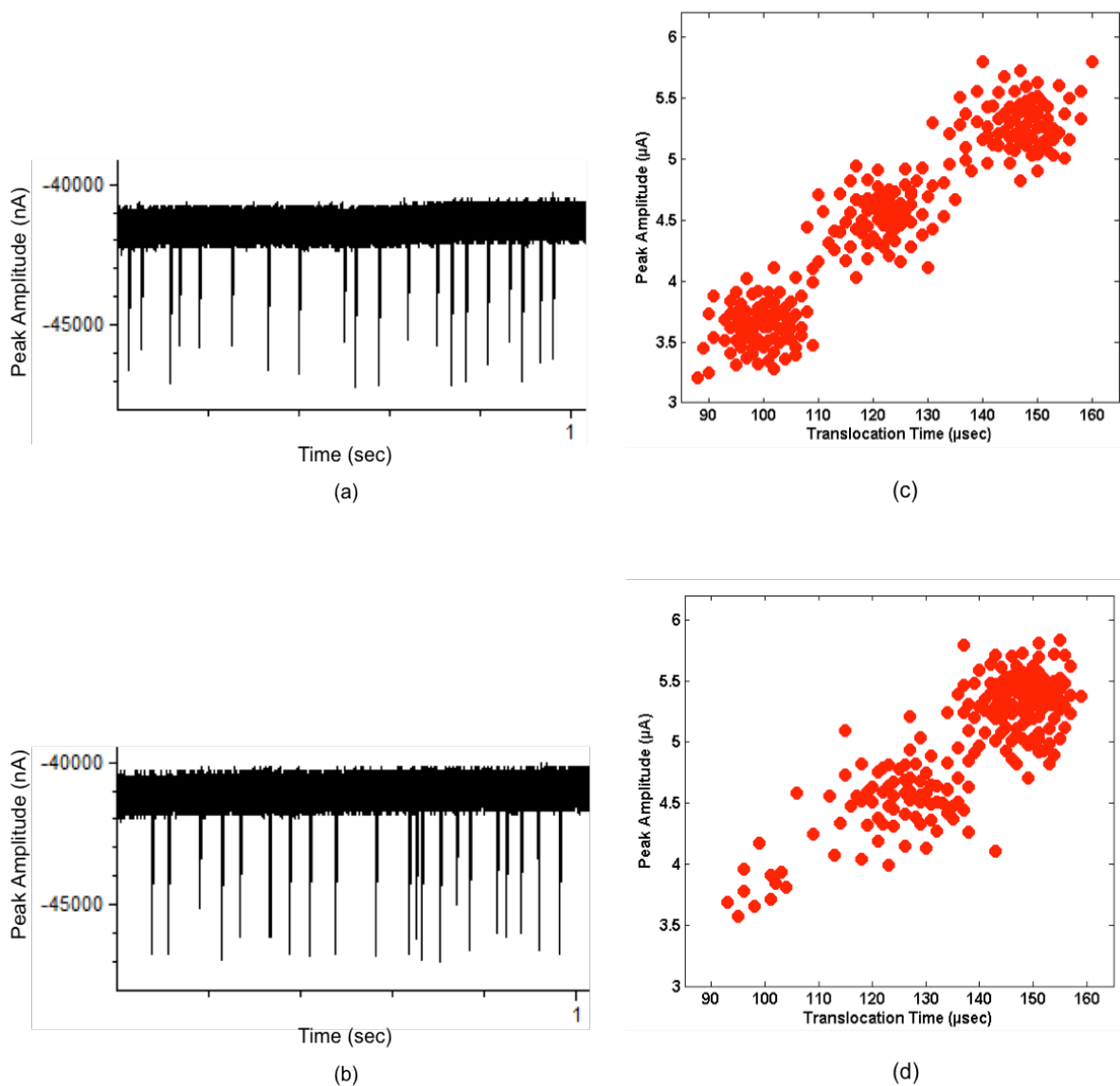


Fig. 6. Signature pulses and scatter plots of mixed suspension of three lung cancer cell lines. Ionic current through a 15 µm micropore showing pulses from the translocation of cell suspensions containing NCI-H1155, A549 and NCI-H460 at ratio of (a) 1:1:1 and (b) 1:5:10 for 1 second duration and their respective scatter plots in (c) & (d). The ratio of the number of pulses from each cell line closely represents the ratio of the number of cells present in each mixture.

These experiments clearly show that different types of NSCLC cells present in a sample were detected as well as quantified with this technology. This differentiation stemmed from their unique mechanophysical properties. The average cell diameters of A549 and NCI-H460 are about the same, whereas NCI-H1155 is significantly smaller than those two lung cancer cells (Fig. 3(a)).

To elucidate the elastic-deformability properties of these cells that transpired into translocation differences, another set of experiments was done with tapered microchannels. The microchannels provided gradually reducing constrictions to the migration of cells. Significantly higher numbers of A549 and NCI-H460 cells completely migrated to the receiving reservoir via the tightly confined microchannels as compared to NCI-H1155 (Fig. 3(b—e)). Higher numbers of A549 cells migrated via the microchannels as compared to NCI-H460 cells, but there was no statistical difference between them. All three cell lines migrated toward the opening of the microchannels ($20 \times 5 \mu\text{m}^2$), but NCI-H1155 cells could not migrate via the ending of the tapered microchannels ($5 \times 5 \mu\text{m}^2$), despite these were smaller in diameter.

Discussion

To differentiate one type of tumor cells from the other using micropore technology, it is necessary that both types of cells are different in their physical, mechanical and molecular properties. This difference is inherent in tumor cells since the cell cytoskeleton is affected during cancer and as a result the cell properties are modified [3, 7, 20, 36, 37]. Depending on the stage and type of cancer, the transformations are much more evident and ultimately the cell attributes are clearly

different. The micropore does electromechanical transduction with high sensitivity to these differences and hence quantifiably differentiates tumor cells. This can be thus used to determine the cancer stage and cancer type, which is very important in cancer diagnosis and treatment [5, 38].

The three subtypes of NSCLC are different from each other in their cell attributes [39, 40]. Even though A549 and NCI-H460 have almost same cell size as shown in Figure 4, but these differ in other cell characteristics like elasticity and flexibility. On the other hand, small sized NCI-H1155 cells faced much less steric hindrance from the micropore walls [33], and were able to translocate easily through the micropore. Between A549 and NCI-H460, the longer translocation time and higher peak amplitude of the pulses for the later indicates that it is less deformable and dynamic as compared to the former and this is exactly what we observed from cell migration behavior of both types of tumor cells through tapered microchannels (Fig 3). There were many more A549 cells that migrated from one side of the microchannel to the other side than for NCI-H460 cells. This directly supports the strength of micropore approach for cancer sensing ability. Among the three tumor cell types, NCI-H1155 cells were the fewer most that were able to migrate from one side of the tapered microchannel to the other. If we relate the fast translocation of NCI-H1155 from the micropore device to their cell migration behavior through tapered microchannel, at first they seem counter-intuitive. But, it is not contradicting because among the three cell types NCI-H1155 is smallest in size. Due to this, even though they are less dynamic and elastic, as seen in the tapered channel migration experiment, they were able to translocate through the micropore easily and quickly. So size is a dominant factor and a prime contributor to the

translocation profile through micropore and cell elasticity, flexibility, cell shape and motility etc. only become important when the cell size is same for the translocating species.

A very important point to note here is that the cells must interact with the micropore walls to discriminate cells on the basis of cell elasticity and flexibility. That is why this device had the pore size close to the size of A549 and H460. For discrimination between smaller cells we would need smaller pores. The system cannot discriminate between cells that do not have to deform or squeeze through in order to pass through the pore. This device cannot discriminate between cell types that have different elasticity and flexibility but are of the same size unless the pore is comparative in size to the cell size. Keeping micropore size comparable to the cell size is key to discriminating cells based on their elasticity/flexibility.

Conclusions

This electromechanical approach to detect and quantify NSCLC cells from a cancer patient sample using a micropore device is the simplest yet very efficient technique. Discriminating different types of tumor cells is a major step in proper disease diagnostic and treatment. The micropore approach can very efficiently translate the difference in tumor cell properties into difference in electrical signals that can be readout easily. Patient's sample can be analyzed with this device without any pre-processing requirements or the need of fluorescent tagging, particle or bead attachment. The required results can be obtained within few hours making it a suitable choice for point-of-care diagnostic application.

Acknowledgements

We are thankful to Dr. Robert Bachoo at UT Southwestern Medical Center for providing the lung cancer cells for experiments. We would also like to thank Dr. M. Arif I. Mahmood for useful discussions and Mr. Raja Raheel Khanzada and Mr. Mohammad Raziul Hasan for help with imaging and graphics. This work was supported by the NSF grant ECCS-1201878 and CPRIT grant RP110041.

Competing Financial Interests

The authors declare no competing financial interests.

References

1. Lennon AM, Wolfgang CL, Canto MI, Klein AP, Herman JM, Goggins M, Fishman EK, Kamel I, Weiss MJ, Diaz LA, et al. 2014. The early detection of pancreatic cancer: what will it take to diagnose and treat curable pancreatic neoplasia? *Cancer Research*; 74(13):3381-9.
2. Carter HB, Albertsen PC, Barry MJ, Etzioni R, Freedland SJ, Greene KL, Holmberg L, Kantoff P, Konety BR, Murad MH, et al. 2013. Early detection of prostate cancer: AUA guideline. *Journal Of Urology*; 190(2):419-26.
3. Chaffer CL, Weinberg RA. 2011. A perspective on cancer cell metastasis. *Science*; 331(6024):1559-64.
4. Gao Y, Yuan Z. 2014. Nanotechnology for the detection and kill of circulating tumor cells. *Nanoscale Research Letters*; 9(1):500.
5. Marino N, Woditschka S, Reed LT, Nakayama J, Mayer M, Wetzel M, Steeg PS. 2013. Breast cancer metastasis: issues for the personalization of its prevention and treatment. *The American Journal of Pathology*; 183(4):1084-95.
6. Fife CM, McCarroll JA, Kavallaris M. 2014. Movers and shakers: cell cytoskeleton in cancer metastasis. *British Journal of Pharmacology*; 171:5507-23.
7. Lukinavicius G, Reymond L, D'Este E, Masharina A, Gottfert F, Ta H, Guther A, Fournier M, Rizzo S, Waldmann H, et al. 2014. Fluorogenic probes for live-cell imaging of the cytoskeleton. *Nature Methods*; 11(7):731-3.
8. Ohnishi Y, Watanabe M, Yasui H, Kakudo K. 2014. Effects of epidermal growth factor on the invasive activity and cytoskeleton of oral squamous cell carcinoma cell lines. *Oncology Letters*; 7(5):1439-42.
9. Pritchard RH, Huang YY, Terentjev EM. 2014. Mechanics of biological networks: from the cell cytoskeleton to connective tissue. *Soft Matter*; 10(12):1864-84.
10. Agus DB, Alexander JF, Arap W, Ashili S, Aslan JE, Austin RH, Backman V, Bethel KJ, Bonneau R, Chen WC, et al. 2013. A physical sciences network characterization of non-tumorigenic and metastatic cells. *Scientific Reports*; 3:1449.
11. Wang Y, Lei R, Zhuang X, Zhang N, Pan H, Li G, Hu J, Pan X, Tao Q, Fu D, et al. 2014. DLC1-dependent parathyroid hormone-like hormone inhibition suppresses breast cancer bone metastasis. *Journal Of Clinical Investigation*; 124(4):1646-59.
12. Chambers AF, Groom AC, MacDonald IC. 2002. Dissemination and growth of cancer cells in metastatic sites. *Nature Reviews Cancer*; 2(8):563-72.
13. Ward KA, Li WI, Zimmer S, Davis T. 1991. Viscoelastic properties of transformed cells: role in tumor cell progression and metastasis formation. *Biorheology*; 28(3-4):301-13.
14. Lekka M, Laidler P, Gil D, Lekki J, Stachura Z, Hryniewicz A. 1999. Elasticity of normal and cancerous human bladder cells studied by scanning force microscopy. *European Biophysics Journal with Biophysics Letters*; 28(4):312-6.
15. Suresh S. 2007. Nanomedicine: elastic clues in cancer detection. *Nature Nanotechnology*; 2(12):748-9.

16. Lee GY, Lim CT. 2007. Biomechanics approaches to studying human diseases. *Trends in Biotechnology*; 25(3):111-8.
17. Ilyas A, Asghar W, Ahmed S, Lotan Y, Hsieh J-T, Kim Y-t, Iqbal SM. 2014. Electrophysiological analysis of biopsy samples using elasticity as an inherent cell marker for cancer detection. *Analytical Methods*; 6(18):7166-74.
18. Benitez R, Toca-Herrera JL. 2014. Looking at cell mechanics with atomic force microscopy: Experiment and theory. *Microscopy Research and Technique*; 77:947-958.
19. De la Rica R, Thompson S, Baldi A, Fernandez-Sanchez C, Drain CM, Matsui H. 2009. Label-free cancer cell detection with impedimetric transducers. *Analytical Chemistry*; 81(24):10167-71.
20. Dehoux T, Abi Ghanem M, Zouani OF, Ducouso M, Chigarev N, Rossignol C, Tsapis N, Durrieu MC, Audoin B. 2014. Probing single-cell mechanics with picosecond ultrasonics. *Ultrasonics*; 56:160-71.
21. Kuznetsova TG, Starodubtseva MN, Yegorenkov NI, Chizhik SA, Zhdanov RI. 2007. Atomic force microscopy probing of cell elasticity. *Micron*; 38(8):824-33.
22. Li QS, Lee GYH, Ong CN, Lim CT. 2008. AFM indentation study of breast cancer cells. *Biochemical and Biophysical Research Communications*; 374(4):609-13.
23. Guo Y-J, Sun G-M, Zhang L, Tang Y-J, Luo J-J, Yang P-H. 2014. Multifunctional optical probe based on gold nanorods for detection and identification of cancer cells. *Sensors and Actuators B-Chemical*; 191:741-9.
24. McGuire MJ, Gray BP, Li S, Cupka D, Byers LA, Wu L, Rezaie S, Liu YH, Pattisapu N, Issac J, et al. 2014. Identification and characterization of a suite of tumor targeting peptides for non-small cell lung cancer. *Scientific Reports*; 4:4480.
25. Han Y, Su C, Liu Z. 2014. Methods for detection of circulating cells in non-small cell lung cancer. *Frontiers in Bioscience*; 19:896-903.
26. Minamimoto R, Toyohara J, Ito H, Seike A, Miyata Y, Morooka M, Okasaki M, Nakajima K, Ito K, Ishiwata K, et al. 2014. A pilot study of 4'-[methyl-11C]-thiothymidine PET/CT for detection of regional lymph node metastasis in non-small cell lung cancer. *EJNMMI Research*; 4(1):10.
27. Tabata O, Asahi R, Funabshi H, Shimaoka K, Sugiyama S. 1992. Anisotropic etching of silicon in TMAH solutions. *Sensors and Actuators A-Physical*; 34(1):51-7.
28. Asghar W, Ilyas A, Billo JA, Iqbal SM. 2011. Shrinking of Solid-state Nanopores by Direct Thermal Heating. *Nanoscale Research Letters*; 6.
29. Asghar W, Ilyas A, Deshmukh RR, Sumitsawan S, Timmons RB, Iqbal SM. 2011. Pulsed plasma polymerization for controlling shrinkage and surface composition of nanopores. *Nanotechnology*; 22(28).
30. Ilyas A, Asghar W, Kim YT, Iqbal SM. 2014. Parallel recognition of cancer cells using an addressable array of solid-state micropores. *Biosensors & Bioelectronics*; 62:343-9.
31. Billo JA, Asghar W, Iqbal SM. 2011. An implementation for the detection and analysis of negative peaks in an applied current signal across a silicon nanopore. *Micro- and Nanotechnology Sensors, Systems, and Applications III*; 8031.

32. Wan Y, Tamuly D, Allen PB, Kim Y-t, Bachoo R, Ellington AD, Iqbal SM. 2013. Proliferation and migration of tumor cells in tapered channels. *Biomedical Microdevices*; 15(4):635-43.
33. Asghar W, Wan Y, Ilyas A, Bachoo R, Kim YT, Iqbal SM. 2012. Electrical fingerprinting, 3D profiling and detection of tumor cells with solid-state micropores. *Lab on a Chip*; 12(13):2345-52.
34. Breitenbuecher F, Hoffarth S, Worm K, Cortes-Incio D, Gauler TC, Kohler J, Herold T, Kurt Werner S, Freitag L, Kasper S, et al. 2014. Development of a highly sensitive and specific method for detection of circulating tumor cells harboring somatic mutations in non-small-cell lung cancer patients. *PLOS One*; 9(1):e85350.
35. Jemal A, Siegel R, Ward E, Hao Y, Xu J, Murray T, Thun MJ. 2008. Cancer statistics, 2008. *CA-A Cancer Journal for Clinicians*; 58(2):71-96.
36. Cross SE, Jin YS, Rao J, Gimzewski JK. 2007. Nanomechanical analysis of cells from cancer patients. *Nature Nanotechnology*; 2(12):780-3.
37. Moeendarbary E, Harris AR. 2014. Cell mechanics: principles, practices, and prospects. *Wiley Interdisciplinary Reviews Systems Biology and Medicine*; 6(5):371-88.
38. Hofman V, Ilie M, Long E, Guibert N, Selva E, Washetine K, Mograbi B, Mouroux J, Venissac N, Reverso-Meinietti J, et al. 2014. Detection of circulating tumor cells from lung cancer patients in the era of targeted therapy: promises, drawbacks and pitfalls. *Current Molecular Medicine*; 14(4):440-56.
39. Shoemaker RH. 2006. The NCI60 human tumour cell line anticancer drug screen. *Nature Reviews Cancer*; 6(10):813-23.
40. McGuire MJ, Gray BP, Li S, Cupka D, Byers LA, Wu L, Rezaie S, Liu Y-H, Pattisapu N, Issac J, et al. 2014. Identification and characterization of a suite of tumor targeting peptides for non-small cell lung cancer. *Scientific Reports*;4.

CHAPTER 4

DIFFERENTIATION OF SPECIFIC CANCER BIOMARKERS WITH

SOLID-STATE NANOPORES

Differentiation of Specific Cancer Biomarkers with Solid-state Nanopores

Waqas Ali^{1,2,3,a}, Mohammed Arif I. Mahmood^{1,2,3,b}, Peter B. Allen^{4,c}, Adam R. Hall^{5,d}, Yuan Wan^{6,7,e}, Muhammad Usman Raza^{1,2,3,f} and Samir M. Iqbal^{1,2,3,8,9,g*}

¹Nano-Bio Lab, ²Department of Electrical Engineering, ³Nanotechnology Research Center, University of Texas at Arlington, Arlington, TX 76019, USA; ⁴Department of Chemistry, University of Idaho, Moscow, ID 83844, USA; ⁵Virginia Tech-Wake Forest School of Biomedical Engineering and Sciences, Wake Forest University School of Medicine, Winston Salem, NC 27101, USA; ⁶Ian Wark Research Institute, University of South Australia, Adelaide, South Australia 5095, Australia; ⁷PMR Institute, Shanghai, China 201203; ⁸Department of Bioengineering, University of Texas at Arlington, Arlington, TX 76019, USA; ⁹Department of Urology, University of Texas Southwestern Medical Center at Dallas, TX 75390, USA.

^awaqas.ali@mavs.uta.edu, ^barif.iftakher@gmail.com, ^cpballen@gmail.com, ^darhall@wakehealth.edu, ^emastermg@163.com, ^fraza.muhammadusman@mavs.uta.edu, ^gsmiqbal@uta.edu

Keywords: Nanopore, Biosensor, Single Molecule Detection, EGFR, Point-of-care, Cancer Diagnosis, Early Detection.

Abstract

Epidermal growth factor receptor (EGFR) is well known as an early biomarker for many cancer types. The current methods for EGFR detection lack the sensitivity and selectivity required to efficiently detect and differentiate EGFR from other proteins. We demonstrate a nanopore-based resistive pulse-sensing technique to selectively detect small amounts of EGFR from a mixture. An anti-EGFR aptamer is used to impart selectivity in the sample solution. The shift in translocation dwell time of samples both with and without a bound anti-EGFR aptamer is used to detect EGFR. EGFR with the bound aptamer results in a translocation dwell time that is about 23% shorter than that of EGFR alone, indicating a greater net charge for the complex. Thrombin is used as a control to demonstrate that the high specificity of the aptamer for EGFR enables differentiation of similar-sized proteins. The use of anti-EGFR aptamer as a targeting agent makes the label free detection of EGFR possible without nanopore surface modification or functionalization.

Introduction

EGFR detection and enumeration promises early cancer detection [1, 2] and the ability to monitor therapy and prognosis [3-5]. Elevated levels of EGFR expression in patients' serum is a strong prognostic indicator for many tumor types [6-8]. For example, Quaranta *et al.* reported the mean EGFR level in brain cancer patients' sera to be nearly twice than that of healthy subjects [9]. The total concentration of EGFR in patient serum is very small (ng/ml) and can be easily obscured by the biological noise. These facts highlight two major challenges in detection of EGFR expression levels in patients' serum: first, a useful biosensor should have molecular level sensitivity and second, it should have very high specificity. In last couple of decades, a variety of detection assays for proteins have been developed using fluorescence, electrochemical, colorimetric, chemiluminescence and surface plasmon resonance means [3, 10]. These assays lack the sensitivity and specificity required for the efficient detection of physiologically relevant EGFR levels.

Development of new approaches for point-of-care (POC) detection of protein biomarkers is a pressing need in early cancer diagnosis. Devices for POC must be ultrasensitive, fast, accurate, low priced and should be easy to use [11]. One candidate technology that has recently emerged as a potent single molecule detector is the solid-state nanopore [12-17] based on the resistive-pulse enumeration. When a molecule hinders the ionic flow through the nanopore, it registers a unique electrical pulse in the baseline ionic current trace. Analysis of these electrical pulses can be used to determine size and charge of molecules [12], length of nucleic acids [14, 18], protein size [19, 20], folding state [20, 21] and molecular agglomeration [22]. They can also be

chemically modified [15, 23] for detection of specific biomarkers [17, 24] and toxic agents [25, 26].

Biological nanopores are unstable and their measurement setup is tedious due to their small fixed diameter (1.5 – 3.6 nm); only polypeptides or denatured proteins are able to translocate there [27, 28]. Moreover, preparation of large-scale protein nanopore arrays faces technical challenges [12]. On the contrary, solid-state nanopores are compatible with proteins of any conformation and size due to the tunable dimensions. These have been successfully used to detect proteins of various sizes and stochastic sensing of proteins [14]. The current approaches have some disadvantages. First, single-ligands functionalized nanopore can only detect one type of target protein; proteins not recognized by ligands are not detected at all. If several proteins need to be simultaneously identified, different kinds of ligands should be respectively immobilized on separate nanopores [29, 30]. This means multiple copies of samples and multiple sets of nanopore frameworks need to be prepared for signal collection, analysis and calibration. Although technically feasible, such strategies for multiplexed protein detection require tremendous workload and would be unreliable from the noise and system artifacts. In addition, due to different sizes of proteins, the nanopore diameter would need to be precisely tuned in order to accommodate each analyte. If the proteins of interest have broad ranges of size that would be another challenge to decide on nanopores with suitable diameters. Another challenge is the immobilization of the specific ligands onto the inner edge of the nanopore. Surface functionalization at such small size scales is not trivial and is expected to result in insufficient immobilization sites and heterogeneous grafting especially when irregular surfaces result into various

charge distribution and variations in the nanopore stoichiometry [12, 29, 30]. An ideal solid-state nanopore system should be able to simultaneously and quickly identify target proteins in a multiplexed fashion from a single miniscule sample. Such detection should be performed, from initial system setup to final data report, on one framework.

This letter reports solid-state nanopores as single-molecule sensors [31-33] for detection and enumeration of EGFR in POC setting. To keep the process simple, instead of using a functionalized nanopore [34], a bare nanopore was used and in-solution binding of EGFR with anti-EGFR aptamer was used to impart selectivity [35]. Anti-EGFR aptamer has very high affinity for EGFR and it is very selective as well [36]. Aptamer binding to the protein altered the overall charge and mass of the complex as compared to the unbound EGFR [37]. Since the speed of the translocating species strongly depended upon its charge [38-40], attachment with aptamer tweaked the translocation time for EGFR only. This change was readily identified from the analysis of registered pulses. As a negative control, the experiments were done with human α -thrombin protein. With thrombin, no change was observed in the translocation time after incubating the protein with the aptamer.

Results and Discussion

Current-voltage (I-V) characteristics of the nanopore in 20 mM Tris-acetate pH 8.2 + 5 mM Mg-acetate + 1 mM K-acetate are shown in Figure 1(b). Conductance of the nanopore was calculated to be 2.5 μ S by a linear fit to the data. For the voltage range of -100 mV to 100 mV, linear I-V characteristics were observed [41, 42]. Open pore current for the nanopore at 50 mV applied bias is shown in Figure 2(a).

EGFR was introduced into the *cis* (negative) side of the nanopore that resulted in significant current blockage events. A snapshot of the nanopore current trace at 50 mV is shown in Figure 2(c). These pulses are for EGFR translocation measured in 10sec. Very uniform current pulses were observed in terms of translocation time and peak amplitude. EGFR translocation through the nanopore registered characteristic current pulses with average peak amplitude of 0.9 ± 0.21 nA and average translocation time of 80 ± 4.06 μ s (Table 1). Only one population of events was observed for the peak amplitude *versus* the translocation time for EGFR translocation through nanopore at 50 mV as shown in Figure 2(d).

TABLE 1. Pulse Statistics for Unbound EGFR & EGFR-aptamer Complex

Translocating Species	Translocation Time [μs]	Peak Amplitude [nA]
EGFR (Unbound)	80 ± 4.06	0.9 ± 0.21
EGFR-aptamer Complex	62 ± 5.24	1.1 ± 0.18

In the next set of experiments, again EGFR was introduced into the *cis* side of the nanopore for translocation but this time sample was incubated with anti-EGFR aptamer for a certain period under conditions mentioned in the experimental section. This time again significant current blockage events were observed. But, in contrast to the previous observations, there were two distinct types of pulses (Figure 3(a)). The two types of pulses were not very different in terms of their peak amplitudes but they were remarkably different in terms of their translocation times. The two types were different from each other by 22.5% with respect to their average translocation times and 18.2% in terms of their average peak amplitudes.

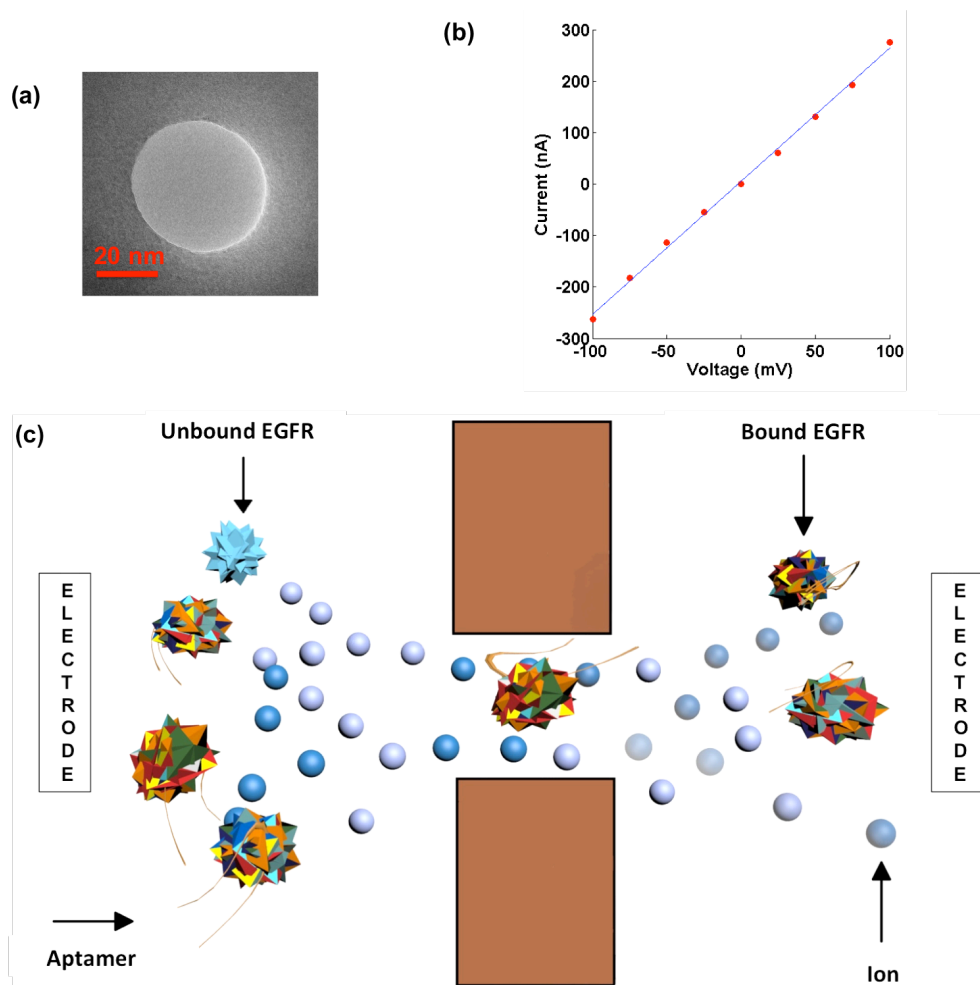


Figure 1. Nanopore for EGFR translocation experiments. (a) TEM image of a 40 nm diameter solid-state nanopore fabricated in 40 nm thick freestanding SiN membrane drilled with focused electron beam from TEM. (b) Linear I-V characteristics for the nanopore show 2.5 μ S conductivity. (c) Incubating EGFR with aptamer allows them to bind with EGFR molecules and form the complex. Complex due to their higher charge and slightly larger excluded volume than unbound EGFR cause electrical pulses that are wider and deeper as compared to those registered by unbound EGFR.

One of the two types of pulses were exactly similar (i.e. same translocation time and peak amplitude) to those that were observed for EGFR translocation without incubation with the aptamer. The second type of pulses had shorter widths i.e. higher

translocation speed, and larger peak amplitudes i.e. more pore blockage, when compared to those for pulses associated with EGFR translocation without incubation with the aptamer. The second type of pulses, characterized by faster translocation speed and more pore blockage, stemmed from the translocation of the complex.

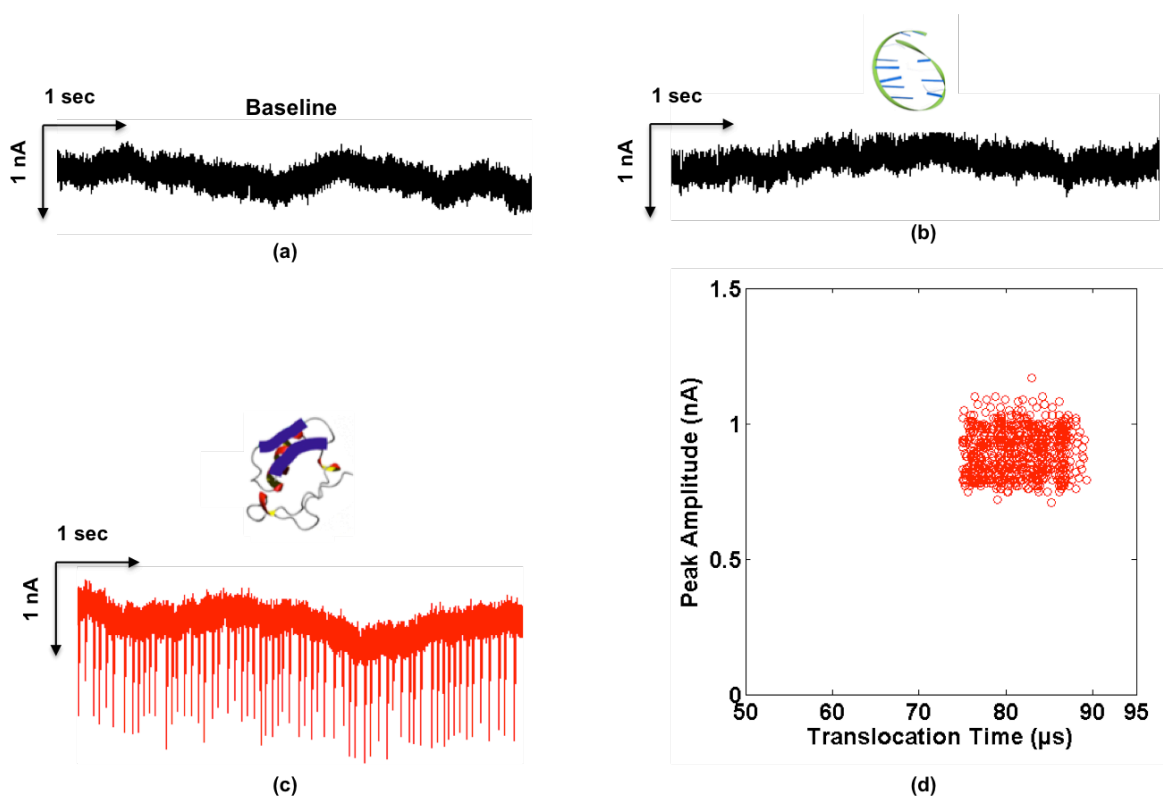


Figure 2. Snapshots of the nanopore current for 10 seconds duration for (a) Baseline, translocation of (b) Anti-EGFR aptamer (unbound only) (c) EGFR (unbound only) and (d) Scatter plot of the translocation time versus peak amplitude of the registered pulses for EGFR translocation through 40 nm nanopore at 50 mV. The registered pulses for EGFR translocation are consistent and form only one cluster of event population on the plot.

The complex translocation through a 40 nm wide and 40 nm thick solid-state nanopore under an applied voltage of 50 mV registered pulses with average peak amplitude of 1.1 ± 0.18 nA and average translocation time of 62 ± 5.24 μ s. The

presence of two distinct types of populations can be clearly seen in Figure 3(d). Another important point to notice from this scatter plot is that the events frequency is not the same for the two types of pulses. There are much more events of EGFR translocation as compared to that of complex translocation. One plausible reason for that could be the abundance of unbound EGFR as compared to the EGFR-aptamer complex. To systematically prove this hypothesis, a titration series was conducted in which the molar concentration of EGFR was kept constant and the molar concentration of anti-EGFR aptamer was gradually increased. Figures 3(b) and 3(c) show the 10 sec current traces when EGFR was incubated with 4 μM and 10 μM anti-EGFR aptamer, respectively. For each case, blockage events are plotted on a scatter plot of translocation time *versus* peak amplitude (Figure 3(e) and 3(f)). A gradual increase in the event frequency for complex translocation was observed as the molar concentration of aptamer increased. The effect was opposite on the event frequency of EGFR translocation. It kept on decreasing. This shifting signal from event population of EGFR to that of complex, with the increase in aptamer concentration, indicates that more EGFR molecules were binding to aptamer as the aptamer concentration increased. So for the first experiment with the complex translocation, there were plenty of unbound EGFR molecules present in the sample (Figure 3(d)) that reduced as the aptamer concentration increased and ultimately very few unbound EGFR molecules were left (Figure 3(f)). This is when the most of the EGFR molecules were bound to the aptamer forming the complex.

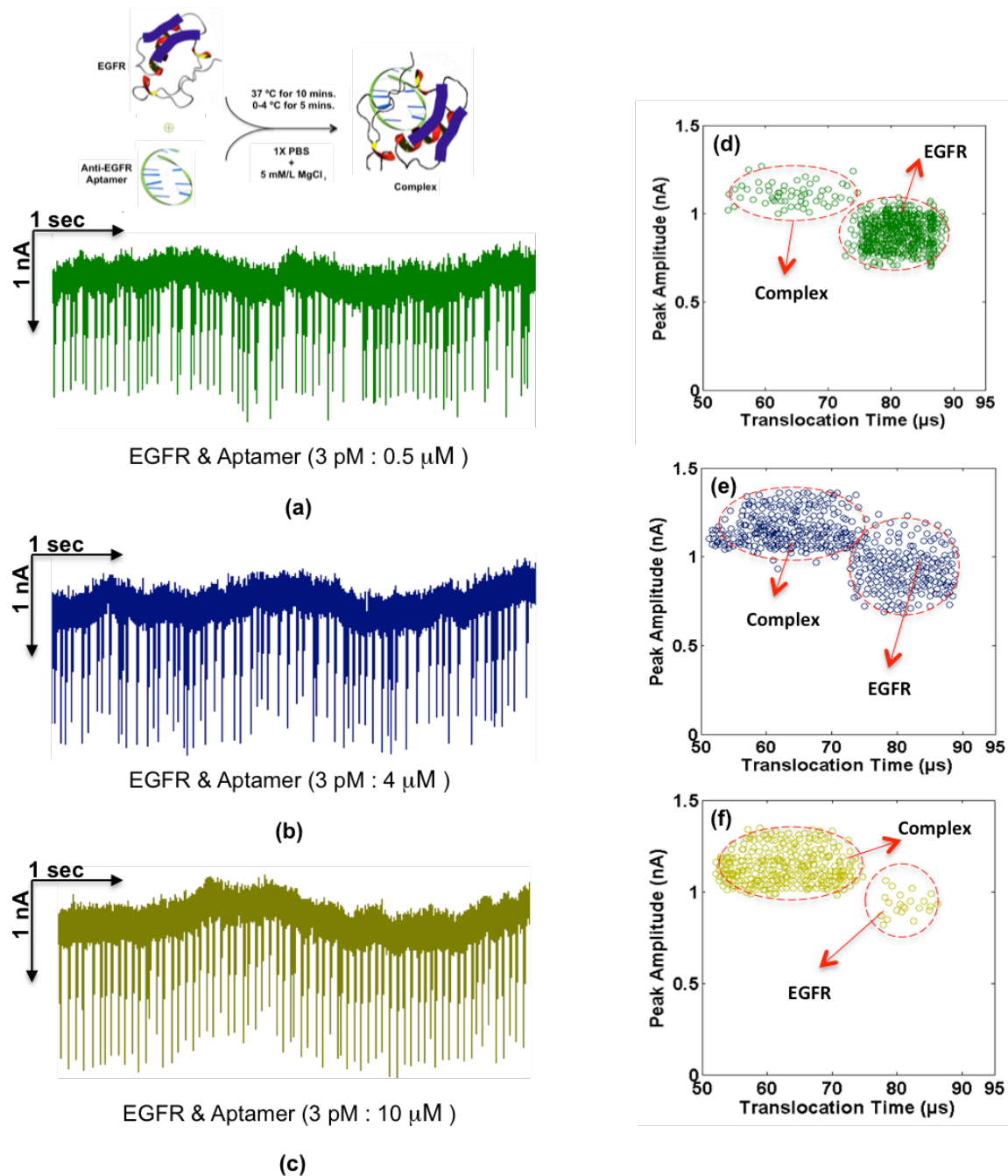


Figure 3. Snapshots of the ionic current trace for 10 seconds of the EGFR (3 pM) translocation when incubated with aptamer at (a) 0.5 μM (b) 4 μM and (c) 10 μM. The scatter plots show the translocation behavior of EGFR (3 pM) when incubated with aptamer at (d) 0.5 μM (e) 4 μM and (f) 10 μM. Two populations are visible: One with higher dwell time corresponds to the translocation of unbound EGFR, and second with shorter dwell time corresponds to complex's translocation.

One might think that the second type of events can be associated with the translocation of free floating anti-EGFR aptamer in the solution. To rule this out, another experiment was carried out to record pulses for the translocation of anti-EGFR aptamer alone through the same nanopore. For this purpose, anti-EGFR aptamer was introduced into the *cis* side of the nanopore and this time no current blockage events were observed. There can be multiple reasons for that but one of the strongest reasons is that a 40 nm nanopore is probably too large to detect the translocation of aptamer (few nanometers in size [43, 44]) because for nanopore based detection scheme, nanopore size should be close to the size of the target [12, 13, 15]. In that case, even if aptamer would be indeed translocating through the nanopore but due to their much smaller size than the pore they are unlikely to block current and hence not registering any pulse, as was observed in these experiments. Another possibility can be that the charge on the aptamer is much smaller than the overall charge of the protein. So even if 50 mV is enough to exert sufficient electrophoretic force on the protein to translocate through the nanopore, it might not be sufficient to push aptamer alone through it due to their small charge. In that case, aptamer will not even be going through the nanopore at all and hence there will be no pulse. Though this is a less likely case but can't be ruled out completely. In any case, the point here is that, out of the two types of events that were observed for the translocation of EGFR after incubating it with aptamer, one was due to the translocation of EGFR alone and the other was due to the translocation of complex and not the free floating aptamer.

Finally, to check the specificity of this assay, experiment was repeated with human α -thrombin protein instead of EGFR. First, thrombin was translocated through a 40 nm

wide and 40 nm thick nanopore at 50 mV. Figure 4(a) shows the current trace for thrombin translocation for 10s duration. The average translocation time and average peak amplitude of the registered pulses from thrombin translocation were determined to be $68 \pm 3.17 \mu\text{s}$ and $0.5 \pm 0.15 \text{ nA}$, respectively. Thrombin ($8 \mu\text{l}$, $50 \text{ ng}/\mu\text{l}$) was then incubated with anti-EGFR aptamer ($10 \mu\text{M}$) and sample was run through the same nanopore at 50 mV. This time again, only one type of pulses were observed that were exact replica of those observed for thrombin without incubation with aptamer. The nanopore current trace for thrombin translocation after incubation with aptamer is shown in Figure 4(b). Figures 4(c) and 4(d) show the population regions of the events recorded by the translocation of unbound thrombin and thrombin-aptamer complex (i.e. after incubation with aptamer), respectively, on translocation time *versus* peak amplitude plot.

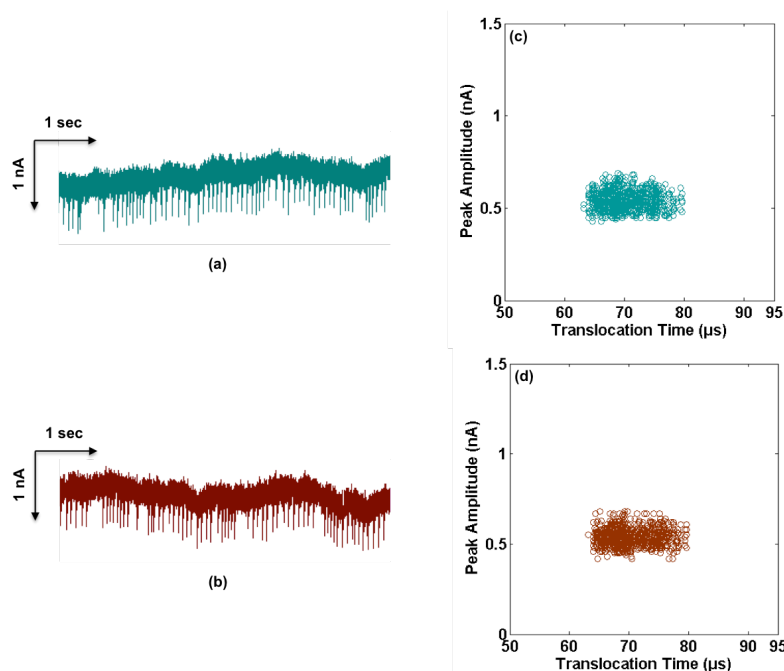


Figure 4. Snapshots of the nanopore ionic current traces for 10 seconds for the translocation of (a) Thrombin (b) Thrombin (11 pM) incubated with 10 pM of aptamer. Scatter plots of the registered pulses for the translocation of (c) Thrombin (d) Thrombin incubated with 10 pM aptamer.

The two populations are exactly same indicating that thrombin translocation profile remained same before and after incubation with aptamer. This is because no aptamer attached to thrombin and the assay was highly selective for EGFR protein. Incubating thrombin with aptamer did not affect their translocation profile since aptamer did not attach to thrombin and no thrombin-aptamer complexes were formed.

The dynamics of protein translocation, in general, through bare as well as chemically-modified solid-state nanopores and the forces involved in this process have already been explored through simulations and experiments [14, 21, 34, 37, 45-48]. EGFR translocation through the nanopore is not different from other proteins. At a pH of 8.2, carboxylic groups in EGFR molecule have negative charge whereas amines are protonated i.e. they attain positive charge. The isoelectric point (pI) for EGFR is 6.7 and at our buffer solution's pH the net charge on EGFR molecule is negative [49]. Due to this charge, after applying biasing voltage, electrophoretic force (EP) pushes the EGFR molecules towards the positive electrode in the *trans* compartment [50]. The velocity of this moving molecule can be calculated using Smoluchowski's equation [51, 52]: $v_{EP} = \frac{\epsilon \eta}{\zeta_{pro}} E$ where ' v_{EP} ' is the electrophoretic velocity of EGFR molecule, ' ϵ ' is the dielectric constant, ' η ' is the solution viscosity, ' ζ_{pro} ' is the zeta potential for protein molecule and ' E ' is the electric field. Electroosmotic flow (EO) in the electrolyte also affects the dynamics of the EGFR movement in nanopores. In some cases EO can also cause a reverse flow of the proteins [47] i.e. negatively charged protein molecules will start moving towards the *cis* side, opposite to the EP. Reverse flow of the EGFR molecule was not observed in the experiments that meant that EO was either in the

direction of EP or even if it was opposite to EP, it was not sufficient to counteract the EP and EP solely was the dominant factor in governing EGFR direction of flow.

The overall translocation process can be split into two stages; (1) Capture step, and (2) Actual translocation through the nanopore. For a 40 nm pore, the capture of EGFR molecule will be diffusion controlled as opposed to the barrier-limited case. The dynamics of this diffusion controlled capture step can be calculated with the Smoluchowski's diffusion equation [40, 51-53]: $J = 2\pi cDr_p$, where ' J ' is the rate at which the EGFR arrives at the nanopore entrance, ' c ' is the bulk analyte concentration, ' D ' is the diffusion constant and ' r_p ' is the nanopore radius. Once EGFR has entered the nanopore, the translocation depends upon the zeta potential of the EGFR molecule and of the nanopore [50]. Cressiot *et al.* simulated the interaction of proteins with nanopore walls formed by FIB as well as TEM. They found that due to the absence of dangling atoms [54] and rearrangement of silica in nanopores formed by TEM, the interaction between proteins and nanopore walls is very weak [48]. Blockage time, $t_b = L/v_{EP}$ (' L ' is nanopore channel length) is a function of the applied voltage [48] as well as the charge of the translocating species [19, 47]. Increasing either of these would increase the EP on the EGFR molecules and hence will decrease the blockage time and vice versa. At fixed applied bias of 50 mV, the pulses were pretty consistent in their width i.e. translocation time or blockage time for EGFR translocation. Coagulation of molecules, if happened, would have either blocked the pore completely or much longer translocation times would have been present [45]. However, none of such events were observed so it can be concluded that no EGFR coagulation occurred under these experimental conditions. Concurrent translocations of multiple EGFR molecules were observed

though, but these events were very few and were discarded from the analysis. From single EGFR translocation events, very consistent pulse depths were observed, that was a clear indication of the uniform excluded volume of the EGFR molecules.

The specificity of anti-EGFR aptamer for EGFR and their attachment chemistry is quite well established [35, 36, 55]. When EGFR is incubated with the aptamer, they form a complex with 1:1 stoichiometry. It is just like aptamer, which has its own charge and mass, riding on the EGFR molecule. Since the estimated pI for aptamer is 5.5, at pH 8.2 it has almost the same charge as the EGFR. The attachment of EGFR with aptamer enhances the overall charge of the complex as well as the complex has more mass now than EGFR alone. These changes influence the overall dynamics of the complex translocation through the nanopore and make the translocation profile of complex different from that of EGFR. The additional charge of the complex very well explains the faster translocation of the complex through the nanopore. One might argue here that due to the additional mass it might be possible that the complex actually moved slower than the EGFR. However this is not the dominant factor in determining the translocation profile of the complex [37], since due to the binding of aptamer with EGFR, the overall change in charge is much more than the overall change in mass. That's why much more shift in the translocation time was observed rather than the peak amplitudes between the pulses associated with complex and EGFR translocation.

The shifting of the EGFR translocation behavior, as the molar concentration of aptamer increased, can be explained with Smoluchowski's diffusion equation. According to this equation, the capture rate ' J ' increases by increasing the analyte concentration ' c ' in the solution. In Figure 3(d), the event rate is low for complex and higher for EGFR but

as we increased the aptamer molar concentration, many more complexes were formed causing the event rate for them to shoot up (Figure 3(e) & 3(f)). With thrombin, since aptamer didn't bind to it, no complexes were formed and the translocation profile remained the same as before when no aptamer was involved.

The nanopores depicted a very selective and sensitive framework for label-free detection of EGFR from a sample. The use of bare nanopore made the process very simple and provided much more flexibility in the choice of nanopore size, unlike functionalized nanopore in which the ligand would be tethered inside the nanopore walls and the target must interact with the nanopore walls [37]. A functionalized nanopore is usable for one type of target and functionalization itself is a time consuming and labor extensive process. The use of bare nanopore with ligands to bind specific targets in solution increase the usability of the device since the same device can be used for multiple targets. There are no stringent limitations on the size of the nanopore as well.

Materials and Methods

Materials: Recombinant Human EGFR/ErbB1 Fc Chimera, CF (EGFR ~134 KDa) was purchased from R&D Systems and human α -thrombin (Thrombin ~37 KDa) was purchased from Abcam, plc. Anti-EGFR aptamer (~10 KDa) had the sequence

GGGCGCUCGACCUUAGUCUCUGUGCCGCUAAUAAUGCACGGAUUAAUCGCCG
UAGAAAAGCAUGUCAAAAGCCGGAACCGUGUAGCACAGCAGAGAAUAAAUGCCC
GCCAUGACCAG [36, 56]. All other chemicals were obtained from Sigma-Aldrich unless specified otherwise.

Nanopore Fabrication and Electrical Measurements: A solid-state nanopore of 40 nm diameter and 40 nm length (Figure 1(a)) was used for all the translocation experiments. The nanopore was drilled in a thin suspended silicon nitride membrane by focusing an electron beam of a transmission electron microscope (TEM). Nanopore diameter was controlled by the exposure time [57]. The detailed fabrication process for membranes is reported elsewhere [58]. The nanopore chip was sandwiched between two PDMS gaskets that were further sandwiched between two Teflon blocks that contained the electrophoresis buffer solution (20 mM Tris-acetate pH 8.2 + 5 mM Mg-acetate + 1 mM K-acetate). Protein unfolding has strong dependence on the applied voltage [21, 48]. To keep proteins in their native states and to avoid any unfolding all the translocation experiments were done at a very low voltage i.e. 50 mV. For current measurement and to apply the voltage, Ag/AgCl electrodes were immersed in the buffer solution and were connected to Axopatch 200B through the headstage. Figure 1(c) shows the schematic of nanopore measurement system. Current recording was done at a bandwidth of 250 kHz whereas filtering was done at 100 kHz with a lowpass Bessel filter. A custom made MATLAB routine [59] was used for analysis of the data. The *t*-test was done for statistical analysis.

In-solution Binding of Protein and Aptamer: For in-solution binding, EGFR protein and anti-EGFR aptamer were mixed in the binding buffer (Figure 2c). The binding buffer constituted of 1X PBS and 5 mM/L MgCl₂. Three separate mixtures were prepared by mixing EGFR and anti-EGFR aptamer in different concentrations. In mixture 1, 8 μl of 50 ng/μl (3 pM) EGFR was mixed with 0.5 μM aptamer. In mixture 2 and 3, EGFR concentration was kept same as mixture 1 but aptamer concentration was 4 μM and 10

μM , respectively. The mixtures were incubated at $37\text{ }^{\circ}\text{C}$ for 10 minutes and then were placed in freezer ($0\text{-}4\text{ }^{\circ}\text{C}$) for 5 minutes. The details on binding dynamics have been explained before [36]. For control experiments, $8\text{ }\mu\text{l}$ of human α -thrombin protein at $50\text{ ng}/\mu\text{l}$ (11 pM) concentration was also mixed with anti-EGFR aptamer ($10\text{ }\mu\text{M}$) and was incubated first at $37\text{ }^{\circ}\text{C}$ for 10 minutes and then at $0\text{-}4\text{ }^{\circ}\text{C}$ for 5 minutes.

Conclusions

In summary, the use of nanopore based resistive-pulse sensors for rapid and reliable detection of EGFR has been presented. Due to high single molecule sensitivity of nanopore sensors, very small amount of EGFR has been detected. EGFR overexpression, though an early biomarker for different types of cancers, have not yet been utilized properly for early cancer detection because available methods are not sensitive enough to detect very small changes in the quantities of EGFR. Besides high sensitivity and rapid detection, the scheme of nanopore with complex detection does not require pre-processing of the samples. The simplicity of this label-free detection method can enable the use of the nanopore device in a POC setting for early cancer diagnosis. The methodology can be further expanded for the detection of other biomarkers as well if there are matching ligands available. Additionally this technique can be used to determine the affinity of the aptamer-protein complex as well.

Acknowledgement

We thank Raja Raheel Khanzada for his help with the graphics of this paper. We would also like to thank Dr. Andrew Ellington from the University of Texas at Austin for

providing us the aptamer molecules. This work was supported by grant ECCS-12000 from National Science Foundation.

References

1. Pepe MS, Etzioni R, Feng Z, Potter JD, Thompson ML, Thornquist M, Winget M, Yasui Y. Phases of biomarker development for early detection of cancer, *Journal of the National Cancer Institute*. 93 (2001) 1054-61.
2. Wulfkuhle JD, Liotta LA, Petricoin EF. Proteomic applications for the early detection of cancer, *Nature Reviews Cancer*. 3 (2003) 267-75.
3. Rusling JF. Multiplexed electrochemical protein detection and translation to personalized cancer diagnostics, *Analytical Chemistry*. 85 (2013) 5304-10.
4. Gabos Z, Sinha R, Hanson J, Chauhan N, Hugh J, Mackey JR, Abdulkarim B. Prognostic significance of human epidermal growth factor receptor positivity for the development of brain metastasis after newly diagnosed breast cancer, *Journal of Clinical Oncology : Official Journal of the American Society of Clinical Oncology*. 24 (2006) 5658-63.
5. Mak MP, William WN, Jr. Targeting the epidermal growth factor receptor for head and neck cancer chemoprevention, *Oral oncology*. 50 (2014) 918-23.
6. Maheswaran S, Sequist LV, Nagrath S, Ulkus L, Brannigan B, Collura CV, Inerra E, Diederichs S, Iafrate AJ, Bell DW, et al. Detection of mutations in EGFR in circulating lung-cancer cells, *The New England Journal of Medicine*. 359 (2008) 366-77.
7. Voldborg BR, Damstrup L, Spang-Thomsen M, Poulsen HS. Epidermal growth factor receptor (EGFR) and EGFR mutations, function and possible role in clinical trials, *Annals of Oncology : Official Journal of the European Society for Medical Oncology / ESMO*. 8 (1997) 1197-206.
8. Mendelsohn J, Baselga J. Epidermal growth factor receptor targeting in cancer, *Seminars in Oncology*. 33 (2006) 369-85.
9. Quaranta M, Divella R, Daniele A, Di Tardo S, Venneri MT, Lolli I, Troccoli G. Epidermal growth factor receptor serum levels and prognostic value in malignant gliomas, *Tumori*. 93 (2007) 275-80.
10. Nam JM, Thaxton CS, Mirkin CA. Nanoparticle-based bio-bar codes for the ultrasensitive detection of proteins, *Science*. 301 (2003) 1884-6.
11. Gubala V, Harris LF, Ricco AJ, Tan MX, Williams DE. Point of care diagnostics: status and future, *Analytical Chemistry*. 84 (2012) 487-515.
12. Venkatesan BM, Bashir R. Nanopore sensors for nucleic acid analysis. *Nature Nanotechnology*. 6 (2011) 615-24.
13. Bell NA, Engst CR, Ablay M, Divitini G, Ducati C, Liedl T, Keyser UF. DNA origami nanopores, *Nano Letters*. 12 (2012) 512-7.
14. Wei R, Gatterdam V, Wieneke R, Tampe R, Rant U. Stochastic sensing of proteins with receptor-modified solid-state nanopores, *Nature Nanotechnology* 7 (2012) 257-63.
15. Iqbal SM, Akin D, Bashir R. Solid-state nanopore channels with DNA selectivity, *Nature Nanotechnology*. 2 (2007) 243-8.
16. Soni GV, Dekker C. Detection of nucleosomal substructures using solid-state nanopores, *Nano Letters*. 12 (2012) 3180-6.

17. Niedzwiecki DJ, Iyer R, Borer PN, Movileanu L. Sampling a biomarker of the human immunodeficiency virus across a synthetic nanopore, *ACS Nano*. 7 (2013) 3341-50.
18. Chen P, Mitsui T, Farmer DB, Golovchenko J, Gordon RG, Branton D. Atomic Layer Deposition to Fine-Tune the Surface Properties and Diameters of Fabricated Nanopores, *Nano Letters* 4 (2004) 1333-7.
19. Fologea D, Ledden B, McNabb DS, Li J. Electrical characterization of protein molecules by a solid-state nanopore, *Applied Physics Letters*. 91 (2007) 539011-3.
20. Talaga DS, Li J. Single-molecule protein unfolding in solid state nanopores, *Journal of the American Chemical Society*. 131 (2009) 9287-97.
21. Rodriguez-Larrea D, Bayley H. Multistep protein unfolding during nanopore translocation, *Nature Nanotechnology*. 8 (2013) 288-95.
22. Uram JD, Ke K, Hunt AJ, Mayer M. Submicrometer pore-based characterization and quantification of antibody-virus interactions, *Small*. 2 (2006) 967-72.
23. Ali M, Bayer V, Schiedt B, Neumann R, Ensinger W. Fabrication and functionalization of single asymmetric nanochannels for electrostatic/hydrophobic association of protein molecules, *Nanotechnology*. 19 (2008) 485711.
24. Majd S, Yusko EC, Billeh YN, Macrae MX, Yang J, Mayer M. Applications of biological pores in nanomedicine, sensing, and nanoelectronics, *Current Opinion in Biotechnology*. 21 (2010) 439-76.
25. Bayley H, Cremer PS. Stochastic sensors inspired by biology, *Nature*. 413 (2001) 226-30.
26. Liu A, Zhao Q, Guan X. Stochastic nanopore sensors for the detection of terrorist agents: current status and challenges, *Analytica Chimica Acta*. 675 (2010) 106-15.
27. Maglia G, Heron AJ, Stoddart D, Japrun D, Bayley H. Analysis of single nucleic acid molecules with protein nanopores, *Methods in Enzymology*. 475 (2010) 591-623.
28. Nivala J, Marks DB, Akeson M. Unfoldase-mediated protein translocation through an alpha-hemolysin nanopore, *Nature Biotechnology*. 31 (2010) 247-50.
29. Movileanu L. Interrogating single proteins through nanopores: challenges and opportunities, *Trends in Biotechnology*. 27 (2009) 333-41.
30. Hernandez-Ainsa S, Keyser UF. DNA origami nanopores: developments, challenges and perspectives, *Nanoscale*. 6 (2014) 14121-32.
31. Payet L, Martinho M, Pastoriza-Gallego M, Betton JM, Auvray L, Pelta J, Mathe J. Thermal unfolding of proteins probed at the single molecule level using nanopores, *Analytical Chemistry*. 84 (2012) 4071-6.
32. Han A, Creus M, Schurmann G, Linder V, Ward TR, de Rooij NF, Staufer U. Label-free detection of single protein molecules and protein-protein interactions using synthetic nanopores, *Analytical Chemistry*. 80 (2008) 4651-8.
33. Howorka S, Siwy Z. Nanopore analytics: sensing of single molecules, *Chemical Society Reviews*. 38 (2009) 2360-84.
34. Rotem D, Jayasinghe L, Salichou M, Bayley H. Protein detection by nanopores equipped with aptamers, *Journal of the American Chemical Society*. 134 (2012) 2781-7.

35. Bunka DH, Stockley PG. Aptamers come of age - at last, *Nature Reviews Microbiology*. 4 (2006) 588-96.
36. Wan Y, Mahmood MA, Li N, Allen PB, Kim YT, Bachoo R, Ellington AD, Iqbal SM. Nanotextured substrates with immobilized aptamers for cancer cell isolation and cytology, *Cancer*. 118 (2012) 1145-54.
37. Mahmood MA, Ali W, Adnan A, Iqbal SM. 3D structural integrity and interactions of single-stranded protein-binding DNA in a functionalized nanopore, *The Journal of Physical Chemistry B*. 118 (2014) 5799-806.
38. He Y, Tsutsui M, Scheicher RH, Fan C, Taniguchi M, Kawai T. Mechanism of how salt-gradient-induced charges affect the translocation of DNA molecules through a nanopore, *Biophysical Journal*. 105 (2013) 776-82.
39. Kowalczyk SW, Dekker C. Measurement of the docking time of a DNA molecule onto a solid-state nanopore, *Nano Letters*. 12 (2012) 4159-63.
40. Plesa C, Kowalczyk SW, Zinsmeister R, Grosberg AY, Rabin Y, Dekker C. Fast translocation of proteins through solid state nanopores, *Nano Letters*. 13 (2013) 658-63.
41. Ho C, Qiao R, Heng JB, Chatterjee A, Timp RJ, Aluru NR, Timp G. Electrolytic transport through a synthetic nanometer-diameter pore, *Proceedings of the National Academy of Sciences of the United States of America*. 102 (2005) 10445-50.
42. Kowalczyk SW, Kapinos L, Blosser TR, Magalhaes T, van Nies P, Lim RY, Dekker C. Single-molecule transport across an individual biomimetic nuclear pore complex, *Nature Nanotechnology*. 6 (2011) 433-8.
43. Zhang H, Li XF, Le XC. Tunable aptamer capillary electrophoresis and its application to protein analysis, *Journal of the American Chemical Society*. 130 (2008) 34-5.
44. van den Hout M, Skinner GM, Klijnhout S, Krudde V, Dekker NH. The passage of homopolymeric RNA through small solid-state nanopores, *Small*. 7 (2011) 2217-24.
45. Yusko EC, Johnson JM, Majd S, Prangko P, Rollings RC, Li J, Yang J, Mayer M. Controlling protein translocation through nanopores with bio-inspired fluid walls, *Nature Nanotechnology*. 6 (2011) 253-60.
46. Kowalczyk SW, Hall AR, Dekker C. Detection of local protein structures along DNA using solid-state nanopores, *Nano Letters*. 10 (2010) 324-8.
47. Firnkies M, Pedone D, Knezevic J, Doblinger M, Rant U. Electrically facilitated translocations of proteins through silicon nitride nanopores: conjoint and competitive action of diffusion, electrophoresis, and electroosmosis, *Nano Letters*. 10 (2010) 2162-7.
48. Cressiot B, Oukhaled A, Patriarche G, Pastoriza-Gallego M, Betton JM, Auvray L, Muthukumar M, Bacri L, Pelta J. Protein transport through a narrow solid-state nanopore at high voltage: experiments and theory, *ACS Nano*. 6 (2012) 6236-43.
49. Ceresa BP, Peterson JL. Cell and molecular biology of epidermal growth factor receptor, *International Review of Cell and Molecular Biology*. 313 (2014) 145-78.
50. Lu B, Hoogerheide DP, Zhao Q, Yu D. Effective driving force applied on DNA inside a solid-state nanopore, *Physical Review E, Statistical, Nonlinear, and Soft Matter Physics*. 86 (2012) 011921.

51. Peters B, Bolhuis PG, Mullen RG, Shea JE. Reaction coordinates, one-dimensional Smoluchowski equations, and a test for dynamical self-consistency, *The Journal of Chemical Physics*. 138 (2013) 054106.
52. Egorova EM. The validity of the Smoluchowski equation in electrophoretic studies of lipid membranes, *Electrophoresis*. 15 (1994) 1125-31.
53. Family F, Meakin P, Deutch JM. Kinetics of coagulation with fragmentation: Scaling behavior and fluctuations, *Physical Review Letters*. 57 (1986) 727-30.
54. Cruz-Chu ER, Aksimentiev A, Schulten K. Ionic Current Rectification Through Silica Nanopores, *The Journal of Physical Chemistry C, Nanomaterials and Interfaces*. 113 (2009) 1850.
55. Wan Y, Tan J, Asghar W, Kim YT, Liu Y, Iqbal SM. Velocity effect on aptamer-based circulating tumor cell isolation in microfluidic devices, *The Journal of Physical Chemistry B*. 115 (2011) 13891-6.
56. Wan Y, Liu Y, Allen PB, Asghar W, Mahmood MA, Tan J, Duhon H, Kim YT, Ellington AD, Iqbal SM. Capture, isolation and release of cancer cells with aptamer-functionalized glass bead array, *Lab On a Chip*. 12 (2012) 4693-701.
57. Fischbein MD, Drndic M. Sub-10 nm device fabrication in a transmission electron microscope, *Nano Letters*. 7 (2007) 1329-37.
58. Asghar W, Ilyas A, Deshmukh RR, Sumitsawan S, Timmons RB, Iqbal SM. Pulsed plasma polymerization for controlling shrinkage and surface composition of nanopores, *Nanotechnology*. 22 (2011) 285304.
59. Billo JA, Asghar W, Iqbal SM. An Implementation for the Detection and Analysis of Negative Peaks in an Applied Current Signal across a Silicon Nanopore, *Micro- and Nanotechnology Sensors, Systems, and Applications III*. 8031 (2011) 80312T.

CHAPTER 5

CONCLUSION & FUTURE DIRECTIONS

5.1 Future Directions

5.1.1 Early Detection of Leukemia from Blood Serum

Leukemia is a type of blood cancer. Such patients are at a higher risk of getting infections. Most common way to diagnose leukemia is from the blood test but at early stage of the disease, a blood test might not show that a person has leukemia.

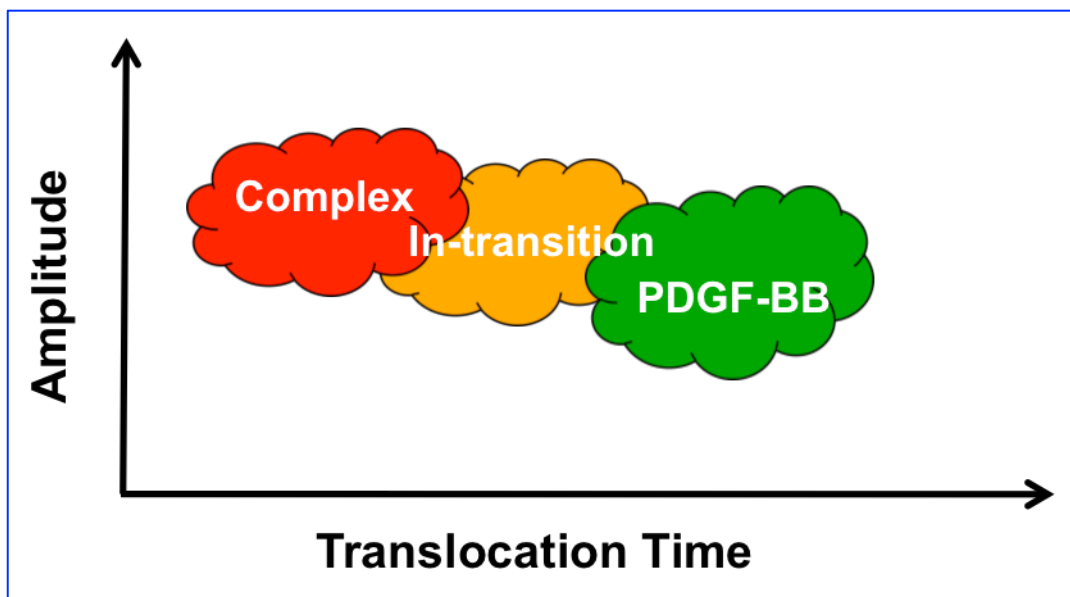


Figure 5.1: Aptamer attachment with PDGF-BB will cause formation of complex. Due to higher net charge complex will translocate faster than PDGF-BB.

Elevated level of platelet derived growth factor receptor protein (PDGF-BB) has been reported in the blood serum of leukemia patients and it's an early biomarker for this disease. Nanopore sensor along with the aptamer that is specific for PDGF-BB can be used to detect this disease at an early stage (Fig. 5.1).

5.1.2 Self-referenced Nanopore Array for Multiple Biomarker Detection

It is the need of the hour to develop a single test that can check the blood serum of a potential cancer patient for all or most of the biomarkers of interest in a single run. A nanopore array that will have several nanopores on a single membrane can be used for this purpose.

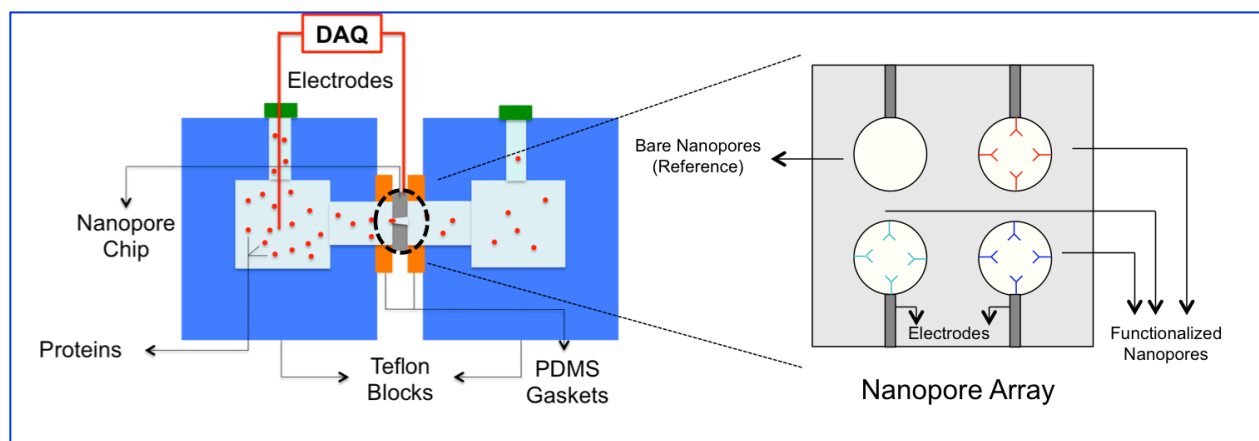


Figure 5.2: System schematic for nanopore array. On the right is a nanopore array with integrated electrodes. Bare nanopore is for referencing whereas other nanopores are functionalized with different aptamers.

Electrodes can be fabricated on the chip along with nanopores to measure the current of individual nanopores. Each nanopore can be functionalized with a different

aptamer to make it selective for a particular target protein (biomarker). Signals from each nanopore can be analyzed to detect the presence of a biomarker. This way there will be no need to check each protein individually with a specialized test rather a single test will be sufficient to check all the important biomarkers present in the blood serum. A system schematic for the device setup is shown in figure 5.2.

5.1.3 Spiral Microfluidics interfaced with Micropore – Lab on a Chip

Just like there is a need for single test to analyze blood serum, the same is required for the whole blood. Whole blood contains several types of cells. A device that can analyze the whole blood of a potential cancer patient, provide the information like count of white blood cells (WBCs), red blood cells (RBCs) and can detect and differentiate CTCs in a single test will make the diagnosis easy, quick and cheap.

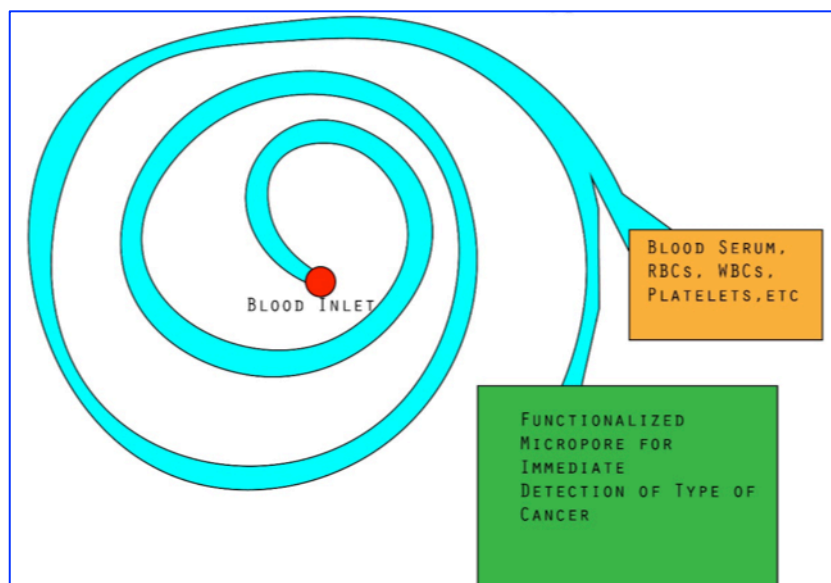


Figure 5.3: A system schematic for a spiral microfluidic device interfaced with micropore.

Keeping that in perspective, a spiral microfluidic device can be combined with the micropore for whole blood processing. There will be a size based filtering through the microfluidic device that will allow us to separate WBCs, RBCs and platelets etc. from the blood. CTCs and other types of cells will pass through the micropore and will be detected and differentiated based on their mechanophysical properties. A general schematic for such a system is shown in Figure 5.3.


5.2 Conclusions

Early detection of CTCs from the blood of a cancer patient is the fruit of advancements in nanotechnology. CTC detection has improved the cancer diagnosis and therapy monitoring but it is not the early detection of cancer since the presence of CTCs in blood is an indication that cancer has metastasized and the only question we can answer by detection and quantification of CTCs is whether it's the start of metastatic stage or its mature state. We can't detect cancer much before its metastatic stage with CTCs detection. Cell deformability has evolved as an inherent cell marker that gives an early indication of cell mutation. We have successfully demonstrated the use of micropore biosensor to electrically differentiate breast cancer cells and lung cancer cells from the difference in their cell deformability. Such differentiation can lead to the detection of tumor at its much earlier stage and proper treatment at that point can prevent cancer to reach its metastatic stage. Our detection efficiency was around 75% that can be further improved by controlling cell clogging and cell agglomeration. We also successfully detected EGFR using nanopore biosensor with detection limit close to that

of ELISA that is the current standard method for detection of EGFR. In contrast to ELISA, nanopore based detection is much simpler and does not require functionalization.

APPENDICES

COPYRIGHT PERMISSIONS

From: eic@langmuir.acs.org 
Subject: RE: Request #9131-6975932 Submitted (Re: Permission to Reuse my Published Work in Dissertation)
Date: May 1, 2016 at 1:26 PM
To: Ali, Waqas waqas.ali@mavs.uta.edu
Cc: eic@id.acs.org



Dear Dr. Waqas:

Thank you for contacting us. [Dr. Winnik approves the use of your published manuscript, DOI: 10.1021/acs.langmuir.6b00016, for use in your dissertation.](#)

The Journal Publishing Agreement that was signed for this manuscript stipulates that [Authors may reuse all or part of the Submitted, Accepted or Published Work in a thesis or dissertation that the Author writes and is required to submit to satisfy the criteria of degree-granting institutions.](#) Such reuse is permitted subject to the ACS' "Ethical Guidelines to Publication of Chemical Research" (<http://pubs.acs.org/ethics>).

Appropriate citation of the Published Work must be made. If the thesis or dissertation to be published is in electronic format, a direct link to the Published Work must also be included using the ACS Articles on Request author-directed link which is available on your ACS Paragon Plus home page.

Please let us know if you have any further questions.

Best regards, Cheryl
Cheryl Shanks
Journal Office Administrator
Langmuir Editor-in-Chief Office

-----Original Message-----

From: "support@services.acs.org" <support@services.acs.org>
Sent: Friday, April 29, 2016 2:19pm
To: "eic@langmuir.acs.org" <eic@langmuir.acs.org>
Subject: Request #9131-6975932 Submitted (Re: Permission to Reuse my Published Work in Dissertation)



[Click here if you have difficulty reading this email >>](#)

Thank you for submitting your help request to the ACS Publications Help Desk. It will be assigned to the appropriate support team.

Support is available 24 hours a day, Monday through Friday.

E-mail Information:

Attachments
cc eic@langmuir.acs.org

Request Information:

Request # 9131-6975932
Date Created 4/29/2016 02:18 PM EDT
Summary Re: Permission to Reuse my Published Work in Dissertation

Hi Lisa

Thanks Lisa. I got permission using the RightsLink but I have been told by mailto:Copyright@acs.org that I need written permission from editorial office as well that is handling my paper. Can I get that too.

Thanks

On Apr 29, 2016, at 7:57 AM,
eic@langmuir.acs.org wrote:

Dear Support,

Could you please assist Dr. Ali's email request which was received
at the Langmuir office.

Thank you,

Lisa

Lisa Tomlin

Administrative Support & Peer Review Services

ACS Managed Support Services
Langmuir

Details

-----Original Message-----

From: "Ali, Waqas" <mailto:waqas.ali@mavs.uta.edu>

Sent: Thursday, April 28, 2016 5:55pm

To: "mailto:eic@langmuir.acs.org" <mailto:eic@langmuir.acs.org>

Cc: "mailto:copyright@acs.org" <mailto:copyright@acs.org>

Subject: Permission to Reuse my Published Work in Dissertation

Dear Dr. Winnik

My name is Waqas Ali and I am a PhD candidate at University of
Texas at Arlington. My article "Differentiating Metastatic and Non-
metastatic Tumor Cells from their Translocation Profile through
Solid-state Micropores" (DOI: 10.1021/acs.langmuir.6b00016)
recently got accepted for publication in Langmuir. I want that paper
to be a part of my PhD Dissertation and for that I need permission
from you. Kindly grant me permission to do that or kindly let me
know what needs to be done on my side to get the permission.

Thanks

Best Regards.

Waqas Ali

Graduate Research Assistant

Nanotechnology Research Center

Electrical Engineering Department

University of Texas at Arlington

817-262-0598 (voice)

mailto:waqas.ali@mavs.uta.edu (mail)

Best Regards.

Waqas Ali

Graduate Research Assistant

Nanotechnology Research Center

Electrical Engineering Department


University of Texas at Arlington

817-262-0598 (voice)

mailto:waqas.ali@mavs.uta.edu (mail)

To update or check the status of this request:

[Click here to access this request online.](#)

From: Permissions permissions@iop.org 
Subject: Re: Permission to Reuse my Published Work in Dissertation
Date: May 3, 2016 at 6:15 AM
To: Ali, Waqas waqas.ali@mavs.uta.edu



Dear Waqas Ali,

Thank you for your email and for taking the time to seek this permission.

When you transferred the copyright in your article to IOP, we granted back to you certain rights, including the right to include the Accepted Manuscript of the article within any thesis or dissertation. Please note you may need to obtain separate permission for any third party content you included within your article.

Please include citation details, "© IOP Publishing. Reproduced with permission. All rights reserved" and for online use, a link to the Version of Record.

The only restriction is that if, at a later date, your thesis were to be published commercially, further permission would be required.

Please let me know if you have any further questions.

In the meantime, I wish you the best of luck with the completion of your dissertation.

Kind regards,

Kathryn Shaw

Copyright & Permissions Team

Gemma Alaway – Rights & Permissions Adviser
Kathryn Shaw - Editorial Assistant

Contact Details

E-mail: permissions@iop.org

For further information: <http://iopscience.iop.org/page/copyright>

Please note: We do not provide signed permission forms as a separate attachment. Please print this email and provide it to your institution as proof of permission.

From: "Ali, Waqas" <waqas.ali@mavs.uta.edu>
To: "permissions@iop.org" <permissions@iop.org>,
Date: 28/04/2016 23:12
Subject: Permission to Reuse my Published Work in Dissertation

Hi

My name is Waqas Ali and I am a PhD candidate at University of Texas at Arlington. My article "Electromechanical transducer for rapid detection, discrimination and quantification of lung cancer cells" (<http://dx.doi.org/10.1088/0957-4484/27/19/195101>) recently got published in IOPScience journal "Nanotechnology". I want that paper to be a part of my PhD Dissertation and for that I need permission from you. Kindly grant me permission to do that or kindly let me know what needs to be done on my side to get the permission.

Thanks

Best Regards.

Waqas Ali
Graduate Research Assistant
Nanotechnology Research Center
Electrical Engineering Department
University of Texas at Arlington
817-262-0598 (voice)

waqas.ali@mavs.uta.edu (mail)

This email (and attachments) are confidential and intended for the addressee(s) only. If you are not the intended recipient please notify the sender, delete any copies and do not take action in reliance on it. Any views expressed are the author's and do not represent those of IOP, except where specifically stated. IOP takes reasonable precautions to protect against viruses but accepts no responsibility for loss or damage arising from virus infection. For the protection of IOP's systems and staff emails are scanned automatically.

IOP Publishing Limited Registered in England under Registration No 467514. Registered Office: Temple Circus, Bristol BS1 6HG
England Vat No GB 461 6000 84.

Please consider the environment before printing this email

- [Home](#)
- [Subjects](#)
- [Journals](#)
- [Books](#)
- [Open Access](#)
- [About Us](#)
- [News & Blogs](#)
- [Contact](#)
-

Copyright Policy

1. OCP acknowledges and agrees that the Author(s) retain(s) the copyright to their work submitted for publication.

2. The author assigns to OCP all rights:

- *to publish the Work, in whole or in part, by various means such as hard copy or electronic copy formats, and in any and all forms of media, now or hereafter known; and*
- *to republish, distribute, promote, publicly perform, and publicly display the Work at any time and in all One Central Press projects.*

3. The author(s) must comply to the following:

- *only submit original work that has neither appeared elsewhere for publication, nor is under review for another refereed publication*
- *should determine whether disclosure of their material, content and photographs requires the prior consent of other parties and, if so, should obtain it; and*
- *research carried out in collaboration with other scholars necessitates that all authors approve of submitting the published work.*

Statements and opinions expressed in the published work are those of the Author(s) and not those of the editors or One Central Press. No responsibility is accepted for the accuracy of information contained in the published work. OCP assumes no responsibility or liability for any damage or injury to persons or property arising out of the use of any materials, instructions, methods or ideas contained inside the published work.

4. By accepting the Copyright Agreement the corresponding Author:

- *warrants that he/she is the Author and has the power and authority to make and execute this assignment*
- *affirms that, for jointly authored Chapters, he/she is empowered to accept this form on behalf of all authors*

- warrants that the Chapter is original, has not previously been published and is not currently under consideration for publication by any other entity
- affirms that permission will be obtained for all previously published and/or copyrighted material contained in this manuscript (to the extent that the chapter incorporates text, passages, figures, data or other material from the work of others), it is the authors collective responsibility to obtain all copyright permissions – they can be obtained during the publishing process and need to be collected before publication; and
- agrees to indemnify One Central Press against all losses, costs and expenses (including legal costs and expenses) arising from claims made by other parties due to the exceptional circumstance that the author has breached any terms, conditions and/or warranties concerning the authorship of the chapter (the whole or parts of it), the rights to publish the chapter or the infringement of any third party's rights.

If the Author has prepared the work as part of that his/her official duties as an employee or officer of a Government agency, public institution or company and has copyrights that belong to the Government agency, public institution, or company, One Central Press agrees to accept their terms and conditions if they are not in conflict with OCP's Copyright Policy.

[CALL FOR CHAPTERS](#)[PUBLISH WITH ONE CENTRAL PRESS](#)

CONTACT DETAILS

[Home](#) | [Subjects](#) | [Books](#) | [Open Access](#) |
[About Us](#) | [News & Blogs](#) | [Contact](#) |
[Publish](#) | [Frequently Asked Questions](#) |
[Copyright Policy](#)



- One Central Press
One Central Park
Northampton Road
Manchester
M40 5BP
United Kingdom
- **Tel:** +44 (0) 161 918 6673
- **@:**
admin@onecentralpress.com

Email:

Subscribe

COAUTHOR PERMISSIONS

To Whom It May Concern

Subject: Permission to reuse/reprint a published/accepted/in-press paper in PhD Dissertation

I am a co-author on the paper titled “Differentiating Metastatic and Non-metastatic Tumor Cells from their Translocation Profile through Solid-state Micropores” DOI: 10.1021/acs.langmuir.6b00016.

I grant permission to Mr. Waqas Ali to reuse/reprint this paper in his PhD dissertation.

Name: AZHAR ILYAS

Signature:  _____

Email: ilyas@bcd.tamhsc.edu

Date: 4/28/2016

To Whom It May Concern

Subject: Permission to reuse/reprint a published/accepted/in-press paper in PhD Dissertation

I am a co-author on the paper titled "Electromechanical transducer for rapid detection, discrimination and quantification of lung cancer cells" DOI: <http://dx.doi.org/10.1088/0957-4484/27/19/195101>.

I grant permission to Mr. Waqas Ali to reuse/reprint this paper in his PhD dissertation.

Name: Loan Bui

Signature:



Email: lbui@mavs.uta.edu

Date: May 2, 2016


To Whom It May Concern

Subject: Permission to reuse/reprint a published/accepted/in-press paper in PhD Dissertation

I am a co-author on the paper titled “Differentiating Metastatic and Non-metastatic Tumor Cells from their Translocation Profile through Solid-state Micropores” DOI: 10.1021/acs.langmuir.6b00016.

I grant permission to Mr. Waqas Ali to reuse/reprint this paper in his PhD dissertation.

Name: Bailey Sayles _____

Signature:  _____

Email: bailey.sayles@mavs.uta.edu _____

Date: 05/05/2016 _____

To Whom It May Concern

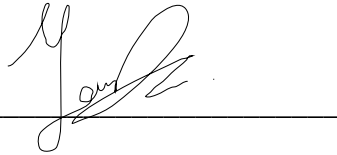
Subject: Permission to reuse/reprint a published/accepted/in-press paper in PhD Dissertation

I am a co-author on the paper titled “Differentiating Metastatic and Non-metastatic Tumor Cells from their Translocation Profile through Solid-state Micropores” DOI: 10.1021/acs.langmuir.6b00016.

I grant permission to Mr. Waqas Ali to reuse/reprint this paper in his PhD dissertation.

Name: Yeun Hur

Signature: _____

A handwritten signature in black ink, appearing to read 'Yeun Hur', is written over a horizontal line. The signature is stylized and cursive.

Email: ushur2002@tamu.edu

Date: 5/1/16

To Whom It May Concern

Subject: Permission to reuse/reprint a published/accepted/in-press paper in PhD Dissertation

I am a co-author on the paper titled "Differentiating Metastatic and Non-metastatic Tumor Cells from their Translocation Profile through Solid-state Micropores" DOI: 10.1021/acs.langmuir.6b00016.

I grant permission to Mr. Waqas Ali to reuse/reprint this paper in his PhD dissertation.

Name: Kim, Young-tae

Signature: 

Email: ykim@uta.edu

Date: 4/28/2016


To Whom It May Concern

Subject: Permission to reuse/reprint a published/accepted/in-press paper in PhD Dissertation

I am a co-author on the paper titled “Differentiating Metastatic and Non-metastatic Tumor Cells from their Translocation Profile through Solid-state Micropores” DOI: 10.1021/acs.langmuir.6b00016.

I grant permission to Mr. Waqas Ali to reuse/reprint this paper in his PhD dissertation.

Name: **SAMIR IQBAL, Ph.D., P.E., FRSC**

Signature:  Dr. Samir Iqbal
cn=Dr. Samir Iqbal, o=UT-
Arlington, ou=Electrical
Engineering,
email=smiqbal@uta.edu, c=US
2016.05.05 00:12:56 -04'00'

Email: **SMIQBAL@uta.edu**

Date: **5 MAY 2016**

To Whom It May Concern

Subject: Permission to reuse/reprint a published/accepted/in-press paper in PhD Dissertation

I am a co-author on the paper titled “Electromechanical transducer for rapid detection, discrimination and quantification of lung cancer cells” DOI: <http://dx.doi.org/10.1088/0957-4484/27/19/195101>.

I grant permission to Mr. Waqas Ali to reuse/reprint this paper in his PhD dissertation.

Name: ___Fatemeh Jelvehi Moghaddam_____

Signature: __F.J.Moghaddam_____

Email: _fatemeh.jelvheimoghaddam@mavs.uta.edu_____

Date: _April/ 28/2016_____


To Whom It May Concern

Subject: Permission to reuse/reprint a published/accepted/in-press paper in PhD Dissertation

I am a co-author on the paper titled "Electromechanical transducer for rapid detection, discrimination and quantification of lung cancer cells" DOI: <http://dx.doi.org/10.1088/0957-4484/27/19/195101>.

I grant permission to Mr. Waqas Ali to reuse/reprint this paper in his PhD dissertation.

Name: Muhammed Usman Raza

Signature: 

Email: raza.muhammadusman@mars.uta.edu

Date: 5/2/16

To Whom It May Concern

Subject: Permission to reuse/reprint a published/accepted/in-press paper in PhD Dissertation

I am a co-author on the paper titled "Differentiating Metastatic and Non-metastatic Tumor Cells from their Translocation Profile through Solid-state Micropores" DOI: 10.1021/acs.langmuir.6b00016.

I grant permission to Mr. Waqas Ali to reuse/reprint this paper in his PhD dissertation.

Name: Loan Bui

Signature:



Email: lbui@mavs.uta.edu

Date: May 2, 2016

To Whom It May Concern

Subject: Permission to reuse/reprint a published/accepted/in-press paper in PhD Dissertation

I am a co-author on the paper titled “Electromechanical transducer for rapid detection, discrimination and quantification of lung cancer cells” DOI: <http://dx.doi.org/10.1088/0957-4484/27/19/195101>.

I grant permission to Mr. Waqas Ali to reuse/reprint this paper in his PhD dissertation.

Name: Bailey Sayles _____

Signature:  _____

Email: bailey.sayles@mavs.uta.edu _____

Date: 05/05.2016 _____

To Whom It May Concern

Subject: Permission to reuse/reprint a published/accepted/in-press paper in PhD Dissertation

I am a co-author on the paper titled "Electromechanical transducer for rapid detection, discrimination and quantification of lung cancer cells" DOI: <http://dx.doi.org/10.1088/0957-4484/27/19/195101>.

I grant permission to Mr. Waqas Ali to reuse/reprint this paper in his PhD dissertation.

Name: Kim, Young-tae

Signature: 

Email: YKim@vta.edu

Date: 4/28/2016

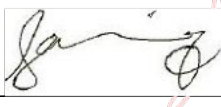
To Whom It May Concern

Subject: Permission to reuse/reprint a published/accepted/in-press paper in PhD Dissertation

I am a co-author on the paper titled “Electromechanical transducer for rapid detection, discrimination and quantification of lung cancer cells” DOI: <http://dx.doi.org/10.1088/0957-4484/27/19/195101>.

I grant permission to Mr. Waqas Ali to reuse/reprint this paper in his PhD dissertation.

Name: SAMIR IQBAL, Ph.D., P.E., FRSC

Signature:  Dr. Samir Iqbal
cn=Dr. Samir Iqbal, o=UT-
Arlington, ou=Electrical
Engineering,
email=smiqbal@uta.edu, c=US
2016.05.05 00:11:37 -0400

Email: SMIQBAL@UTA.EDU

Date: 5 MAY 2016


To Whom It May Concern

Subject: Permission to reuse/reprint a published/accepted/in-press paper in PhD Dissertation

I am a co-author on the paper titled “Differentiation of Specific Cancer Biomarkers with Solid-state Nanopores” that is currently in review for publication at Functional Nanostructures.

I grant permission to Mr. Waqas Ali to reuse/reprint this paper in his PhD dissertation.

Name: __M Arif I Mahmood_____

Signature: _____

Email: arif.iftakher@gmail.com _____

Date: _5/5/2016_____

To Whom It May Concern

Subject: Permission to reuse/reprint a published/accepted/in-press paper in PhD Dissertation

I am a co-author on the paper titled "Differentiation of Specific Cancer Biomarkers with Solid-state Nanopores" that is currently in review for publication at Functional Nanostructures.

I grant permission to Mr. Waqas Ali to reuse/reprint this paper in his PhD dissertation.

Name: PETER ALLEN

Signature: 

Email: pballen@uidaho.edu

Date: 5/5/2016

To Whom It May Concern

Subject: Permission to reuse/reprint a published/accepted/in-press paper in PhD Dissertation

I am a co-author on the paper titled “Differentiation of Specific Cancer Biomarkers with Solid-state Nanopores” that is currently in review for publication at Functional Nanostructures.

I grant permission to Mr. Waqas Ali to reuse/reprint this paper in his PhD dissertation.

Name: Adam R. Hall

Signature: 

Email: arhall@wakehealth.edu

Date: 05/05/16

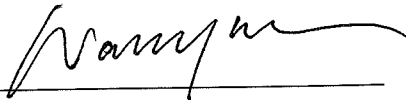
To Whom It May Concern

Subject: Permission to reuse/reprint a published/accepted/in-press paper in PhD Dissertation

I am a co-author on the paper titled "Differentiation of Specific Cancer Biomarkers with Solid-state Nanopores" that is currently in review for publication at Functional Nanostructures.

I grant permission to Mr. Waqas Ali to reuse/reprint this paper in his PhD dissertation.

Name: Yuan Wang

Signature: 

Email: wang33@psu.edu

Date: 5/5/2016

To Whom It May Concern

Subject: Permission to reuse/reprint a published/accepted/in-press paper in PhD Dissertation

I am a co-author on the paper titled "Differentiation of Specific Cancer Biomarkers with Solid-state Nanopores" that is currently in review for publication at Functional Nanostructures.

I grant permission to Mr. Waqas Ali to reuse/reprint this paper in his PhD dissertation.

Name: Muhammad Usman Reza

Signature: 

Email: raza.muhammad.usman@maus.uta.edu

Date: 5/5/16

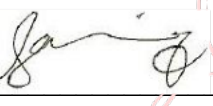
To Whom It May Concern

Subject: Permission to reuse/reprint a published/accepted/in-press paper in PhD Dissertation

I am a co-author on the paper titled “Differentiation of Specific Cancer Biomarkers with Solid-state Nanopores” that is currently in review for publication at Functional Nanostructures.

I grant permission to Mr. Waqas Ali to reuse/reprint this paper in his PhD dissertation.

Name: **SAMIR IQBAL, Ph.D., P.E., FRSC**

Signature:  Dr. Samir Iqbal
cn=Dr. Samir Iqbal, o=UT-
Arlington, ou=Electrical
Engineering,
email=smiqbal@uta.edu, c=US
2016.05.05 00:29:20 -04'00'

Email: **SMIQBAL@uta.edu**

Date: **5 MAY 2016**